NASA CR-54665

ONE AND TWO-DIMENSIONAL STEADY STATE LOW PRESSURE DISCHARGE THEORY

by

E. K. Shaw

M. L. Report No. 1495

Microwave Laboratory

W. W. HANSEN LABORATORIES OF PHYSICS

STANFORD UNIVERSITY · STANFORD, CALIFORNIA

Interim Report

(Summary Report II)

Prepared for

National Aeronautics and Space Administration

Contract NAS 3-4100

NOTICE

This report was prepared as an account of Government sponsored work. Neither the United States, nor the National Aeronautics and Space Administration (NASA), nor any person acting on behalf of NASA:

A.) Makes any warranty or representation, expressed or implied, with respect to the accuracy, completeness, or usefulness of the information contained in this report, or that the use of any information, apparatus, method, or process disclosed in this report may not infringe privately owned rights; or

B.) Assumes any liabilities with respect to the use of, or for damages resulting from the use of any information, apparatus, method or process disclosed in this report.

As used above, "person acting on behalf of NASA" includes any employee or contractor of NASA, or employee of such contractor, to the extent that such employee or contractor of NASA, or employee of such contractor prepares, disseminares, or provides access to, any information pursuant to his employment or contract with NASA, or his employment with such contractor.

Requests for copies of this report should be referred to

National Aeronautics and Space Administration
Office of Scientific and Technical Information
Attention: AFSS-A
Washington, D. C. 20546

ABSTRACT

This study was motivated by the recent upsurge of interest in ion propulsion devices wherein thrust is obtained by accelerating ions out of the plasma of a dc discharge. In order to be able to understand and thus improve the operation of these devices it is necessary to be able to analyze and solve complicated one- and two-dimensional dc discharge problems.

In this work it is shown that a pressure theory approach, although approximate, when modified to take into account ion generation can be used to accurately describe a wide variety of dc discharges in the low- and medium-pressure regimes. This modified pressure theory or fluid approach makes use of the "moment method" of solution of the Boltzmann equation to obtain differential equations which describe low pressure discharges in terms of measurable macroscopic parameters.

Solutions are found for the parameters of the discharges in one-dimensional planar, cylindrical, and coaxial geometries for various generation rates and including both the effects of ion-neutral collisions and an applied magnetic field. The results for the one-dimensional collisionless cases are compared with the more exact formulation of Langmuir and found to be in good agreement.

In the limit of a small inner conductor, the one-dimensional coaxial solutions are shown to be useful in determining the properties of cylindrical Langmuir probes in the ion collection regime. The results are compared to present collisionless probe theories and found to be in good agreement. The one-dimensional coaxial solutions are then extended to include the effects of collisions and an applied magnetic field on the characteristics of a cylindrical probe.

For the most important case of ion generation proportional to electron density, two-dimensional solutions for the parameters of the discharges in a rectangular box, a finite length cylinder, and between finite length concentric coaxial cylinders are found for the first time.

Calculated parameters for both the one- and two-dimensional discharges are presented graphically for a number of representative cases and the equations are tabulated and summarized in such a way as to be easily applied to other cases.

The theory is also used to describe the behavior of two experimental devices: the so-called oscillating-electron ion source and the Kaufman ion source. Only qualitative agreement between experiment and theory is obtained when the two-dimensional theory is used to approximate the behavior of the oscillating-electron ion source. However, a one-dimensional theory which includes both primary or beam electrons and secondary or Maxwellian electrons is found to give good agreement between theory and experiment for the Kaufman ion source.

ACKNOWLEDGEMENTS

I wish to express my gratitude to Professor Gordon S. Kino, my research advisor, for his encouragement and guidance throughout the duration of this study.

I also wish to thank Dr. Kenneth J. Harker of the Hansen Laboratory and Dr. S. A. Self of the Stanford University Institute for Plasma Research for their many helpful suggestions and enlightening discussions.

Finally, I am grateful to the staff of Hansen Laboratories for their excellent professional services.

PRECEDING PAGE BLANK NOT FILMED.

TABLE OF CONTENTS

LIST OF FIGURES

LIST OF TABLES

CHAPTER I

INTRODUCTION AND HISTORICAL BACKGROUND

In this work it is shown that a pressure theory, modified to take into account generation, can be used to describe one- and two-dimensional steady state discharges in the low pressure (collisionless) and medium pressure regimes where the collision dominated or diffusion theory is no longer applicable. For the first time, solutions are found for the discharges in a two-dimensional rectangular box, a two-dimensional finite length cylinder, and both one- and two-dimensional coaxial geometries.[1] The effects of ion neutral collisions and a uniform magnetic field are also included in the analysis of each of the above cases. In the limit of a small inner conductor, the one-dimensional coaxial solutions are found to be useful in determining the properties of cylindrical Langmuir probes thus making possible, for a first time, a quantitative study of the effects of a magnetic field and collisions on probe characteristics in the ion collection regime.

Using this pressure theory or Eulerian approach two different experimental discharges are analyzed and the results compared with experimental measurements, the first device being a so-called oscillating-electron ion source[2,3] and the second, an idealized model of the Kaufman ion source.[4] Reasonably good correlation between theory and experiment is obtained.

This study was motivated by the recent upsurge of interest in ion propulsion devices wherein thrust is obtained by accelerating ions out of the plasma of a dc discharge.[3,5,6] Considerable experimental work has been done on the Kaufman type of ion thrustor,[7-9] but in order to be able to fully understand, analyze, and improve the operation of this device it is necessary to be able to solve rather complicated one- and two-dimensional dc discharge problems. Although this study is generally directed toward analyzing discharges employing heavy ions which could be used for ion propulsion, the results are presented in such a way as

to be meaningful and useful for the study of a broad range of low and medium pressure, steady-state discharge problems which heretofore were very difficult, if not impossible, to formulate and solve.

The foundation for nearly all the later theoretical work on low pressure discharges was established in a classic paper by Tonks and Langmuir in 1929.[10] They developed a collisionless theory involving a rather complicated integral equation which they then used to solve several simple one-dimensional problems. This theory was verified by and used to explain a large number of experiments by Langmuir and his co-workers which extended over a period of some fifteen years.[11] The early theoretical work was later verified and extended by, among others, S. A. Self in a series of papers starting in 1962,[12-14] Harrison and Thompson in 1959,[15] and Caruso and Cavaliere in 1962.[16]

In the intervening years between the theoretical work of Langmuir and Self a great many experiments were carried out on various aspects of the low-pressure discharge. As examples of this type of work we cite the excellent experiments of Klarfeld[17] in 1938 and Bickerton and Engle[18] in 1955. Almost without exception, any theory accompanying these experiments is based upon the collisionless theory developed by Langmuir.[10] Unfortunately, as mentioned above, the formulation developed by Langmuir leads to a complicated integral equation which cannot be easily extended to include the intermediate region between the free-fall and collision dominated cases or to two-dimensional problems. Indeed, it is not at all evident that an extension of Langmuir's exact formulation to these problems can be made. Thus, it becomes necessary to look for an approach which does not have the limitations of Langmuir's formulation. We have found that a fluid or macroscopic approach, although approximate when modified for the low pressure regime, gives meaningful results for the parameters of low-pressure discharges. This pressure theory approach which leads to differential equations rather than the more complicated integral equation formulation of Langmuir is somewhat similar to that of Persson.[19,20] However, several important extensions of and departures from his approach have been made: In solving the collisionless one-dimensional problems we have included the pressure term and the third

moment equation which is known to be a more accurate approach; we have solved the previously unsolved coaxial discharge which has useful applications in the study of probe theory; the possibility of neutral density variation has also been considered together with finite ion temperatures at generation; we have successfully applied the theory to two-dimensional discharges in rectangular, cylindrical, and coaxial geometries including both collisions and a magnetic field; and finally we have been able to extend the theory to include a three-component plasma in which there are two types of electrons, primary beam elements and the secondary Maxwellian distribution of electrons. This approximates the behavior of the Kaufman type ion source.

The development in the following chapters proceeds in the logical manner of increasing complexity: First, we give a discussion of the method of solution and assumptions which define the dc discharge model. Next, we proceed to a solution of some simple one-dimensional planar and cylindrical discharges which are used to verify the validity of the theory. Then we give a rather complete discussion of the heretofore unsolved one-dimensional coaxial discharge. Next, we discuss the more complicated two-dimensional cases. We then discuss the more difficult numerical solution of the general dc discharge problem. Finally, we present the application and correlation of the theory to two experimental devices. A more detailed discussion of the contents of the various chapters follows below.

In Chapter II, the general low pressure discharge problem is formulated in terms of the fluid or Eulerian approach by solving the Boltzmann-Vlasov equation using the "moment method" of solution to generate macroscopic equations of motion. This formulation leads to particularly useful solutions because the parameters in the equations are relatively easily measured quantities. In this same chapter, the limitations of the theory and the assumptions made to simplify the problem are discussed in detail.

In Chapter III, using the theory developed in Chapter II, one-dimensional planar and cylindrical dc discharges are solved for various generation rates. In order to demonstrate the validity of this approach, the results are compared to those obtained by the more exact formulation

of Langmuir and Self.[10,14] Good agreement is obtained for the parameters of interest throughout the discharge regions. Chapter III also contains the results obtained for the parameters of the one-dimensional coaxial discharge both with and without ion-neutral collisions and a magnetic field. The results are presented graphically so that the effect of collisions and a magnetic field can be easily studied for various coaxial geometries.

Using the solutions of the one-dimensional coaxial discharge, the ion current to a small cylindrical probe is calculated and found to agree very closely with other collisionless probe theories. The quantitative effect of collisions and a magnetic field on the ion density near a probe are found for the first time for the intermediate pressure regime and a small magnetic field.

At the end of Chapter III tables summarizing all of the solutions and equations for the one-dimensional discharge are presented with the equations and expansions of parameters near the origin written in such a way as to be easily programmed for computer solution of cases not covered.

Chapter IV contains detailed results of the formulation and solution of two-dimensional problems in rectangular, cylindrical and coaxial geometry. As far as is known these results represent the first solutions of this type of problem in the low and medium pressure regimes. The effect of ion-neutral collisions is also included and for a somewhat more restricted case an applied magnetic field is also considered. Again, the equations and solutions of the two-dimensional discharges are summarized at the end of the chapter in such a way as to make easy the computation of cases not covered in the body of the chapter.

Numerical procedures for solving more general discharge problems are discussed in Chapter V. The considerable difficulties in formulating and solving the discharge as a general boundary value problem are reviewed. Two different numerical methods of solution are given which have been used with some success to solve the general one-dimensional problem. One of these methods is applied to the two-dimensional problem where a solution is obtained for a limited range of parameters.

Although this work was intended to be mostly theoretical in nature, the availability of a two-dimensional experimental device made it attractive to compare the theoretical analysis with some experimental data. Some qualitative agreement between experiment and theory was obtained for a two dimensional oscillating-electron ion source.[2] The results of comparing this experiment with the theory are presented in the first part of Chapter VI. Also included in Chapter VI is the comparison of a theoretical analysis of an idealized one-dimensional model of the Kaufman type ion source,[4] with experimental results obtained at the California Institute of Technology.[8] This analysis further demonstrates the versatility of the pressure theory approach in that other components which may be in the plasma such as beam or primary cathode electrons are easily included as a third component in the analysis.

CHAPTER II

FORMULATION OF THE PROBLEM

We are concerned in this work with solving one- and two-dimensional steady-state gaseous discharge problems. More particularly, we wish to develop mathematical models which describe plasmas in the low and medium pressure regimes where the collision dominated theory is no longer applicable.

In general, the low-pressure discharges which we will be discussing in the following chapters are assumed to have the following characteristics: Ions are generated throughout the discharge with low or zero initial velocity and proceed toward the walls undergoing a number of collisions with neutral atoms, depending on the pressure. The potential has a maximum at the center of the discharge and decreases monotonically toward the walls. Recombination within the body of the plasma (volume recombination) is neglected. Ionization occurs throughout the plasma with a functional form dependent upon the type of discharge. Steady-state conditions prevail throughout the plasma. The electrons are in thermal equilibrium corresponding to a uniform temperature and have a Boltzmann distribution of density for all cases except those with a magnetic field.

In this chapter, the equations governing the behavior of steady-state discharges are developed from a particular form of the Boltzmann equation. This is followed by a detailed discussion of the assumptions made in arriving at the final mathematical models.

A. THE BOLTZMANN-VLASOV EQUATION

The equation which we are going to use to describe the various components (electrons, ions, neutrals) of the plasma is commonly called the Boltzmann equation. More precisely, it is a combination of the

Boltzmann equation and the Vlasov equation since it includes both uncorrelated space charge forces and short range binary collisions.[21] An excellent discussion of the derivation and limitations of both the Vlasov and Boltzmann equations is given by Delcroix.[21]

For our purposes, it is convenient to write the Boltzmann-Vlasov equation in the following form

$$\frac{\partial f}{\partial t}(\vec{r},\vec{w},t) + \vec{w} \cdot \frac{\partial f}{\partial \vec{r}}(\vec{r},\vec{w},t) + \vec{a} \cdot \frac{\partial f}{\partial \vec{w}}(\vec{r},\vec{w},t) = \left(\frac{\partial f}{\partial t}(\vec{r},\vec{w},t)\right)_c , \tag{1}$$

where $f(\vec{r},\vec{w},t)$ is the distribution function defined such that the number density of a particular component is given by

$$n(\vec{r},t) = \int_{-\infty}^{\infty} f(\vec{r},\vec{w},t)\, d\vec{w} \quad ; \tag{2}$$

$\vec{w}$ is the velocity, and $\vec{a}$ is the sum of the acceleration of the particles due to external applied forces plus the acceleration due to uncorrelated space charge forces.

The term on the right-hand side of Eq. (1) represents in a non-explicit way changes in the distribution function which are due to all short range collisional processes such as elastic collisions, ionizing collisions, recombination, and charge exchange. Much more will be said about this particular term in the next two sections of this work.

B. SOLUTION OF THE BOLTZMANN-VIASOV EQUATION

There are two different commonly used methods of solving Eq. (1): a perturbation technique, and the "moment method." The first named method is normally used when the solution is known to be near a given distribution function. Since we are concerned with relatively rarified plasmas where the distribution function for the ions and in some cases the electrons is not known and may be quite different from any standard distribution function, the perturbation technique of solution cannot be

used and we must resort to the "moment method" of solution. Although this method of solution is discussed in some detail by a number of authors,[22-24] the particular formulation which we need, including particle generation, has not been developed fully heretofore. We therefore discuss the "moment method" of solution in some detail.

In the most general "moment method" the Boltzmann equation is multiplied by a general function of velocity, position and time and then integrated over all velocity space. If we let $A(\vec{r},\vec{w},t)$ be the general function of velocity, position, and time; multiply Eq. (1) by A ; and then integrate over all velocity space, we obtain the result

$$\frac{\partial}{\partial t}\left(n\langle A\rangle\right) - n\langle\frac{\partial A}{\partial t}\rangle + \nabla_r \cdot n\langle\vec{w}A\rangle - n\langle\vec{w}\cdot\nabla_r A\rangle - n\langle\vec{a}\cdot\nabla_w A\rangle = \int_{-\infty}^{\infty} A\left(\frac{\partial f}{\partial t}\right)_c d\vec{w} , \tag{3}$$

where the symbol $\langle\ \rangle$ means the average over all the velocities is to be taken.

The most useful equations for our purposes are obtained by letting $A(\vec{r},\vec{w},t)$ be increasingly higher integral powers of the velocity, $\vec{w}$. When this approach is used we obtain what are commonly called the transport equations or the macroscopic equations of motion. These equations are useful in a practical way because, as we will see below, they result in relationships between measurable, macroscopic quantities. If we let $A = 1$, Eq. (3) becomes

$$\frac{\partial n}{\partial t} + \nabla\cdot(n\vec{v}) = G , \tag{4}$$

the well-known <u>equation of continuity</u> with a generation term, G , on the right-hand side defined such that

$$G = \int_{-\infty}^{\infty}\left(\frac{\partial f}{\partial t}\right)_c d\vec{w} = \int_{-\infty}^{\infty}\left(\frac{\partial f}{\partial t}\right)_g d\vec{w} , \tag{5}$$

where $(\partial f/\partial t)_g$ is the change in the distribution function due to generation (ionizing collisions), and where $\vec{v} = \langle w\rangle$, the average macroscopic velocity.

We next let $A = \vec{w}$ and make the substitution $\vec{w} = \vec{v} + \vec{u}$ (where $\vec{u}$ is the random part of the velocity) to obtain

$$\frac{\partial}{\partial t}(n\vec{v}) + n(\vec{v} \cdot \nabla\vec{v}) + \vec{v}\,\nabla \cdot (n\vec{v}) + \frac{\nabla \cdot \overleftrightarrow{\Psi}}{M} - n\vec{a} = \int \vec{w} \left(\frac{\partial f}{\partial t}\right)_c d\vec{w} \quad , \tag{6}$$

where $\overleftrightarrow{\Psi}$ is the kinetic stress tensor defined by

$$\overleftrightarrow{\Psi} = Mn\langle \vec{u}\,\vec{u} \rangle \quad , \tag{7}$$

and M is the mass of the component (ion, neutral, electron) under consideration. In Eq. (7) the term $\vec{u}\,\vec{u}$ is the product of two vectors, a tensor. Equation (6) is usually called the momentum transfer equation.

The next higher-order "moment equation," the heat transfer equation, is obtained by setting $A = (\vec{w} - \vec{v})(\vec{w} - \vec{v})$. For this value of $A(\vec{w})$ Eq. (3) becomes

$$\left(\frac{\partial}{\partial t} + \vec{v} \cdot \nabla + \nabla \cdot \vec{v}\right)\overleftrightarrow{\Psi} + \overleftrightarrow{\Psi} \cdot \nabla\vec{v} + (\overleftrightarrow{\Psi} \cdot \nabla\vec{v})^T + \nabla \cdot \overleftrightarrow{Q} - \vec{\omega}_c \times \overleftrightarrow{\Psi} - (\vec{\omega}_c \times \overleftrightarrow{\Psi})^T = \int_{-\infty}^{\infty} (\vec{w} - \vec{v})(\vec{w} - \vec{v}) \left(\frac{\partial f}{\partial t}\right)_c d\vec{w} \quad , \tag{8}$$

where $\overleftrightarrow{Q}$ is the heat or energy flux tensor defined by

$$\overleftrightarrow{Q} = Mn\langle \vec{u}\,\vec{u}\,\vec{u} \rangle \quad , \tag{9}$$

$\overleftrightarrow{\Psi} \cdot \nabla\vec{v}$ is the scalar product of two tensors, and $(\overleftrightarrow{\Psi} \cdot \nabla\vec{v})^T$ is the transposed tensor of this scalar product. A good explanation of this notation is given by Delcroix.[23] In the derivation of the above equation we have assumed that the only velocity dependent force is the

Lorentz force where

$$\vec{\omega}_c = -\frac{q}{M}\vec{B} \quad . \tag{10}$$

Equations (4), (6), and (8) describe the macroscopic behavior of a plasma with one set of the three equations for each component of the plasma. Provided the collision, generation, and acceleration terms are known, Eqs. (4), (6), and (8) give three equations in the four unknowns, $\overleftrightarrow{\Psi}$, n, $\vec{v}$, and $\overleftrightarrow{Q}$. Thus, in order to form a closed set of equations, it is necessary to generate one more equation. This is done by assuming that $\nabla \cdot \overleftrightarrow{Q}$ is either equal to zero or given as a known function or that $\nabla \cdot \overleftrightarrow{\Psi}$ is given in Eq. (6) and then using Eqs. (4) and (6) to form a closed set. In this work we usually assume that $\nabla \cdot \overleftrightarrow{\Psi} = 0$ for the ions. However, we shall solve some one-dimensional problems more accurately by assuming $\nabla \cdot \overleftrightarrow{Q} = 0$. More will be said about these assumptions in the next section.

C. ASSUMPTIONS DEFINING THE MODEL

In order to make the mathematics of the analysis tractable it is necessary to make certain assumptions about the plasma of the discharges which are to be analyzed. In this section each of the necessary assumptions is discussed in detail and the limitations, if any, which a particular assumption puts on the model are pointed out. Since we are most interested in mercury discharges because of the possible application to ion propulsion, some of the assumptions are evaluated in terms of the low pressure mercury discharge.

1. Steady-state conditions are assumed to prevail throughout the plasma, thus we set $\partial/\partial t = 0$ for all variables. As we shall see, in the relatively low-pressure discharges which we are considering, this does not mean that the electron and ion temperatures are equal or that the electrons and ions are in thermal equilibrium with each other.

2. Quasi-neutrality is assumed to exist throughout the discharge. This means that we assume

$$n_i \approx n_e = n \quad , \tag{11}$$

where n_i is the total ion density and n_e is the total electron density. Such an assumption is equivalent to neglecting the left-hand side of Poisson's equation. The validity of this assumption can only be rigorously checked after the solution of a particular problem; that is, only after the term $\nabla^2\phi$ where ϕ is the potential can be evaluated and compared to the difference

$$\left|\frac{q}{\epsilon_0}(n_i - n_e)\right| \quad .$$

It is well known that the assumption of quasi-neutrality breaks down at the edge of the plasma where a sheath of a few debye lengths thickness[25] is formed. The sheath region has been analyzed by Self[12] and by Caruso and Cavaliere.[16] However, it will be seen in the next chapter that even at edge of the plasma this assumption gives good approximations to the ion current and most of the other parameters of the discharge.

At this point we would like to emphasize that the general "moment method" approach discussed in the preceding section is not dependent upon the assumption of approximate charge neutrality. If one is willing to use the complete Poisson equation,

$$\nabla^2\phi = -\frac{q}{\epsilon_0}(n_i - n_e) \quad ,$$

as an added differential equation connecting the number densities and the potential, then Eqs. (4), (6), and (8) apply for any amount of charge separation.

3. For all of the cases solved in the following chapters, with the exception of those with an applied magnetic field, the <u>electrons</u> are assumed to be <u>in thermal equilibrium</u> corresponding to a <u>uniform temperature</u>, T_e . The electron density is then given by the Boltzmann distribution

$$n = n_{e0}\, e^{e\phi/kT_e} \quad , \tag{12}$$

where n_{e0} is the electron density at the center of the discharge, ϕ

is the potential relative to the center of the discharge, k is the Boltzmann constant, and T_e is the electron temperature.

Measurements by Langmuir in 1925, 1927, and 1928 of the electron velocity distribution in the positive column[26-28] seemed to indicate that the electrons had a Maxwellian distribution even though electron-neutral and electron-electron collisions were too rare to establish such a steady-state distribution. These unexplainable results are called "Langmuir's Paradox."[29] Recently much more sophisticated measurements by Vorob'eva, Kagan and their co-workers have confirmed that the electrons in a typical low-pressure mercury discharge are indeed Maxwellian out to at least 12 eV for pressures below approximately 10 microns.[30,31]

There is still some controversy concerning the mechanism which provides the electrons for the high energy "tail" of the distribution. The latest and most comprehensive discussion and study of this problem was made by Crawford and Self in 1964.[32] Their explanation is that the scattering of axially accelerated electrons is an adequate source of the high energy tail and they refer to recent experimental work by Ott[33] in 1963 and Harp[34] in 1964, for verification of the condition that a dc discharge can exist with an approximately Maxwellian electron distribution without the existance of rf energy-scattering effects.

For discharges where an external magnetic field is applied, the relation given by Eq. (12) can no longer be used and it is necessary to use the macroscopic equations for the electrons as well as for the ions.

4. We assume the only short range elastic collisions of importance are electron-neutral and ion-neutral collisions. Electron-ion, electron-electron and ion-ion collisions are assumed to be so rare as to be negligible in comparison to electron-neutral and ion-neutral collisions. For very low pressure discharges (pressure below 1μ in mercury) one can also neglect the ion-neutral collisions. For this pressure the ion-neutral collision frequency calculated using the experimental mobility values of von Engel[35] is less than one-fifth of the ionizing collision frequency measured by Klarfeld[17] and thus to a reasonably good approximation can be neglected. Most of the cases discussed below in Chapters II, III, and IV are generalized to include ion-neutral collisions with calculated

results showing how the parameters of the discharge vary as the ion-neutral collision frequency becomes comparable to the ionization frequency.

In order to take elastic collisions into account in the momentum transfer equation one must be able to evaluate the collision term

$$\int_{-\infty}^{\infty} \left(\frac{\partial f}{\partial t}\right)_c \vec{w}\, d\vec{w} \quad .$$

For hard sphere type collisions with $1/r^5$ attractive forces, Allis[36] shows that the above expression is independent of the distribution function and may be written for electron-neutral collisions as

$$\int_{-\infty}^{\infty} \left(\frac{\partial f}{\partial t}\right)_c \vec{w}\, d\vec{w} = -\nu_{en}\, n_e(\vec{v}_e - \vec{v}_n) \quad , \qquad (13)$$

where ν_{en} is the ion-neutral collision frequency, $\vec{v}_n$ is the neutral gas average velocity and $\vec{v}_e$ is the average velocity of the electrons. If the condition of $1/r^5$ attractive forces is not met, Eq. (13) can still be used for the electrons provided a suitable average value of electron neutral collision frequency is used.[24] Equation (13) is thus a general expression which applies reasonably well to electron neutral collisions.

For ion-neutral collisions the similar expression

$$\int_{-\infty}^{\infty} \left(\frac{\partial f}{\partial t}\right)_c \vec{w}\, d\vec{w} = -\nu_{in}\, n_i(\vec{v}_i - \vec{v}_n) \qquad (14)$$

may be used provided the mean free time between collisions is constant. In the above equation ν_{in} is the ion-neutral collision frequency and $\vec{v}_i$ is the average ion velocity. When the background neutral gas density is uniform ν_{en} and ν_{in} are taken to be constants. If the neutral density is not constant, the collisions frequencies must be written as

$$\nu_{en} = n_n \alpha_{en} \qquad (15)$$

$$\nu_{in} = n_n \alpha_{in} \quad , \qquad (16)$$

where n_n is the neutral gas density and Eqs. (15) and (16) define the α's . The assumption of uniform neutral density is examined in more detail in Appendix A where it is seen that reasonable (less than 10%) variations in the neutral density have little effect on the parameters of the one-dimensional collisionless planar discharge.

It is well to keep in mind that Eq. (14) is only approximate, applying reasonably well to mercury discharges but only very approximately to the noble gases. Each discharge must be examined on its own merits to determine how closely the condition of constant mean free time between ion-neutral collisions is satisfied. Most of the measured data give the collision probability, P_c , as a function of incident particle energy, $e\phi$, in electron volts. Since the mean free time is given by[37]

$$\tau \propto \frac{1}{\sqrt{e\phi\ P_c}} \tag{17}$$

for τ to be constant at a given pressure as the incident particle energy changes, the collision probability must be inversely proportional to the square root of the energy.

5. We assume that ions are generated with zero velocity throughout the entire volume of the discharge. With these assumptions, the ionization part of the collision integral becomes

$$\int_{-\infty}^{\infty} \left(\frac{\partial f}{\partial t}\right)_g A(\vec{w})\ d\vec{w} = \int_{-\infty}^{\infty} G\ \delta w(0)\ A(\vec{w})\ d\vec{w} = G\ A(0) \quad , \tag{18}$$

where G is the generation term equal to the number of ions generated per second per unit volume. For the first three moment equations this gives

$$G\ A(0) = G \quad , \tag{19}$$

$$G\ A(0) = G(\vec{w})_0 = 0 \tag{20}$$

and

$$G\,A(0) = G(\vec{w} - \vec{v})(\vec{w} - \vec{v}) = G\,\vec{v}\,\vec{v} \quad , \tag{21}$$

where $A = 1$, $\vec{w}$, and $(\vec{w} - \vec{v})(\vec{w} - \vec{v})$, respectively.

The consequences of assuming the ions to be generated at zero velocity rather than the more realistic gas temperature is discussed in Appendix B. It is shown that for the ratio of neutral gas temperature to electron temperature found in low-pressure discharges, the effects of neglecting the initial ion velocity are negligible.

For each ion generated we also make the reasonable assumption that an electron is generated at the background electron temperature with a Maxwellian distribution of velocity.

It is convenient to write the generation function, G , as

$$G = \nu^I n_{e0}\, g \quad , \tag{22}$$

where n_{e0} is the electron density at the center of the discharge, ν^I is the ionization frequency, and g is normalized to have the value unity at the center of the discharge. We write g as

$$g = e^{\gamma e\phi/kT} = \left(\frac{n_e}{n_{e0}}\right)^{\gamma} \quad , \tag{23}$$

where $\gamma = 0$, 1 , and 2 correspond to the three cases of generation: everywhere uniform, proportional to electron density, and proportional to electron density squared. The case of uniform generation ($\gamma = 0$) corresponds to ionization by an electron beam or a light beam, the case of generation proportional to electron density squared ($\gamma = 2$) corresponds to multiple ionization processes, and the case of generation proportional to electron density ($\gamma = 1$) corresponds to the most frequent case of ionization by the electrons in the plasma. As discussed by Self,[12] for $\gamma = 1$, ν^I is identifiable as the average ionizing collision frequency per electron. In the other two cases ν^I has no simple physical significance.

If the neutral density is not uniform then the generation term, G is given by

$$G = \alpha^I n_{e0} n_n g \tag{24}$$

where α^I is defined by

$$\alpha^I = \frac{\nu^I}{n_n} \quad . \tag{25}$$

6. We assume that the acceleration term $\vec{a}$ is due to only the self consistent Coulomb force, $q\vec{E}/M$ plus in some cases an external Lorentz force, $q(\vec{v} \times \vec{B})/M$.

D. FINAL EQUATIONS

Using the above definitions and approximations, the transport equations for the ions become

$$\nabla \cdot (n_i v_i) = \nu^I n_{e0} g \quad , \tag{26}$$

$$n_i \vec{v}_i \cdot \nabla \vec{v}_i + \vec{v}_i(\nabla \cdot n_i \vec{v}_i) + \frac{\nabla \cdot \overleftrightarrow{\Psi}_i}{M} = \frac{e}{M} n_i(\vec{E} + \vec{v}_i \times \vec{B}) - \nu_{in} n_i \vec{v}_i \quad , \tag{27}$$

and

$$(\vec{v}_i \cdot \nabla + \nabla \cdot \vec{v}_i)\overleftrightarrow{\Psi}_i + \overleftrightarrow{\Psi}_i \cdot \nabla \vec{v}_i + (\overleftrightarrow{\Psi}_i \cdot \nabla \vec{v}_i)^T = + \vec{\omega}_{c_i} \times \overleftrightarrow{\Psi}_i$$

$$+ \left(\vec{\omega}_{c_i} \times \overleftrightarrow{\Psi}\right)^T + GM\vec{v}_i\vec{v}_i + \int_{-\infty}^{\infty} (\vec{w}_i - \vec{v}_i)(\vec{w}_i - \vec{v}_i)\left(\frac{\partial f}{\partial t}\right)_c d\vec{w} \quad , \tag{28}$$

where we have assumed that the velocity of the neutral gas is zero and the neutral gas density is uniform. In Eq. (28) we have not evaluated

the collision term since we only use the first two moment equations when we solve problems with collisions. It is very important to note also that we have included the $\vec{v}_i \cdot \nabla\vec{v}_i$ inertial term since the average ion velocity is not small compared to the random ion velocity.

CHAPTER III
ONE-DIMENSIONAL CASES

In order to check the accuracy of the formulation given above, several one-dimensional planar and cylindrical geometry problems have been solved and results compared with values obtained by the more exact methods of Langmuir and Self.[10,14] One-dimensional planar and cylindrical discharges have been analyzed for the three different generation rates, corresponding to $\gamma = 0$, 1 and 2 with collisions neglected. The particular one-dimensional geometries analyzed below are shown in Fig. 1.

Agreement with the more exact theory is shown to be quite good even for the assumption of negligible kinetic pressure. A further indication of the validity of this macroscopic pressure theory approach to dc discharge problems has been furnished by Self and Ewald.[38] Using this approach, they have obtained excellent agreement with the experimental results of Klarfeld[17] for a one-dimensional cylindrical discharge.

Also included as a major portion of this chapter are the first known solutions to the one-dimensional coaxial discharge (Fig. 1c) including ion neutral collisions and a magnetic field. The coaxial solutions are of interest for at least two reasons: First, the solutions represent reasonable approximations to "long" coaxial discharges with an emitting inner conductor, provided the electron density is such that the Maxwellian electrons rather than the beam electrons provide a major portion of the ionization; Second, and more importantly, the solutions can be applied to probe theory to give answers to several important questions in this area such as: What is the magnitude of the error in probe measurements when the probe is not negligible in size compared to the plasma; by what magnitude does the ion density at the edge of the sheath of a small cylindrical probe differ from the undisturbed value, and what are the effects of a magnetic field and or collisions on the density of ions at the edge of the probe sheath? All of the above questions are answered in this chapter, using the coaxial solutions.

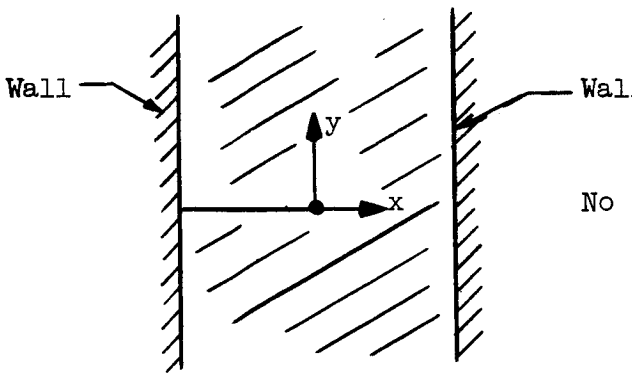

No y or z variations

a. Planar Geometry

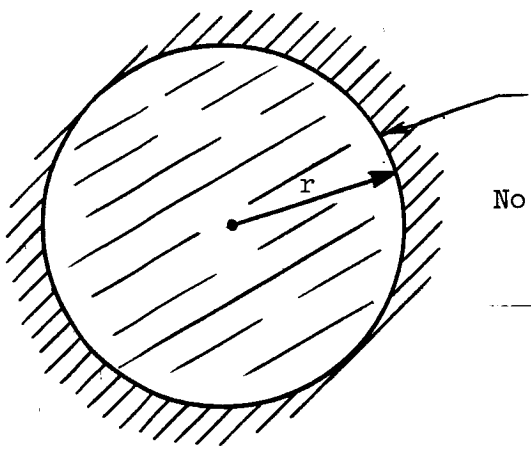

No θ or z variations

b. Cylindrical Geometry

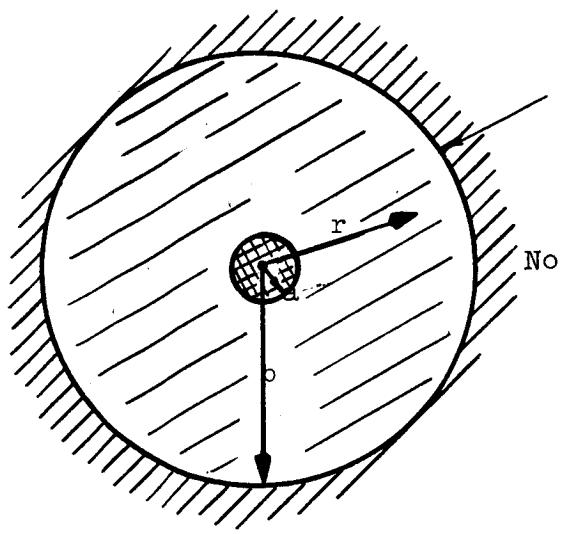

No θ or z variations

c. Coaxial Geometry

FIG. 1--Geometries of the one-dimensional discharges.

At the end of the chapter all of the solutions and equations describing the one-dimensional discharges are tabulated in a form useful for computation purposes, so that cases other than those treated in this chapter may be easily calculated.

A. CORRELATION WITH THE LANGMUIR'S THEORY

1. Neglecting Kinetic Pressure

Assuming $\nabla \cdot \overleftrightarrow{\Psi} = 0$ in Eq. (27), neglecting ion-neutral collisions, and considering variations only in the x-direction, Eq. (26) and (27) for the ions form the closed set of equations

$$\frac{1}{x^{\beta}} \frac{d}{dx} (x^{\beta} n v) = n_{e0} \nu^{I} g \tag{29}$$

and

$$\frac{1}{x^{\beta}} \frac{d}{dx} (x^{\beta} n v^{2}) = - \frac{e}{M} n \frac{d\Phi}{dx} , \tag{30}$$

where the distance from the center of the discharge is taken to be x ; the subscript on the velocity has been dropped since in one dimension $v_i = v_e = v$; and $\beta = 0$, $\beta = 1$, $\beta = 2$ correspond to the planar cylindrical and spherical cases, respectively.

The above equations may be put in dimensionless form by the substitution

$$s = \nu^{I} \left(\frac{M}{2kT_e} \right)^{1/2} x \tag{31}$$

$$v_1 = \left(\frac{M}{2kT_e} \right)^{1/2} v \tag{32}$$

and

$$\eta = \frac{-e\Phi}{kT_e} . \tag{33}$$

Using Eqs. (31), (32) and (33(, together with the assumption of charge neutrality [Eq.(11)], Eqs. (29) and (30) become

$$\frac{1}{s^{\beta}} \frac{d}{ds} (s^{\beta} e^{-\eta} v_1) = g \qquad (34)$$

and

$$\frac{1}{s^{\beta}} \frac{d}{ds} (s^{\beta} e^{-\eta} v_1^2) = \frac{e^{-\eta}}{2} \frac{d\eta}{ds} \quad . \qquad (35)$$

(a) Planar Case

For $\beta = 0$ (planar case) explicit analytic expressions for η and v_1 as functions for s can be obtained by solving Eqs. (34) and (35). With $\beta = 0$, Eq. (34) and (35) become

$$\frac{d}{ds} (e^{-\eta} v_1) = g \qquad (36)$$

and

$$\frac{d}{ds} (v_1^2) = (v_1^2 + \frac{1}{2}) \frac{d\eta}{ds} \quad . \qquad (37)$$

Integration of Eq. (37) yields the result

$$v_1^2 = \frac{1}{2} (e^{\eta} - 1) \quad , \qquad (38)$$

where the initial conditions $v_1(0) = \eta(0) = 0$ have been used. Substitution of Eq. (38) into (36) then gives the relation

$$\frac{1}{4} \frac{e^{-\eta}}{v_1} \frac{d\eta}{ds} (1 - 2v_1^2) = g \quad . \qquad (39)$$

It can be seen that $d\eta/ds \to \infty$ at $s = s_0$, $\eta = \eta_0$, where $v_1^2 = v_{10}^2 = 1/2$, and hence where [from Eq. (38)] $\eta_0 = 0.692$. This then is the edge of the plasma, sometimes called the Tonks-Langmuir boundary, for it is where s is a maximum $(ds/d\eta = 0)$. The condition that $v_{10} = 1/\sqrt{2}$ at the boundary was determined by Bohm[39] to be a necessary

condition for the formation of a sheath and is called the Bohm Criteria. It is interesting to note that the Bohm Criteria comes out as a natural result of solving the one-dimensional problems using this modified pressure theory approach and that the Bohm Criteria is satisfied independent of the value one chooses for the generation rate, g . It can be seen from Eq. (38) that the potential at the edge of the plasma is independent of the generation function g , just as it is in the Tonks-Langmuir theory. When $\gamma = 0$, the solutions of Eqs. (38) and (39) are

$$s = \frac{1}{e^{\eta}} \sqrt{\frac{e^{\eta}-1}{2}} \tag{40}$$

and

$$s = \frac{v_1}{2v_1^2 + 1} \tag{41}$$

for $\gamma = 1$

$$s = -\sqrt{\frac{e^{\eta}-1}{2}} + \sqrt{2} \tan^{-1} \sqrt{e^{\eta}-1} \tag{42}$$

and

$$s = -v_1 + \sqrt{2} \tan^{-1} \left(\sqrt{2v_1}\right) \quad ; \tag{43}$$

for $\gamma = 2$

$$s = \sqrt{\frac{e^{\eta}-1}{2}} \left[1 - \frac{1}{3} (e^{\eta}-1)\right] \tag{44}$$

and

$$s = v_1 \left(1 - \frac{2}{3} v_1^2\right) \quad . \tag{45}$$

The values of η vs s are plotted in Figs. 2,3, and 4, where the more exact values from Self[14] are also shown.

Of considerable interest is the value of ion current density at the boundary. This current density can be calculated from the relation

$$J_i = \left(\frac{2kT_e}{M}\right)^{1/2} n_{e0}\, e\, j_0 \quad , \tag{46}$$

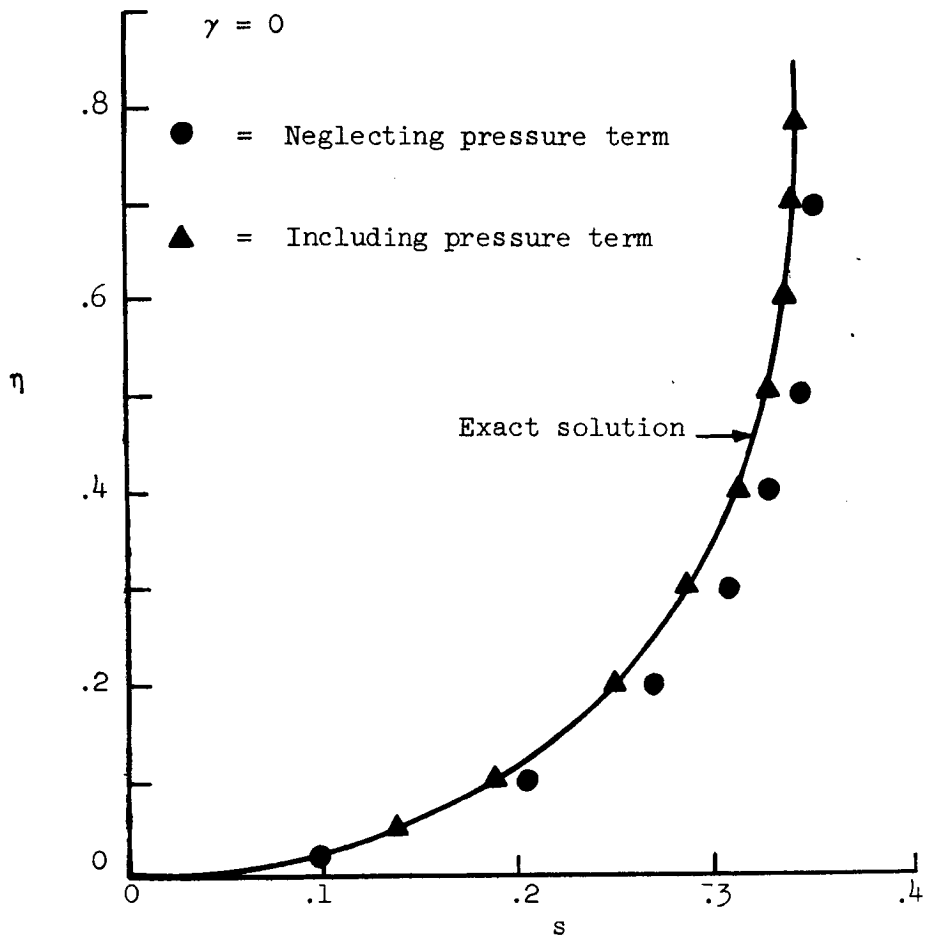

FIG. 2--Normalized potential as a function of position in the planar discharge ($\gamma = 0$) .

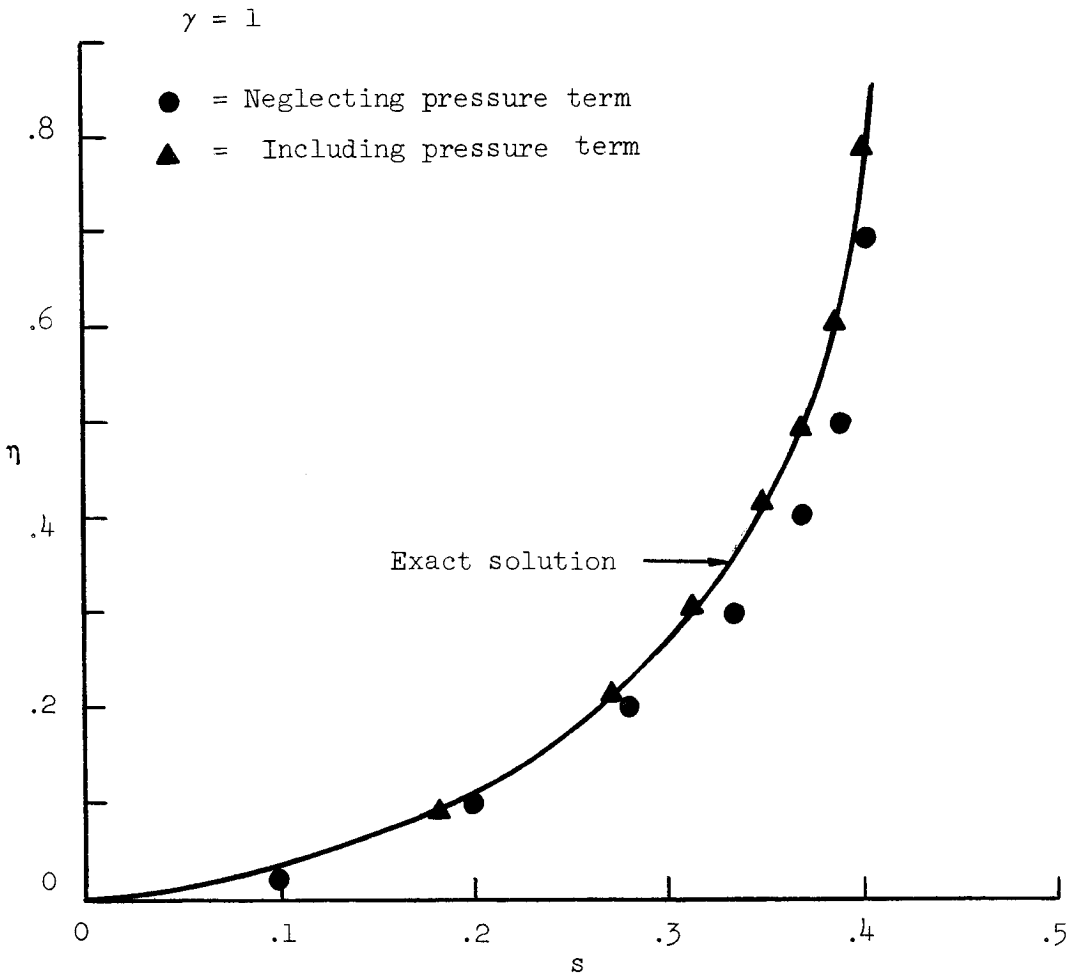

FIG. 3--Normalized potential as a function of position in the planar discharge ($\gamma = 1$) .

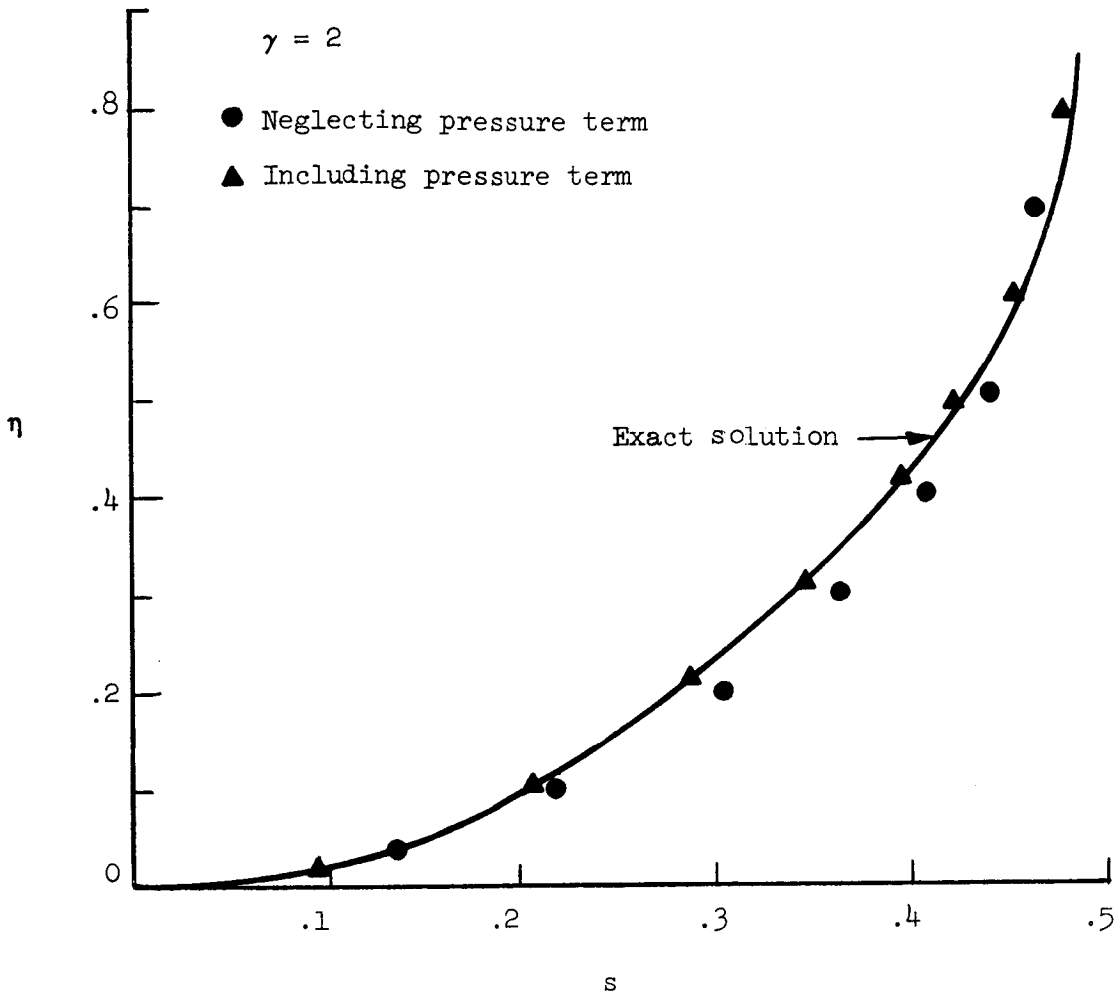

FIG. 4--Normalized potential as a function of position in the planar discharge ($\gamma = 2$) .

where

$$j_0 = v_{10} e^{-\eta_0} \quad , \tag{47}$$

v_{10} is the average normalized ion velocity at the boundary (η_0 , s_0) , and J_i is the ion current density.

Another quantity of interest at the Tonks-Langmuir boundary is the ion energy. In normalized form we write this energy as

$$U_0 = v_{10}^2 \quad . \tag{48}$$

In Table I the values of distance, s_0 ; potential, η_0 ; ion current, j_0 and energy, U_0 ; calculated using the above equations, are compared with the more accurate results of Self. It will be seen that for all three cases the value of s_0 at the edge of the plasma obtained by this method is in excellent agreement with the calculations of Self, as is the current density at the edge. Fortunately, these are the macroscopic parameters of the plasma which are usually measured in ion propulsion devices and Langmuir probes. The potential and ion energy at the edge of the plasma are not in such good agreement with the more exact theory.

(b) Cylindrical case

When we take $\beta = 1$ (cylindrical geometry) in Eqs. (29) and (30), only the case $\gamma = 0$ can be solved explicitly. Again, the Bohm Criteria is satisfied at the Tonks-Langmuir boundary for all three cases of ion generation $(\gamma = 0 , 1 , \text{and } 2)$. The equations for all three cases are given at the end of the chapter in Table IV. The results for $\gamma = 0$ are

$$s_r = \frac{\sqrt{e^{2\eta} - 1}}{e^{2\eta/3}} \tag{49}$$

and

$$s_r = \frac{2v_1}{(4v_1^2 + 1)^{3/4}} \quad . \tag{50}$$

TABLE I

COMPARISON OF PARAMETERS AT THE TONKS-LANGMUIR

BOUNDARY-PLANAR CASES

	$\gamma = 0$				$\gamma = 1$				$\gamma = 2$			
	η_0	s_0	j_0	U_0	η_0	s_0	j_0	U_0	η_0	s_0	j_0	U_0
Exact Values	0.854	0.344	0.344	0.675	0.854	0.405	0.344	0.675	0.854	0.492	0.344	0.675
Neglecting Pressure Term	0.693	0.354	0.354	0.500	0.693	0.403	0.354	0.500	0.693	0.471	0.354	0.500
Including Pressure Term	0.786	0.345	0.345	0.60	0.786	0.398	0.345	0.60	0.786	0.478	0.345	0.60

For $\gamma = 1$ and 2, the Runge-Kutta method was used on an IBM 7090 digital computer to obtain values of η and v_1 vs s_r. The results for all three cases are plotted in Figs. 5, 6, and 7. Again, the exact values are plotted for comparison. For these cylindrical cases, the values of η_0, s_0, j_0 and U_0 are compared with the more exact values in Table II. Although Self does not give the asymptotic values of the parameters for the case $\gamma = 2$, they are also included for completeness in Table II.

2. Including Kinetic Pressure Term

A more exact result is obtained if the kinetic pressure term is not neglected in the momentum transfer equation. We then make the assumption that

$$\nabla \cdot \vec{q} = 0 \quad ,$$

or that the heat flow is negligible. The equation of heat transfer in one dimension then becomes

$$v_1 \frac{d}{ds}\left(e^{-\eta}\langle u_1^2\rangle\right) + e^{-\eta}\frac{\langle u_1^2\rangle}{s^\beta}\frac{d(s^\beta v_1)}{ds} + 2e^{-\eta}\langle u_1^2\rangle\frac{dv_1}{ds} = gv_1^2 \quad , \tag{51}$$

where we have used the normalization of Eqs. (31), (32), and (33) together with the normalization

$$\langle u_1^2\rangle = \frac{M}{2kT_e}\langle u^2\rangle \quad . \tag{52}$$

The equation of continuity is unchanged. However, the momentum transfer equation now has the added kinetic pressure term and becomes

$$\frac{1}{s^\beta}\frac{d}{ds}\left(s^\beta e^{-\eta} v_1^2\right) + \frac{1}{s^\beta}\frac{d}{ds}\left(s^\beta s^{-\eta}\langle u_1^2\rangle\right) = \frac{1}{2}\frac{d\eta}{ds} \quad . \tag{53}$$

TABLE II

COMPARISON OF PARAMETERS AT THE TONKS-LANGMUIR

BOUNDARY-CYLINDRICAL CASES

	$\gamma = 0$				$\gamma = 1$				$\gamma = 2$			
	η_0	s_0	j_0	U_0	η_0	s_0	j_0	U_0	η_0	s_0	j_0	U_0
Exact Values	1.056	0.583	0.291	0.730	1.155	0.772	0.270	0.772	___	___	___	___
Neglecting Pressure Term	0.822	0.620	0.310	0.50	0.840	0.784	0.304	0.50	1.18	0.967	0.267	0.50
Including Pressure Term	0.975	0.586	0.292	0.643	1.062	0.771	0.272	0.665	1.295	1.335	0.225	0.751

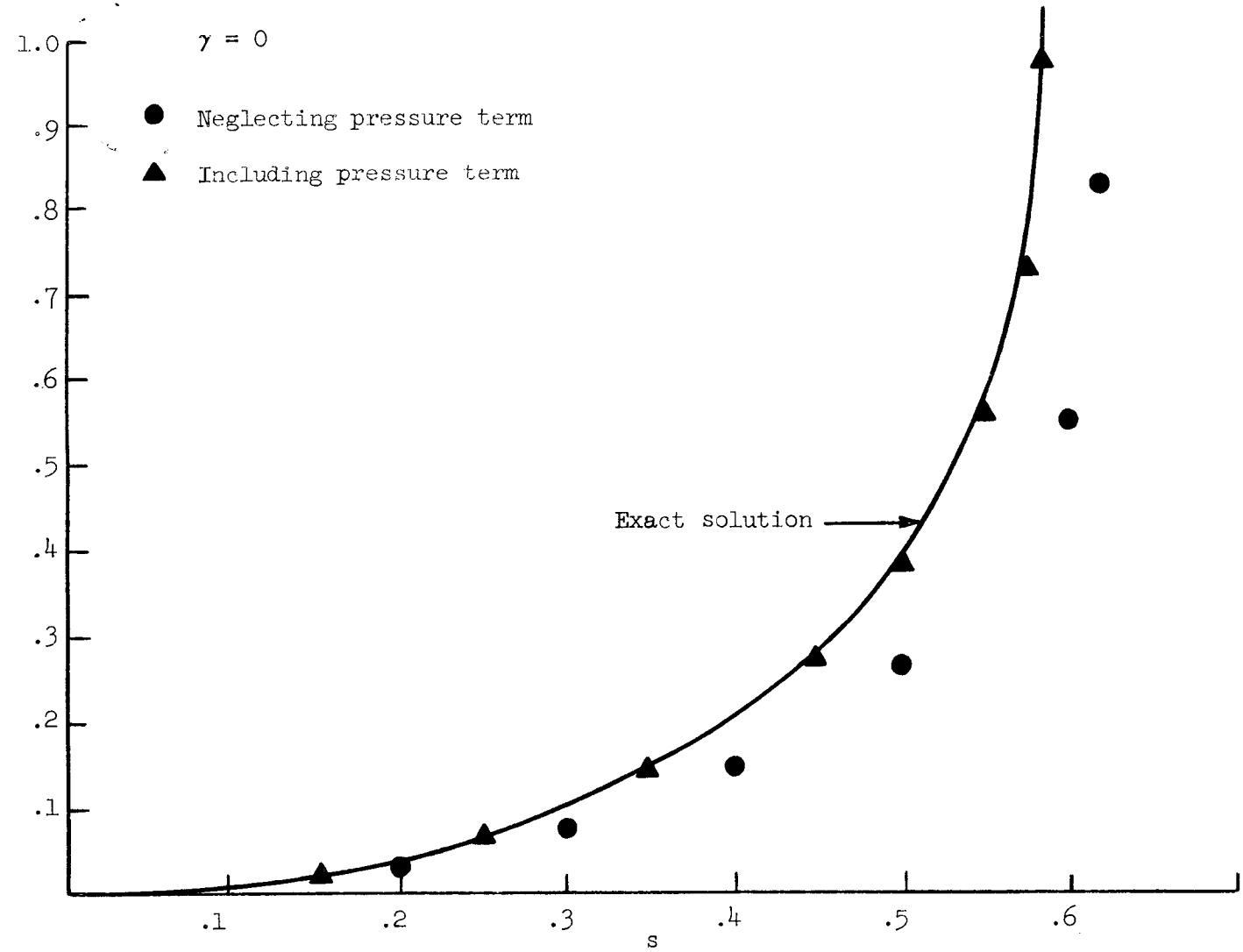

FIG. 5--Normalized potential as a function of position in the cylindrical discharge ($\gamma = 0$) .

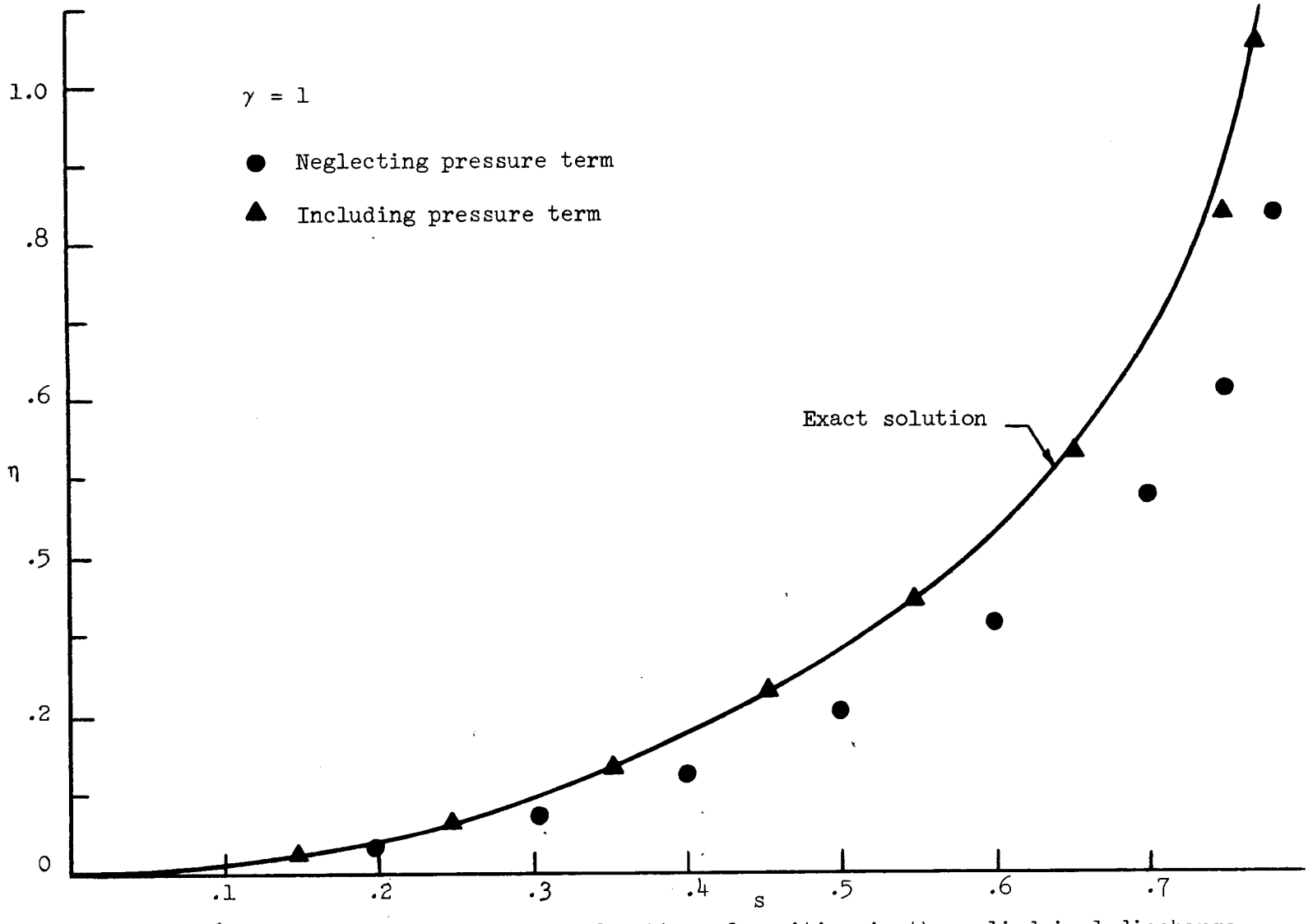

FIG. 6--Normalized potential as a function of position in the cylindrical discharge ($\gamma = 1$).

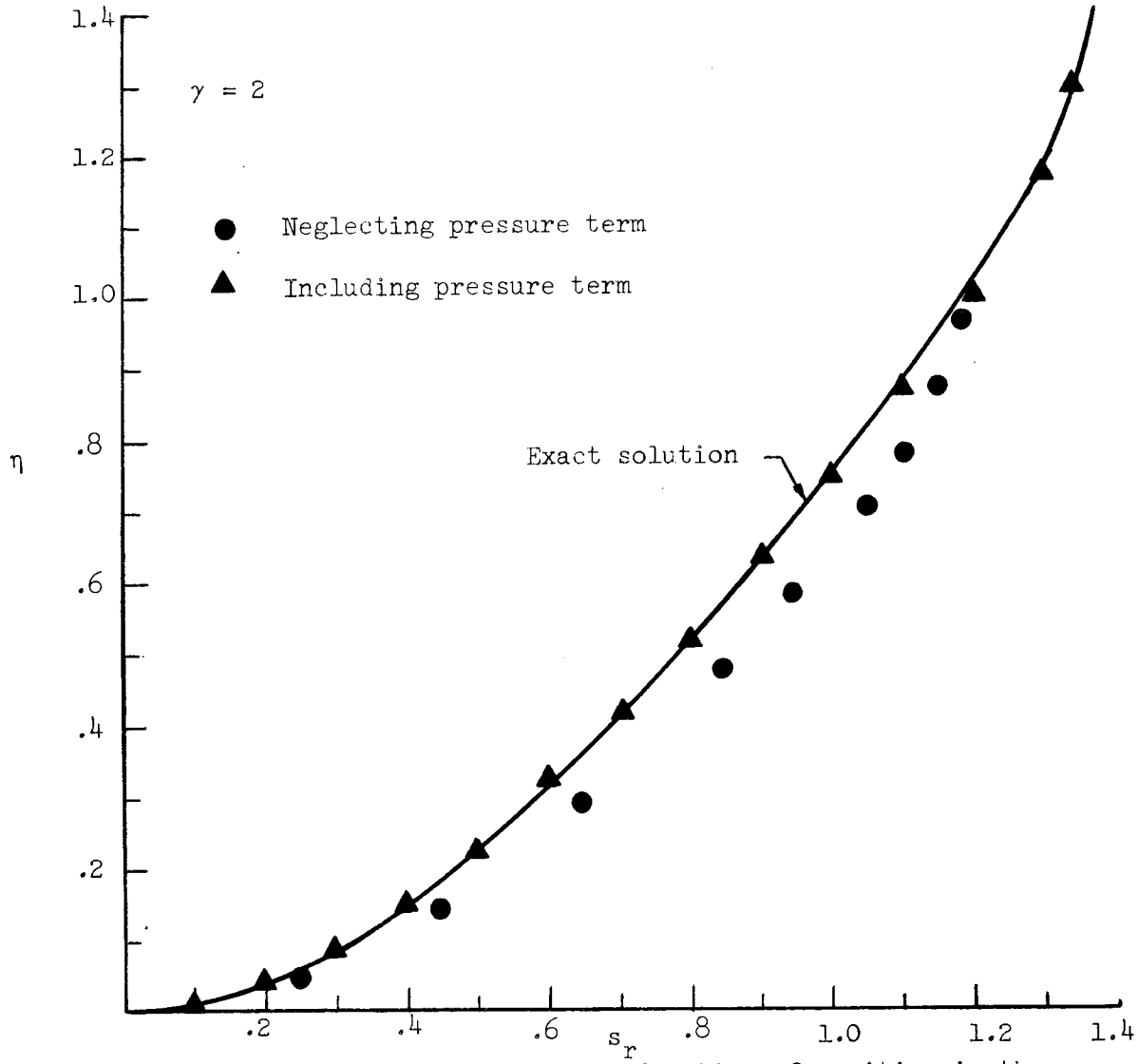

FIG. 7--Normalized potential as a function of position in the cylindrical discharge ($\gamma = 2$).

(a) Planar Case ($\beta = 0$)

For this case the momentum transfer equation becomes

$$\frac{d}{ds}\left(v_1^2 + \langle u_1^2\rangle\right) - \left(v_1^2 + \langle u_1^2\rangle\right)\frac{d\eta}{ds} = \frac{1}{2}\frac{d\eta}{ds} \quad , \qquad (54)$$

with the solution

$$v_1^2 + \langle u_1^2\rangle = \frac{1}{2}\left(e^{\eta} - 1\right) \quad . \qquad (55)$$

Using this result to eliminate $\langle u_1^2\rangle$ from Eq. (51), and after some rearrangement, we obtain the equation

$$\frac{d}{dU}\left(e^{-\eta}\, U^{3/2}\right) = \frac{3}{2}\frac{U^{1/2}}{(4U + 1)} \quad , \qquad (56)$$

where $U = v_1^2$. Since Eq. (56) does not depend upon either s or $\langle u^2\rangle$, we again see that the value of potential at the edge of the plasma is independent of the generation term g . Integrating Eq. (56), we obtain

$$e^{-\eta}\, v_1^3 = \frac{3}{4}\left(v_1 - \frac{1}{2}\tan^{-1} 2v_1\right) \quad . \qquad (57)$$

Equation (57), together with the equation of continuity, can be solved to give an explicit relationship between η and s only for the case $\gamma = 0$. The result is

$$e^{2\eta}\, s^3 = \frac{3}{4}\left(s\, e^{\eta} - \frac{1}{2}\tan^{-1} 2se^{\eta}\right) \quad . \qquad (58)$$

For $\gamma = 1$ and $\gamma = 2$, the Runge-Kutta method programmed for the IBM 7090 digital computer was again used to obtain the solutions. The results, which show excellent agreement with the more exact theory, are plotted in Figs. 2, 3 and 4, and tablulated in Table I. It will be seen that the values of J_0 and s_0 agree very closely with the values obtained by Self. The values of "wall" potential (η_0) and ion energy (U_0) also agree more closely with the exact values. The normalized wall

potential is 0.786 compared to the exact value of 0.854 and to the value of 0.693 calculated neglecting kinetic pressure. The ion energy is 0.60 compared to the exact value of 0.675 and to the value of 0.50 calculated neglecting the kinetic pressure term.

The Bohm Criteria that the normalized average velocity is given by $1/\sqrt{2}$ at the boundary is no longer satisfied. The velocity is greater than $1/\sqrt{2}$, thus resulting in the more exact value of ion energy. It is interesting to note, as we will see later, that the Bohm Criteria is satisfied for all the cases where we neglect the kinetic pressure term, including those of a magnetic field and collisions, but is not satisfied for cases with the kinetic pressure included.

(b) Cylindrical Case ($\beta = 1$)

For the one-dimensional cylindrical cases with kinetic pressure included, it is necessary to use numerical methods on all three cases ($\gamma = 0$, 1, and 2). Again, including the kinetic pressure term improves the accuracy of the results. The potential vs distance for this higher order approximation is also plotted in Figs. 5, 6, and 7. The values of potential, distance, energy, and ion current density at the boundary are given in Table II. The equations for the cylindrical discharge are tabulated at the end of this chapter.

B. COAXIAL SOLUTIONS

Langmuir tried to determine the solution for the one-dimensional collisionless coaxial discharge in 1929 using the exact integral formulation.[10] However, he was unable to solve the integral equation due to convergence problems in the assumed series solution. Later Self,[40] using the same general approach, found that the series solution assumed by Langmuir was not uniformly convergent. Fortunately, the macroscopic approach used in this work leads to meaningful differential equations with convergent solutions. As mentioned at the beginning of this chapter, not only is the coaxial discharge of interest because of its possible application to coaxial type discharges but it also has direct application to the analysis of cylindrical probes.

Below, we find solutions for the coaxial discharge under several conditions. First, neglecting the kinetic pressure term, we solve the collisionless, "free-fall" case and then proceed to solve the more complex cases including collisions and a magnetic field. We then solve the collisionless coaxial discharge including the kinetic pressure term.

Finally, we relate the coaxial solutions to probe theory and discuss the usefulness of the results in probe theory calculations.

1. Neglecting Kinetic Pressure

(a) "Free-fall case.

The normalized equations governing this discharge follow immediately from Eq. (29) and Eq. (30) since the operators in cylindrical and coaxial geometry are the same. Thus, for the ions we have

$$\frac{1}{s_r}\frac{d}{ds}\left(s_r e^{-\eta} v_1\right) = g \qquad (59)$$

and

$$\frac{1}{s_r}\frac{d}{ds_r}\left(s_r e^{-\eta} v_1^2\right) = \frac{1}{2} e^{-\eta}\frac{d\eta}{ds_r} \quad , \qquad (60)$$

where $g = 1$, $e^{-\eta}$, or $e^{-2\eta}$ depending on the type of generation. We are again assuming that

$$n_e = n_i = n_{e0} e^{-\eta} \quad . \qquad (61)$$

For the case $\gamma = 0$, $g = 1$ Eq. (59) can be integrated immediately to give

$$s_r e^{-\eta} v_1 = \frac{s_r^2}{2} + c \quad . \qquad (62)$$

For coaxial geometry we suppose that at some distance, $s_r = s_m$ say the normalized potential, η , goes through a minimum with

$$\frac{\partial \eta}{\partial s_r}(s_m) = 0 \quad ,$$

$$v_1(s_m) = 0 \quad ,$$

and

$$\eta\ (s_m) = 0 \quad .$$

Physically, what this means is that we are assuming a sheath forms at both the inner and outer "walls" of the coaxial system, that a potential maximum occurs between the inner and other "walls," and that the ions thus fall in the self consistent electric field toward the walls. Ions created at a position of s greater than s_m fall to the outer wall and ions created at a position of s less than s_m fall to the inner wall.

In order to satisfy the initial conditions, we see that the constant in Eq. (62) must be equal to $-s_m^2/2$, thus

$$\eta = \ell n \left[\frac{2s_r\ v}{s_r^2 - s_m^2} \right] \quad . \tag{63}$$

This is about as far as we can go with the solution without using numerical methods. For computation purposes we rearrange the equations in the following forms:

$$\left(v_1^2 - \frac{1}{2} \right) \frac{d\eta}{ds_r} = \frac{v_1^2}{s_r} - 2v_1\ e^{(1-\gamma)\eta} \tag{64}$$

and

$$\left(v_1^2 - \frac{1}{2} \right) \frac{dv_1}{ds} = \frac{v_1}{2s_r} - \left(v_1^2 + \frac{1}{2} \right) e^{(1-\gamma)\eta} \quad . \tag{65}$$

The results of solving Eqs. (64) and (65) for various values of inner to outer radii are shown in Figs. 8 through 11. Both the normalized ion density and potential are plotted as a function of position in the discharge region. Only the most important case of generation proportional to electron density is plotted since we will find more accurate solutions for the other cases $(\gamma = 0,2)$ in part 2. However, the other cases may be found from the equations given in Table IV. The ion current at the boundary can be found from a knowledge of either the density or the potential since the normalized velocity is always equal to $1/\sqrt{2}$ at the

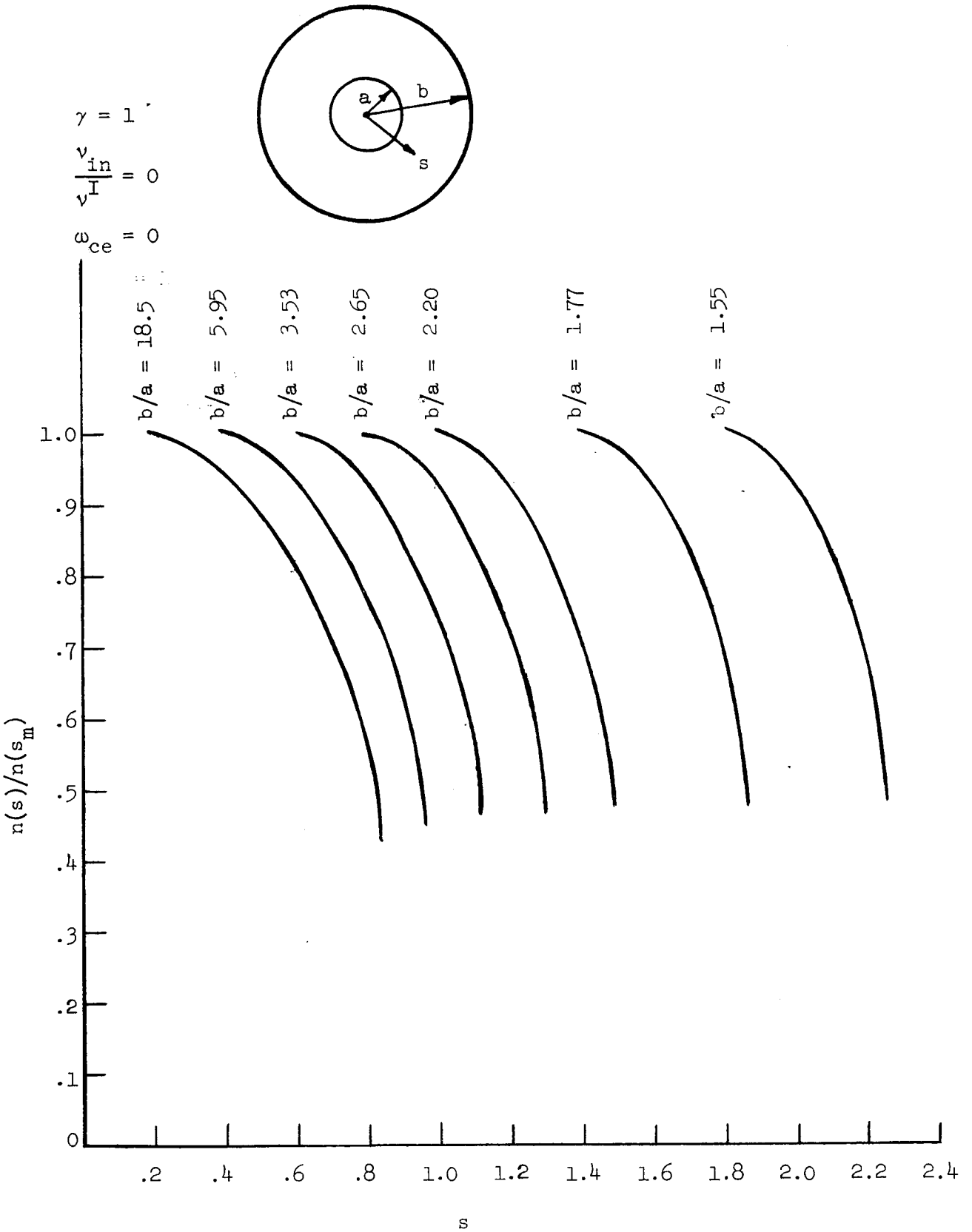

FIG. 8--Normalized ion density as a function of position in the coaxial discharge without collisions or a magnetic field.

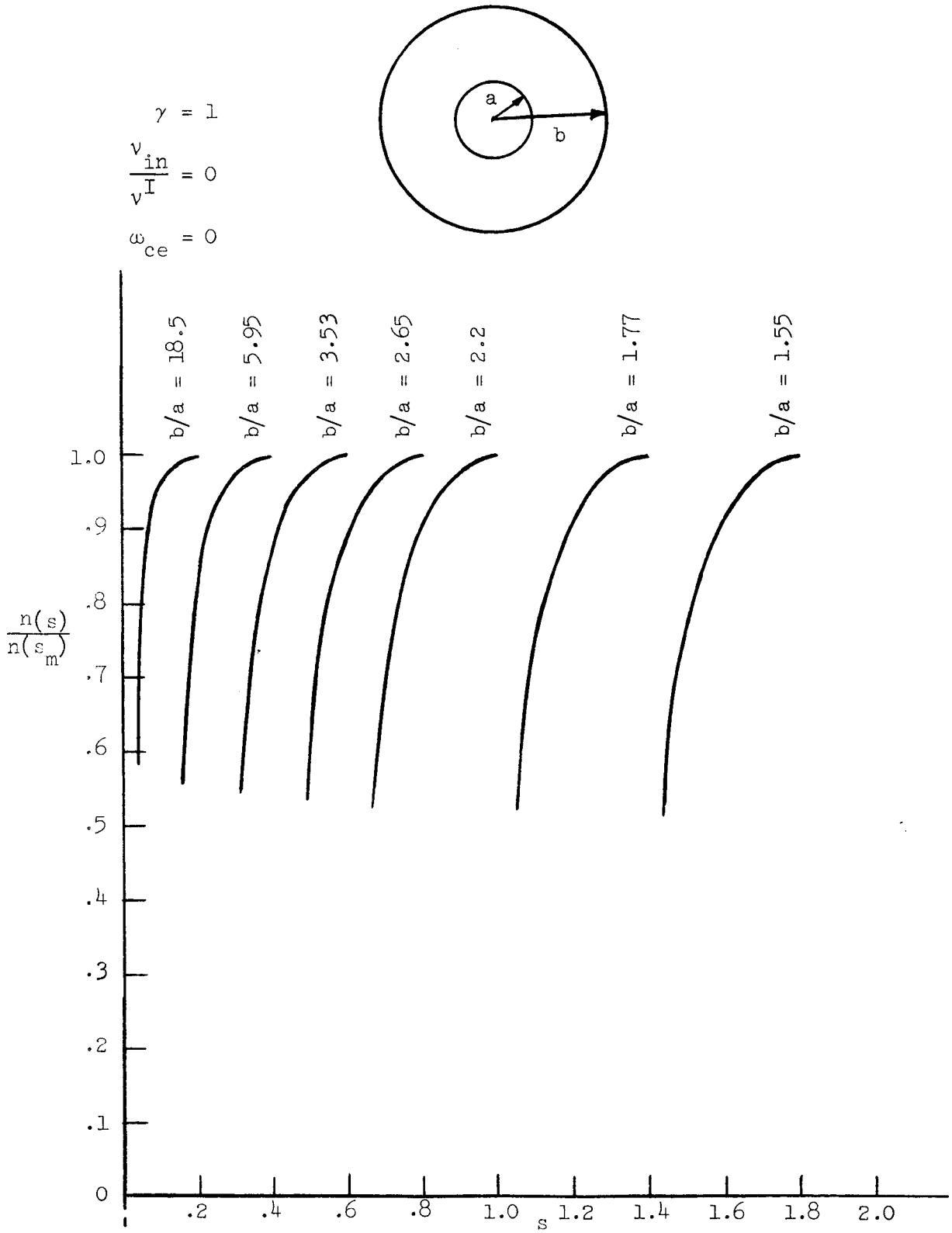

FIG. 9--Normalized ion density as a function of position in the coaxial discharge without collisions or a magnetic field

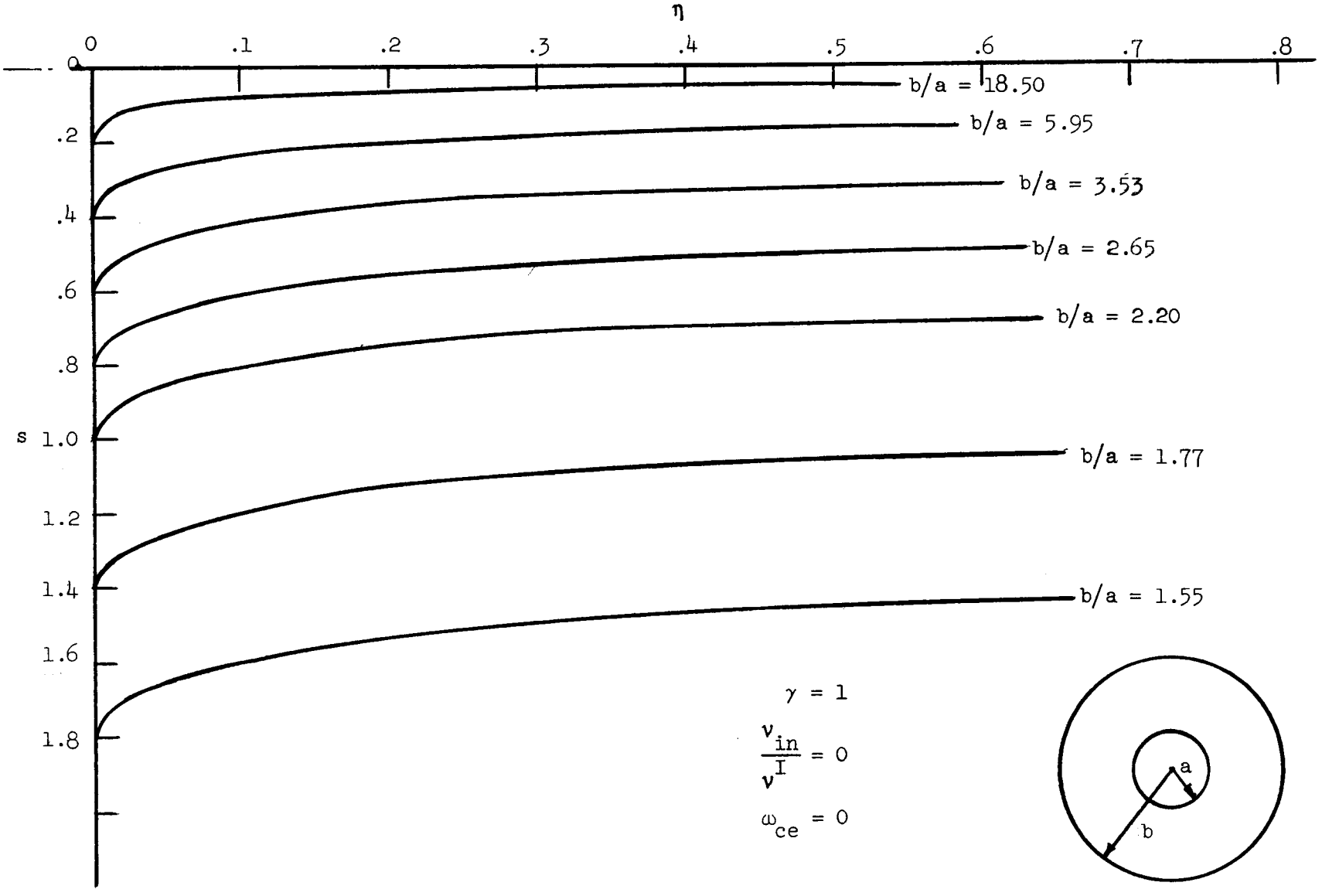

FIG. 10--Normalized potential as a function of position in the coaxial discharge without collisions or a magnetic field.

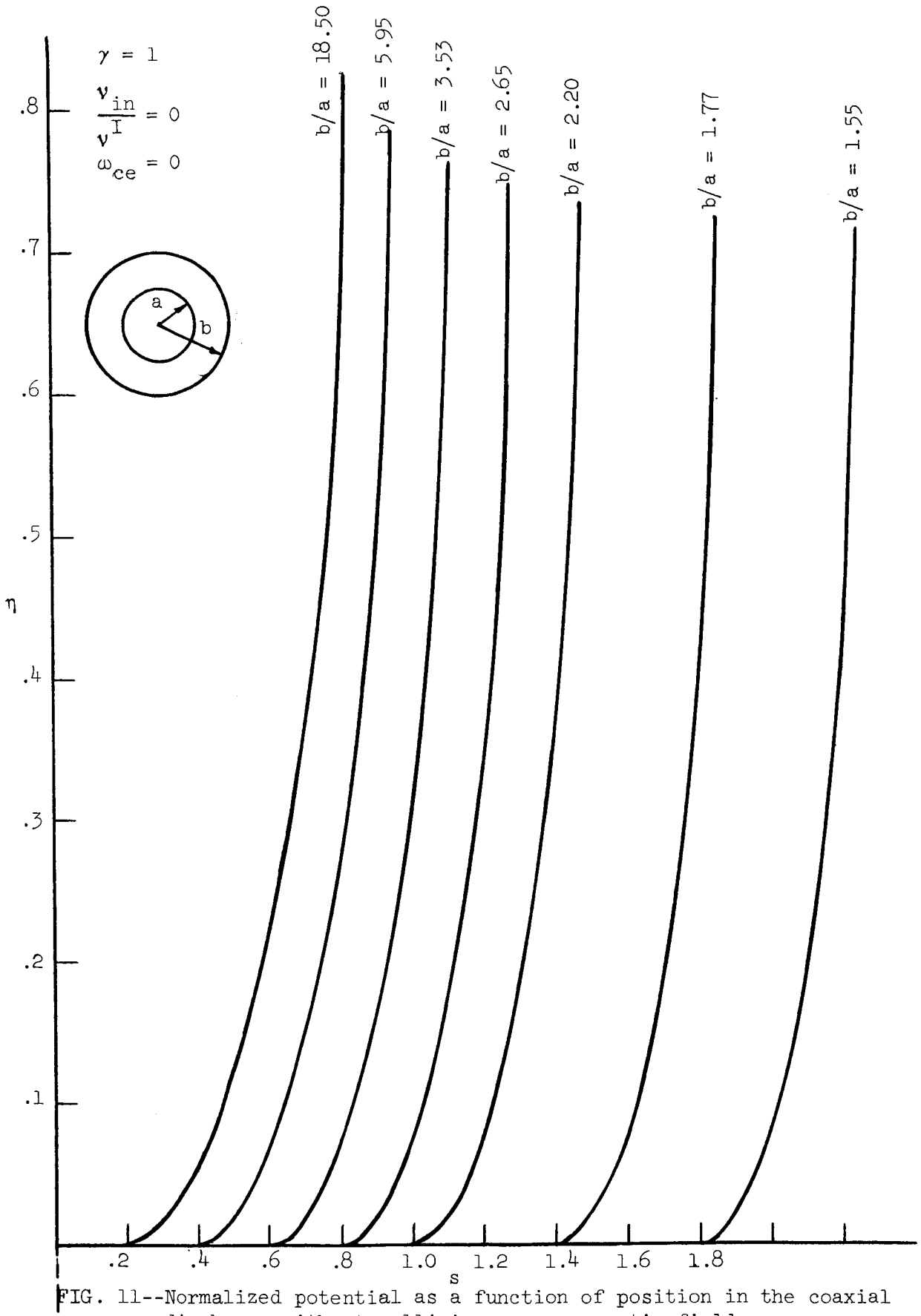

FIG. 11--Normalized potential as a function of position in the coaxial discharge without collisions or a magnetic field.

boundary and the potential and density are related by

$$n/n_{e0} = e^{-\eta}$$

For the normalized current we thus obtain

$$j_0 = n/n_{e0}\, v_1 = 0.707e^{-\eta} \quad .$$

We note that the potentials (and therefore the densities) at the inner and outer walls are approaching the limiting case of a planar discharge as the ratio of inner to outer radii approaches unity. For the case of outer to inner radii ratio equal to 1.55 we see that the two curves of Fig. 10 and Fig. 11 which apply to this case are nearly symmetrical, with potentials at the wall of 0.660 for the inner "wall" and 0.715 for the outer wall. Both of these values are near the limiting value for a planar discharge of 0.693 and we would expect that any discharge with a ratio of inner to outer radii of less than approximately 1.5:1 could be reasonably represented by a planar discharge. It is also of interest to compare the normalized wall distance in the case of a planar discharge and the one discussed above. From Table I, for a planar discharge with $\gamma = 1$, the normalized wall distance is 0.354 while for the case of $b/a = 1.55$ the wall distances are 0.36 and 0.44 for the outer and inner walls, respectively.

As the radius of the inner conductor becomes smaller and smaller we would expect the potential and density in the discharge to approach that of a cylindrical discharge except for points very near the center. For a cylindrical discharge the potential at the wall for this case is (from Table II) $\eta = 0.840$ and the normalized wall distance is 0.784. Looking at Fig. 11 for the case of a ratio of outer to inner radii of 18.5:1 we see that the potential at the wall is 0.850 while the wall distance is 0.830. Both of these values differ from the cylindrical case by less than 10%. All the curves of Figs. 8 through 11 thus are useful in estimating the error one would obtain in assuming the limiting cases.

(b) Including collisions and a longitudinal magnetic field

When a magnetic field is applied transverse to the direction of motion of the ions and electrons as shown in Fig. 12, the electrons no longer have the Boltzmann distribution of density given by Eq. (12). This is because the application of a small magnetic field causes the electrons to cycloid such that the collision and magnetic field terms in Eq. (27) begin to dominate the equation and the approximation to Eq. (20)

$$\frac{kT_e}{m}\frac{\nabla n}{n} = \frac{e}{m}\nabla\Phi$$

is no longer valid. We must therefore use macroscopic equations of motion for the electrons as well as the ions.

Assuming a uniform magnetic field, B_z, in the z-direction, the equations of continuity and momentum transfer for the electrons are, respectively,

$$\nabla \cdot (n_e \vec{v}_e) = G \tag{66}$$

and

$$(n_e(\vec{v}_e \cdot \nabla v_e) + G\,\vec{v}_e = -\frac{e}{m} n_e(\vec{E} + \vec{v}_e \times B_z) - \nu_{en}\, n_e\, \vec{v}_e - \frac{kT_e}{m}\nabla n_e \quad , \tag{67}$$

where ν_{en} s the electron-neutral collision frequency, k is Boltzmann's constant, and T_e is the electron temperature. In the above equations we have assumed that the electron temperature is constant throughout the discharge. We know that the average electron velocity is small compared to the random velocity and we thus neglect second order terms in the average velocity in Eq. (67). Writing Eq. (67) in component form for the radial direction, we have

$$v_{er}(\nu^I n_e^{\gamma-1} + \nu_{en}) + \frac{kT_e}{m}\frac{\partial U_e}{\partial r} = \frac{e}{m}\frac{\partial \Phi}{\partial r} + \frac{e}{m} v_{e\theta} B_z \quad , \tag{68}$$

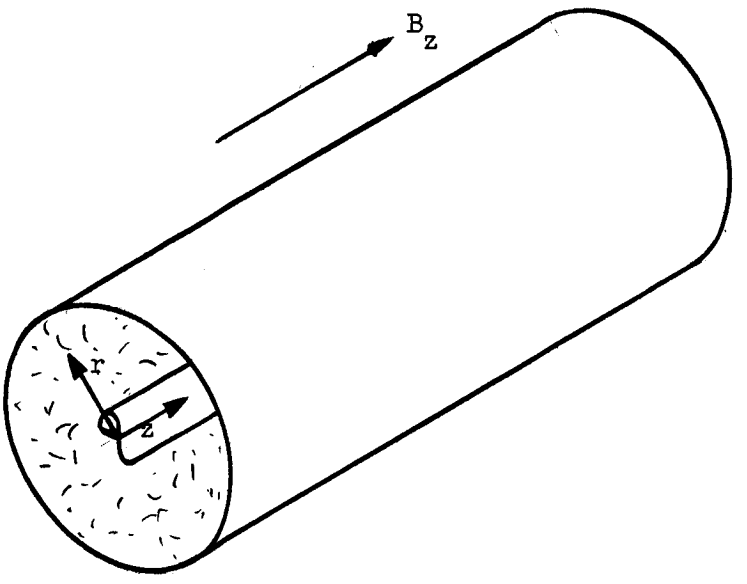

FIG. 12--One-dimensional coaxial discharge with an applied magnetic field.

where v_{er} and $v_{e\theta}$ are the electron velocity in the r and θ directions, respectively, and $U_e = \ell n\, n_e/n_{e0}$

In the θ direction we find that

$$v_{e\theta}(\nu^I n_e^{\gamma-1} + \nu_{en}) = -\frac{e}{m}(v_{er} B_z) \quad . \tag{69}$$

Using Eq. (69) in Eq. (68) to eliminate $v_{e\theta}$ and using the standard normalizations of Eqs. (31), (32), and (33) we obtain the result

$$v_{el}\left[n_e^{(\gamma-1)} + \frac{\nu_{en}}{\nu^I} + \frac{\omega_{ce}^2}{\nu^I(\nu^I n_e^{\gamma-1} + \nu_{en})}\right] - \frac{1}{2} R_m \frac{\partial U_1}{\partial s_r} = -\frac{1}{2} R_m \frac{\partial \eta}{\partial s_r} \quad , \tag{70}$$

where

$$U_1 = -\ln(n/n_{e0}) \tag{71}$$

$$R_m = \frac{M}{m} \quad . \tag{71}$$

Since we assume that $n_i \approx n_e$ everywhere in the discharge and since

$$\nabla \cdot (n_e \vec{v}_e) = \nabla \cdot (n_i \vec{v}_i) = G \quad ,$$

the radial velocity components of the ions and the electrons must also be equal so that

$$v_{er} = v_{ir} = v_r \quad .$$

We therefore drop the subscripts e and i on both the velocity and density terms.

Only the case of small magnetic fields, i.e., magnetic fields for which the ion cyclotron radii are much greater than the radius of the discharge, will be considered. For this low magnetic field case, the normalized equations for the ions are uneffected by the magnetic field

and thus are given by

$$v_1 \frac{\partial v_1}{\partial s_r} + v_1 \left(n^{\gamma-1} + \frac{\nu_{in}}{\nu^I} \right) = \frac{1}{2} \frac{\partial \eta}{\partial s_r} \tag{72}$$

and

$$\frac{\partial v_1}{\partial s_r} - v_1 \frac{\partial U_1}{\partial s_r} = n^{\gamma-1} \quad . \tag{73}$$

Only the most interesting case of ion generation directly proportional to electron density will be treated in detail. However, Eq. (66), (70), (72), and (73) form a closed set of equations in the unknowns η , v_1 , n , and U_1 which can be easily solved by standard numerical methods for any value of γ .

For $\gamma = 1$, we thus want to solve the following three equations:

$$v_1 \frac{\partial v_1}{\partial s_r} + v_1 \left(1 + \frac{\nu_{in}}{\nu^I} \right) = \frac{1}{2} \frac{\partial \eta}{\partial s_r} \tag{74}$$

$$\frac{\partial v_1}{\partial s_r} - v_1 \frac{\partial U_1}{\partial s_r} = 1 \tag{75}$$

and

$$\left(\frac{\nu_{en}^2 + \omega_{ce}^2}{\nu_{en} \nu^I} \right) v_1 = \frac{1}{2} Rm \left(\frac{\partial U_1}{\partial s_r} - \frac{\partial \eta}{\partial s_r} \right) \quad , \tag{76}$$

where we have used the condition that

$$\nu_{en} \gg \nu^I$$

for all cases of interest.

It is now convenient to define two parameters, A and B , to be

$$A = \frac{\nu_{en}^2 + \omega_{ce}^2}{\nu_{en} \nu^I} \tag{77}$$

and

$$B = 1 + \frac{\nu_{in}}{\nu_I} \quad . \tag{78}$$

In order to be able to use the Runge-Kutta procedure of solving a system of nonlinear equations, it is necessary to have Eqs. (74), (75), and (76) in the form

$$\frac{dF_1}{ds} = f(F_1, F_2, \ldots F_n) \tag{79}$$

$$\vdots$$

$$\frac{dF_n}{ds} = f_n(F_1, F_2, \ldots F_n) \quad . \tag{80}$$

The final equations which are solved are thus

$$\frac{dv_1}{ds_r} = \left[- v_1^2 \left(\frac{A}{Rm} + B \right) + \frac{1}{2} \frac{v_1}{s_r} - \frac{1}{2} \right] \Bigg/ \left(v_1^2 - \frac{1}{2} \right) \tag{81}$$

$$\frac{dU_1}{ds_r} = \left[- \left(1 + B + \frac{A}{Rm} \right) v_1 + \frac{v_1^2}{s_r} \right] \Bigg/ \left(v_1^2 - \frac{1}{2} \right) \tag{82}$$

and

$$\frac{d\eta}{ds_r} = \left[- (1 + B) v_1 + \frac{v_1^2}{s_r} - \frac{2 v_1^2 A}{Rm} \right] \Bigg/ \left(v_1^2 - \frac{1}{2} \right) \quad . \tag{83}$$

Figures 13 and 14 show the normalized density as a function of radial position in the discharge for various values of inner to outer radii and for two different values of the parameter B, which is a measure of the ratio of ion-neutral to ionization frequencies.

Plotted in Figs. 15 and 16 are the densities and potentials at the inner and outer "walls" of the coaxial discharge as a function of inner to outer radii, b/a, for three different values of collision frequency.

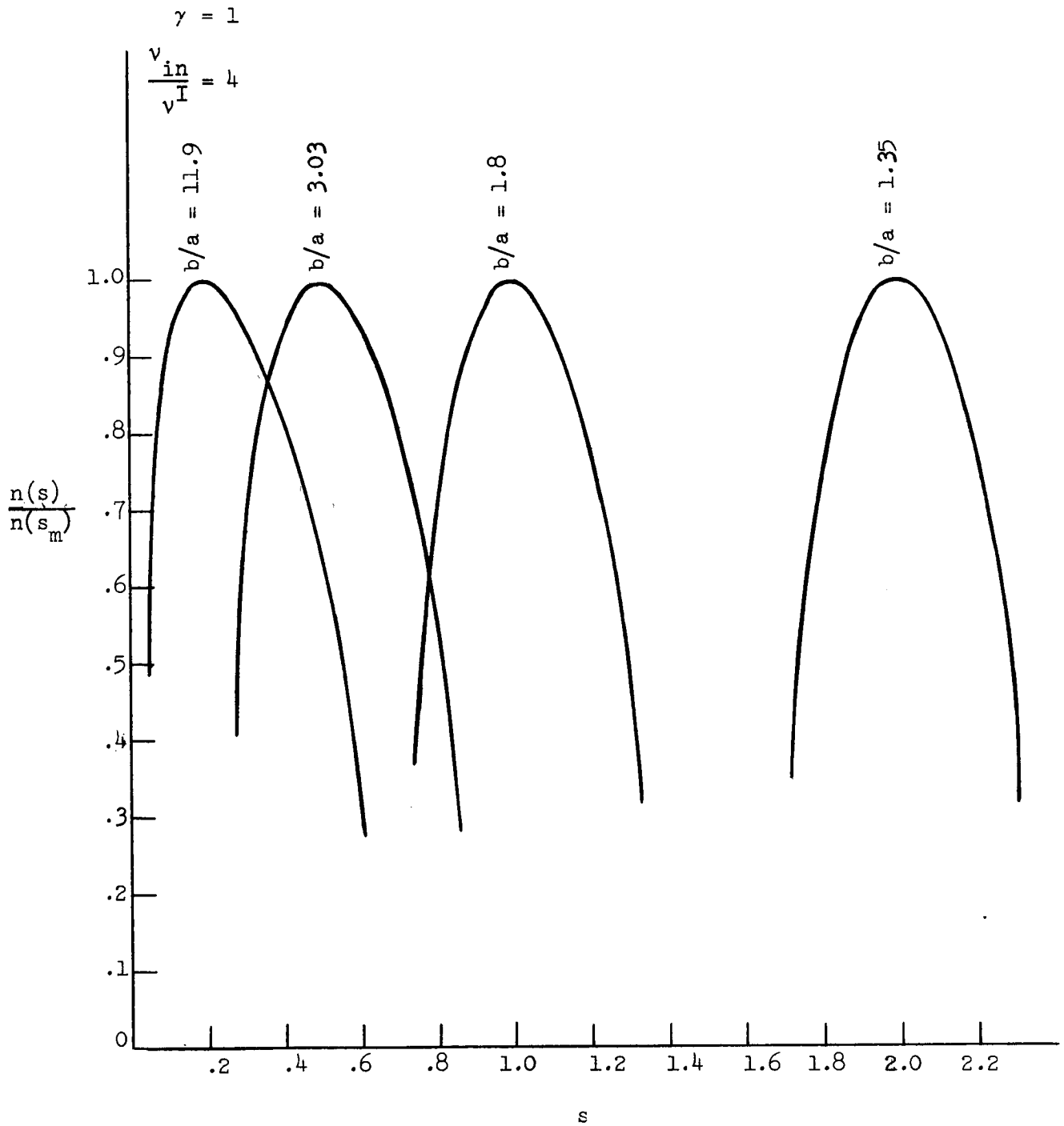

FIG. 13--Normalized ion density as a function of position in the coaxial discharge with collisions.

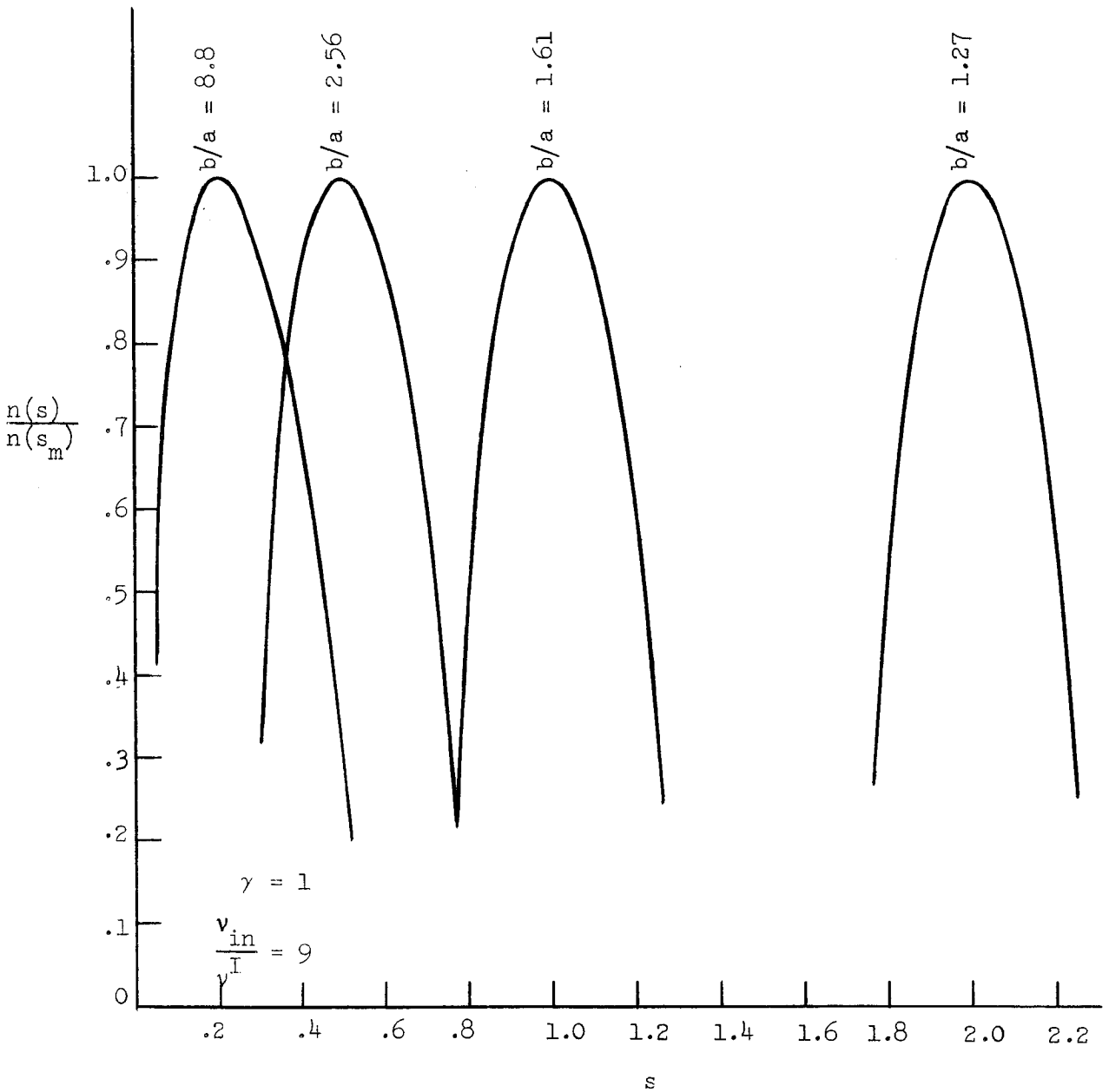

FIG. 14--Normalized ion density as a function of position in the coaxial discharge with collisions.

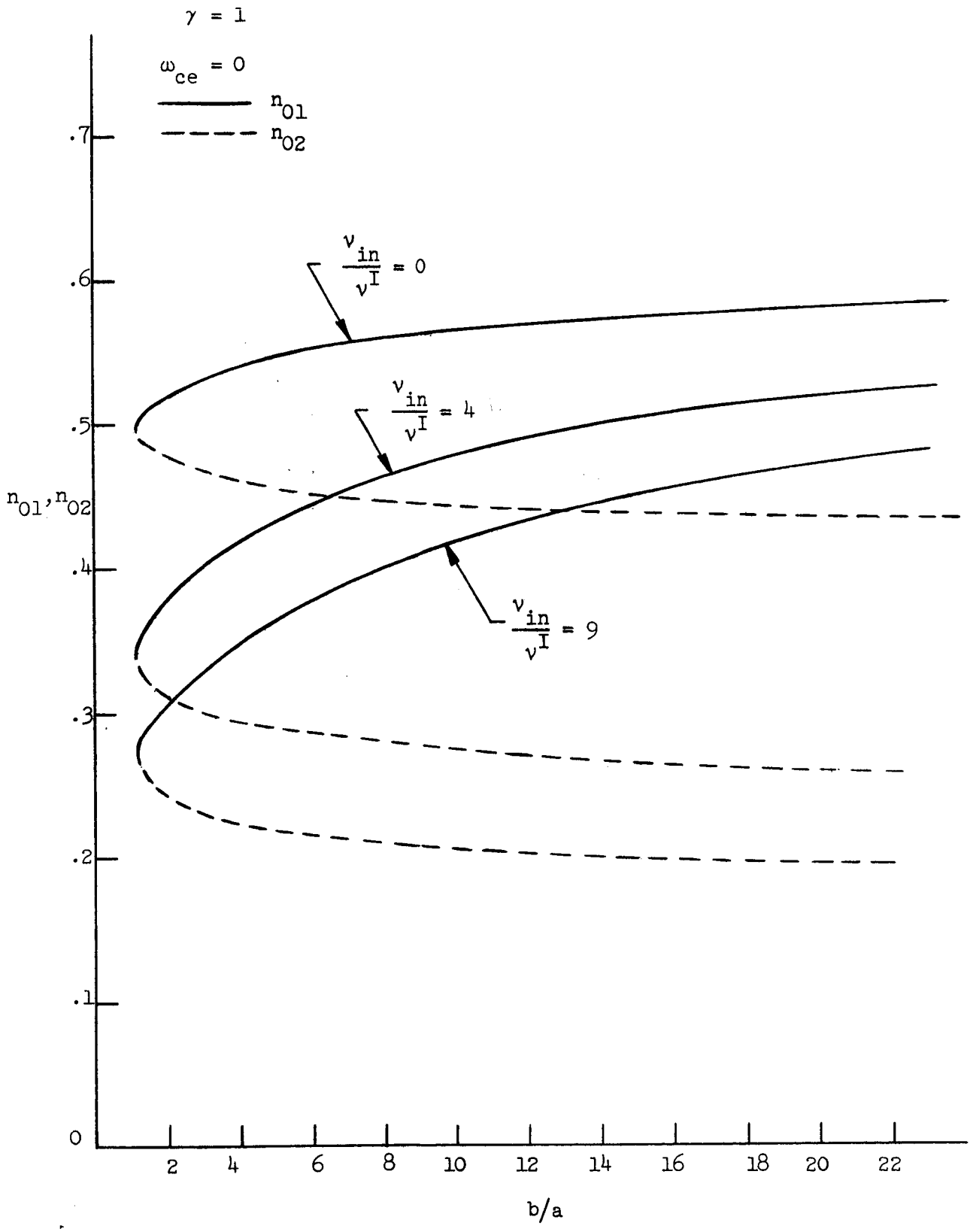

FIG. 15--Normalized "wall" density in the coaxial discharge with collisions as a function of the ratio of outer to inner wall radii.

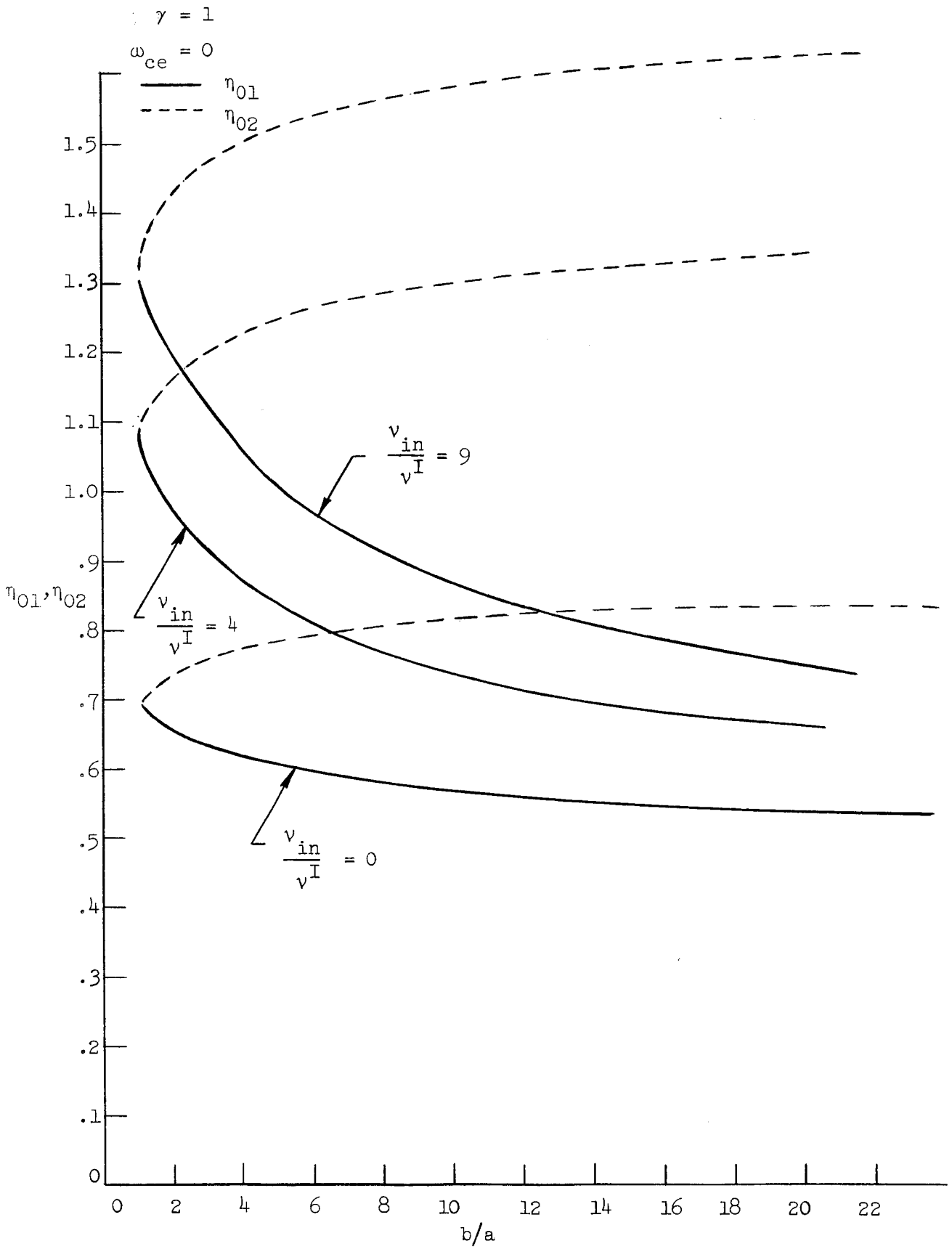

FIG. 16--Normalized "wall" potential in the coaxial discharge as a function of the ratio of outer to inner wall radii.

As expected, for a given b/a, a higher collision frequency results in a lower value of density. This is due to the fact that the rate of ion loss to the walls is reduced when ion-neutral collisions are occurring.

The effect of a magnetic field and a magnetic field plus collisions are shwon in Figs. 17, 18, and 19. Notice that the magnetic field has much the same effect on the "wall" ion density as ion neutral collisions.

More will be said about these results in the discussion of probe theory which follows the next section.

2. Including Kinetic Pressure Term

When we include the kinetic pressure term, $\nabla \cdot \overleftrightarrow{\psi}$, in the equations of the collisionless coaxial discharge more accurate solutions are obtained. These more accurate equations follow immediately from Eqs. (34), (51), and (53) for the cylindrical discharge. Again for purposes of computation, we put Eqs. (34), (51), and (53) in the form of Eq. (79) and obtain

$$\frac{dv_1}{ds_r} = \left[\frac{v_1}{2s_r} - \left(\frac{1}{2} + 2v_1^2\right)e^{(1-\gamma)\eta}\right] \Bigg/ \left(v_1^2 - \frac{1}{2} - 3\overline{u_1^2}\right) \tag{84}$$

$$\frac{d\eta}{ds_r} = \left[\frac{v_1^2}{s_r} - \frac{3\overline{u_1^2}}{s_r} + 3\left(\overline{u_1^2}/v_1 + v_1\right)e^{(1-\gamma)}\right] \Bigg/ \left(v_1^2 - \frac{1}{2} - \overline{u_1^2}\right) \tag{85}$$

and

$$\frac{\partial \overline{u_1^2}}{\partial s_r} = \left[-\frac{\overline{u_1^2}}{s_r} + \left(\frac{3\overline{u_1^2}}{2v_1} + \frac{3(\overline{u_1^2})^2}{v_1} + v_1^3 - \frac{v_1}{2}\right)e^{(1-\gamma)\eta}\right] \Bigg/ \left(v_1^2 - \frac{1}{2} - 3\overline{u_1^2}\right). \tag{86}$$

The above equations were solved by again using the Runge-Kutta procedure starting the solutions off with a Taylor series expansion of each of the above equations about the point $s = s_m$. Figure 20, 21, and 22

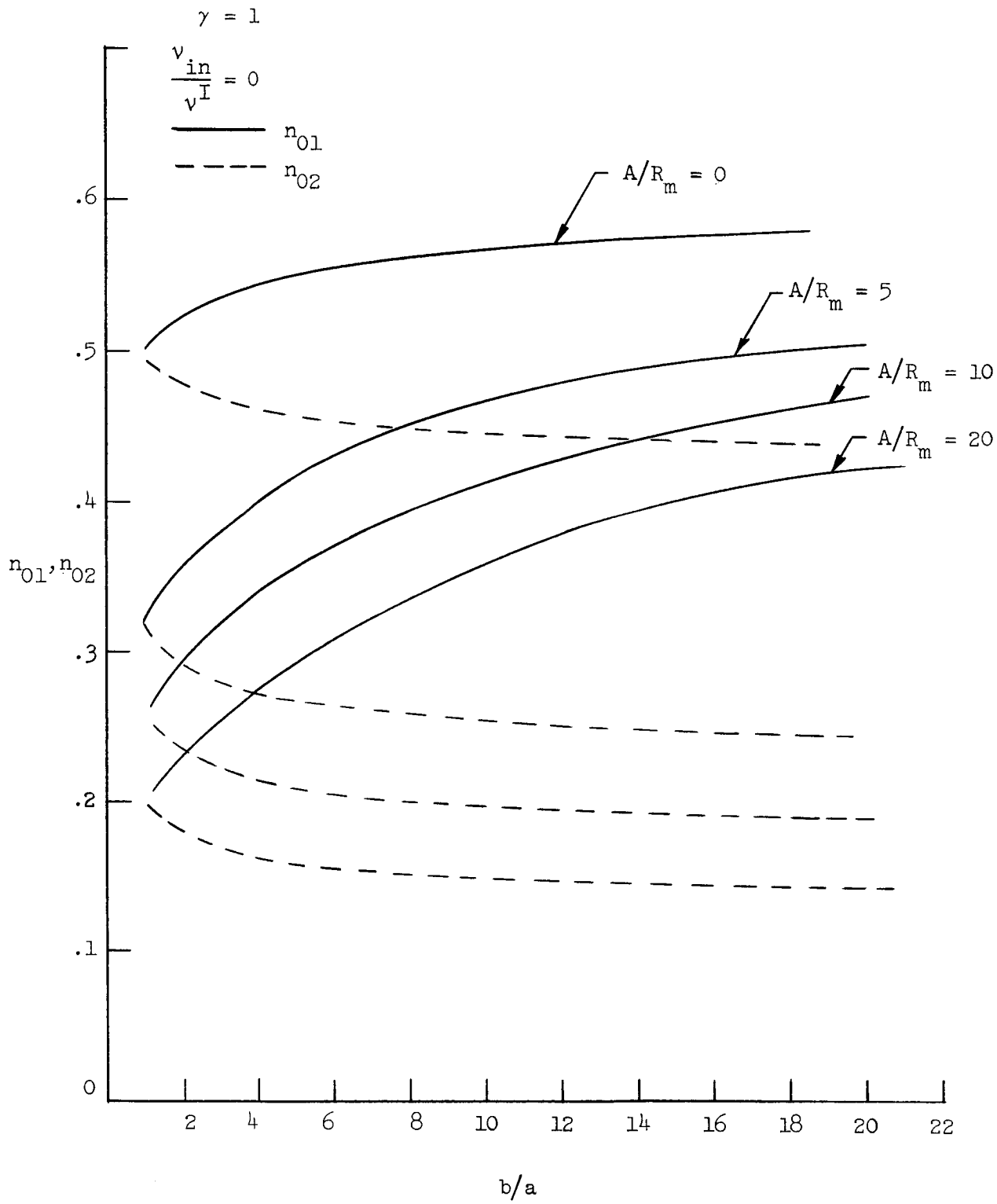

FIG. 17--Normalized "wall" density in the coaxial discharge with a magnetic field as a function of the ratio of outer to inner wall radii.

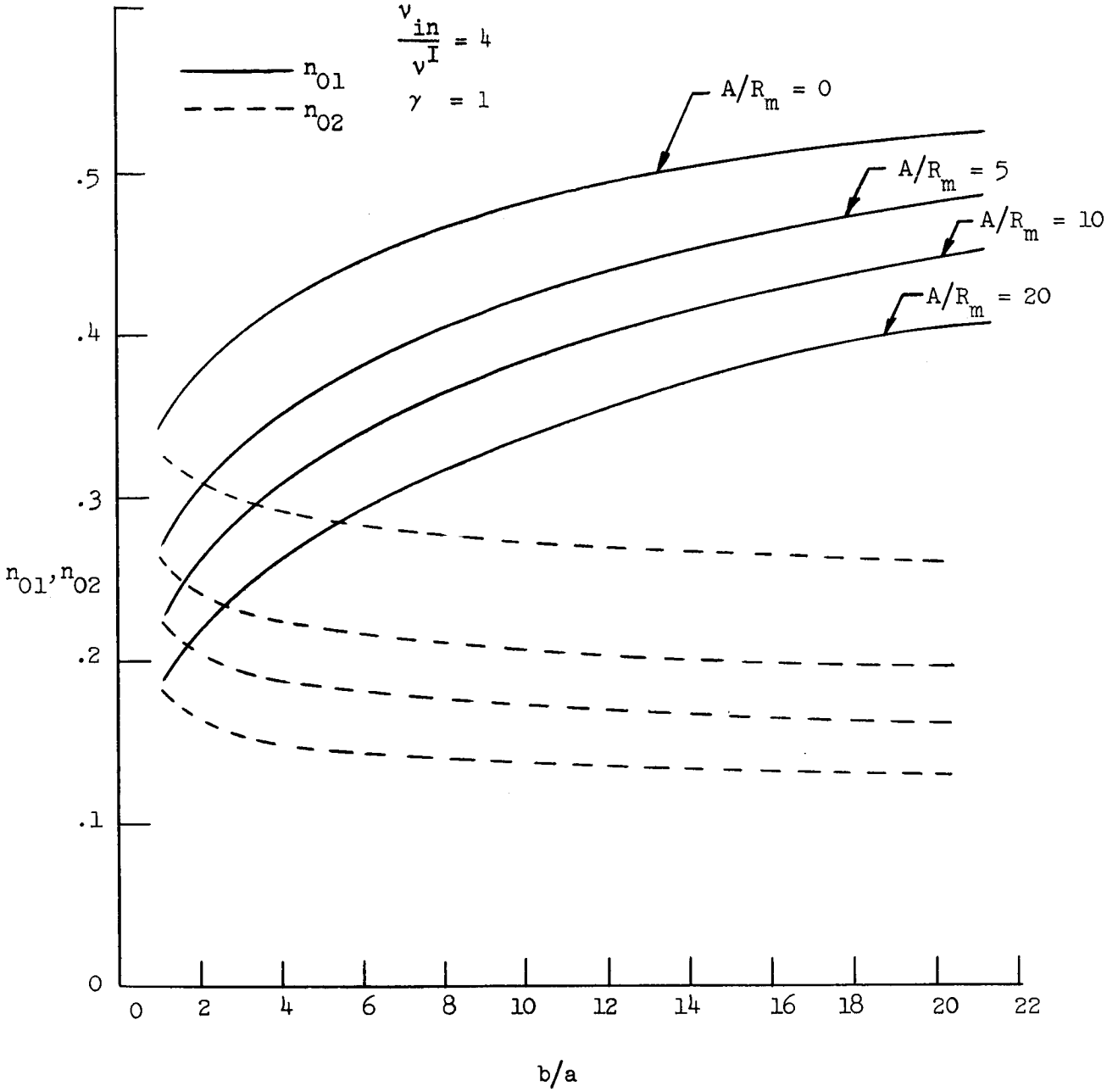

FIG. 18--Normalized "wall" density in the coaxial discharge with magnetic field and collisions as a function of the ratio of outer to inner wall radii

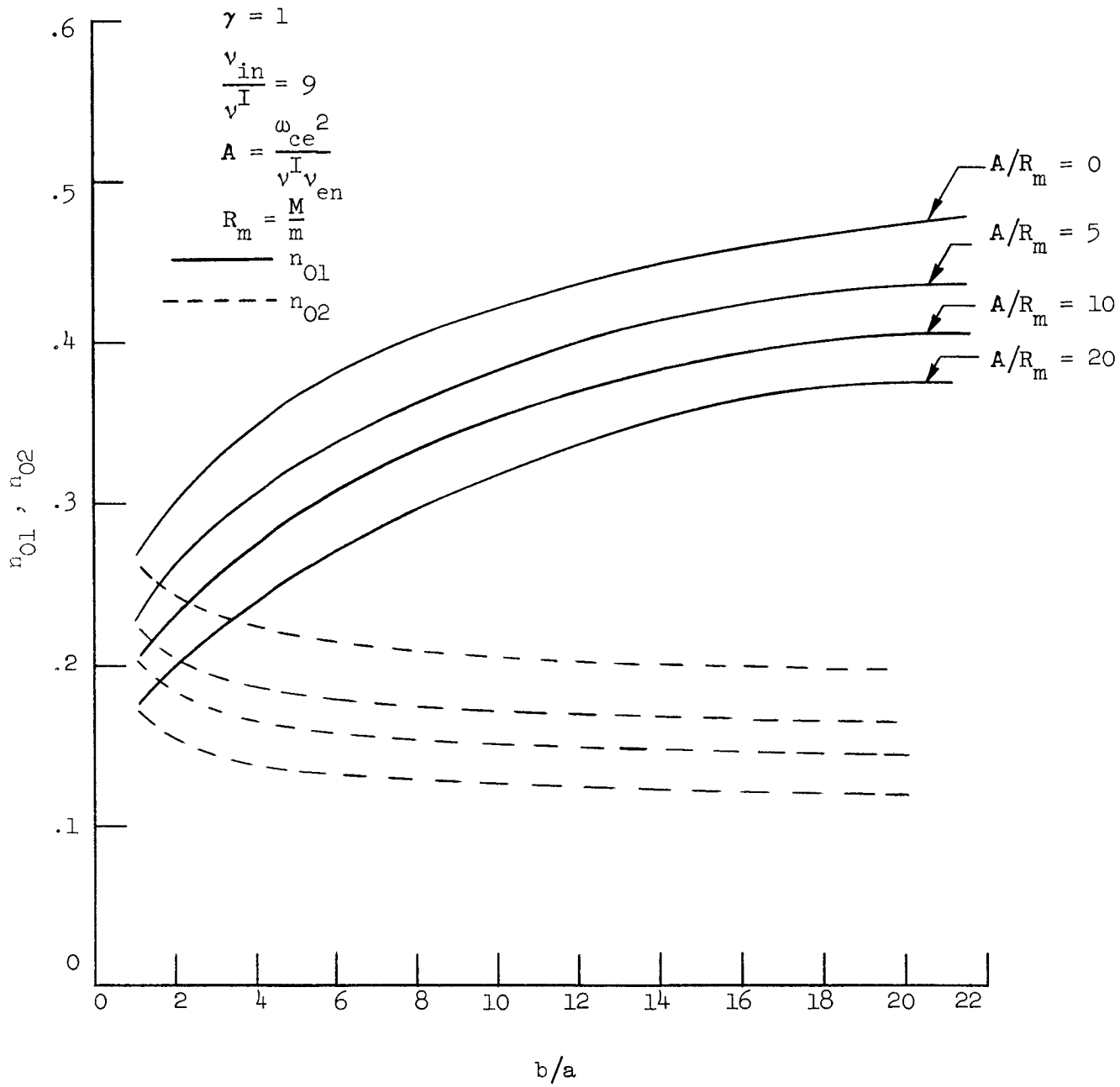

FIG. 19--Normalized "wall" density in the coaxial discharge, with collisions and a magnetic field, as a function of the ratio of outer to inner wall radii.

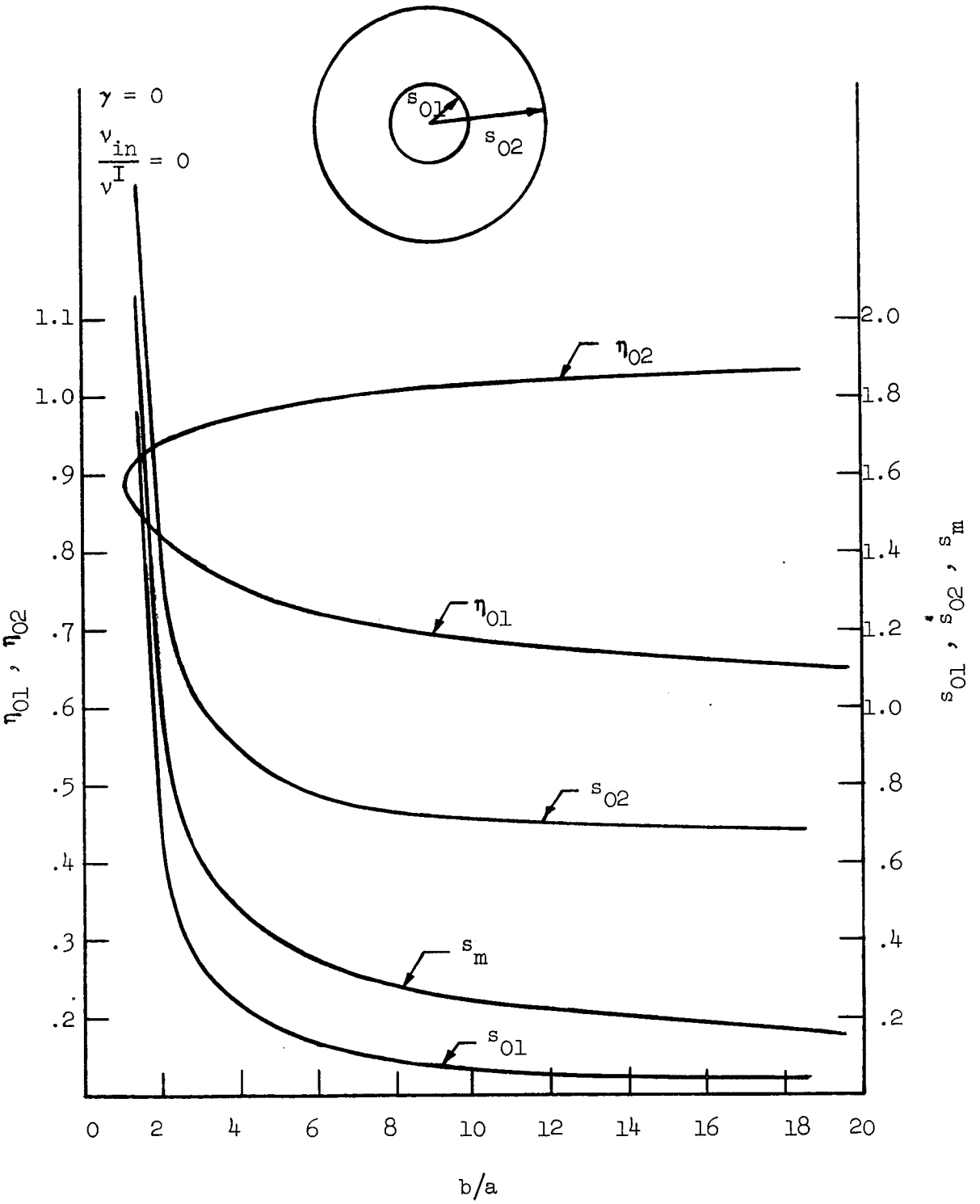

FIG. 20--Inner and outer wall parameters of the one-dimensional coaxial discharge as a function of the ratio of outer to inner radii with kinetic pressure included ($\gamma = 0$) .

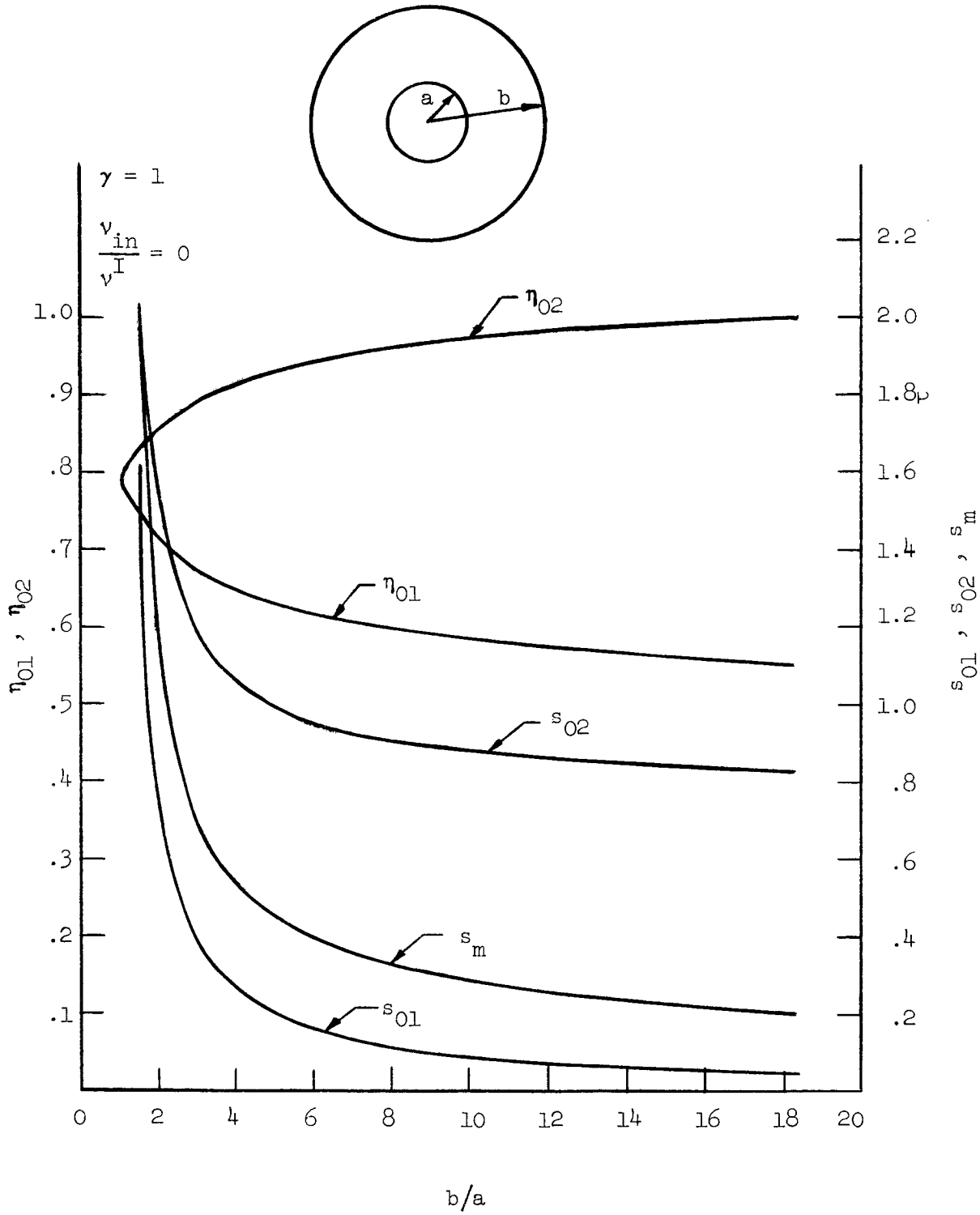

FIG. 21--Inner and outer "wall" parameters of the one-dimensional coaxial discharge as a function of the ratio of outer to inner radii with kinetic pressure included ($\gamma = 1$) .

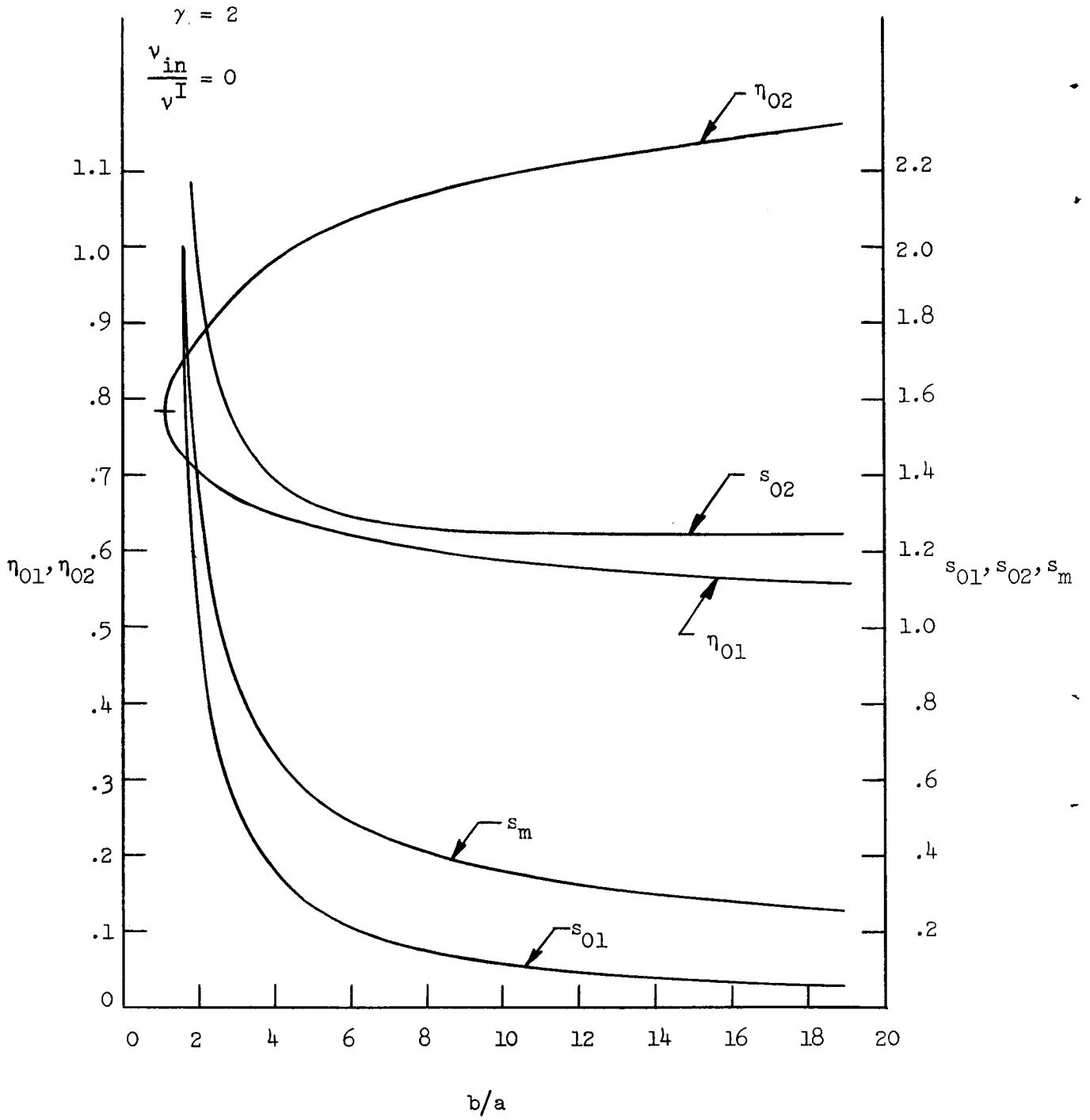

FIG. 22--Inner and outer "wall" parameters of the one-dimensional coaxial discharge as a function of the ratio of outer to inner radii with kinetic pressure included ($\gamma = 2$).

show how the "wall" parameters vary as the ratio of outer to inner diameter is changed for the cases $\gamma = 0$, 1 , and 2 .

It is comforting to note that in all cases the values of the "wall" parameters approach the previously calculated values for the planar discharge and the cylindrical discharge as $b/a \rightarrow 1$ and $b/a \rightarrow \infty$, respectively.

3. The Coaxial Discharge and Probe Theory

As the ratio of outer to inner radii (b/a) of the coaxial discharge becomes large, the discharge begins to approximate a "small" cylindrical probe in an "infinite" plasma. The solutions thus become applicable to the problems connected with probe theory. Several interesting and useful results of applying the solutions for a large b/a to probe theory are discussed below.

One immediate quantitative result which can be obtained is the effect of the probe size on a discharge or, what is the same thing, the distance away from the edge of the discharge a probe must be in order not to effect the probe measurements. The parameter of interest at the sheath boundary is the ion density. From Figs. 20, 21, and 22, we see that in this collisionless case, the potential is asymptoting to a normalized value of 0.575 for all three generation rates corresponding to $\gamma = 0$, 1 , and 2 . We obtain the same asymptotic value for the potential (and thus, the density) independent of the generation since there is very little generation between s_m and the probe, i.e., in the sheath region. This gives a normalized ion density at the sheath of $n_i = 0.562$. Again from Figs. 20-22 we see that for less than a 10% error in this value of ion density the value of b/a must be greater than approximately 8:1. This means that the radius of the sheath surrounding the probe, which may be larger than the probe, should be at least 8 sheath radii away from the edge of the plasma in order to keep the error in ion density to less than 10%.

The ion current to a cylindrical probe may be written as

$$I_p = n_s e v_s A_s \quad , \tag{87}$$

where I_p is the current to the probe, n_s is the ion density at the sheath, v_s is the ion velocity at the sheath, and A_s is the area of the sheath. Using the value of v_s determined by the Bohm Criteria and a value of ion density determined by obtaining the potential at the T-L Boundry, Bohm, Burhop, and Massey[41] found an expression which gives ion collection in terms of undisturbed ion density, n_0 . Their result is

$$I_p = .40\, n_0\, e \sqrt{\frac{2kT_e}{M}}\, A_s \quad . \tag{88}$$

Provided that the area of the probe is approximately equal to the area of the sheath, the above expression can be used to calculate the ion density when the electron temperature is known.

Using the theory developed in this work it is possible to not only verify the work of Bohm, Burhop and Massey (B.B.M) but to extend it also to the cases of a plasma with collisions and in a magnetic field. In the collisionless cases of Figs. 20-22 the value of density at the sheath appears to be asymptoting to a value of $n_s = 0.562$. The normalized ion velocity at the sheath for all three values of generation ($\gamma = 0,1,2$) is given very closely by $v_s = 0.720$. Substituting values into Eq. (87) we obtain the result

$$I_p = .404\, n_0\, e \sqrt{\frac{2kT_e}{M}}\, A_s \quad , \tag{89}$$

which is very close indeed to the value obtained by B.B.M. In the limit of probe radius to electron Debye length becoming very large, Allen, Boyd, and Reynolds[42] also obtain essentially the same result.

It is interesting to compare the result of Eq. (89) obtained by using three moment equations and including kinetic pressure to the result obtained by only using the first two-moment equations and neglecting kinetic pressure. From Fig. 17 we see that for $\gamma = 1$ the value of ion density at the sheath is given by

$$n_s \approx 0.580$$

for large b/a . The normalized ion velocity at the sheath is again the same value as given by the Bohm criteria, namely

$$v_s = 0.707 \quad .$$

Equation (87) thus becomes for this case

$$I_p = 0.410\, n_0 \sqrt{\frac{2kT_e}{M}}\, A_s e \quad , \qquad (90)$$

which again is very close to the value obtained by B.B.M. We would thus expect the theory used in this work to give reasonably accurate results when extended to the cases of collisions and a magnetic field even when the pressure term is neglected.

With the assumptions that the sheath is small compared to the mean free path for collision and also small compared to the cycloidal radius of ions, a similar expression to Eq. (90) can be obtained for various collision rates and/or a magnetic field. The results should give reasonably good accuracy for the ion density in the plasma provided that the sheath thickness is small compared to the probe radius. If the sheath thickness is not small compared to the probe radius, the results given below are still useful as long as the Child-Langmuir Law can be used to find the area A_s of the sheath.

In order to make the presentation of the results more compact, we rewrite Eq. (87) in the following form:

$$I_p = \frac{n_s n_0}{\sqrt{2}} \sqrt{\frac{2kT_e}{M}} A_s e \quad , \tag{91}$$

where the value of n_s is found for various collision rates and magnetic fields from the calculated curves of Fig. 23.

It is interesting to note that ion-neutral collisions have the same qualitative effect on the undisturbed ion density as a magnetic field, both causing a increase in the undisturbed ion density because both tend to inhibit diffusion of ions across the plasma. From Fig. 23 we see that a relative ion-neutral collision frequency of ten results in an actual undisturbed ion density 10% higher than that calculated neglecting collisions. When both collisions and a magnetic field are present, the error in undisturbed ion density calculated with the theory of B.B.M is even greater. A relatively small magnetic field can give a large value of the parameter A/R_m . We see that neglecting collisions with $A/R_m = 20$ the error in undisturbed ion density would be greater than 20% if one used the theory of B.B.M.

As far as is known, the curves of Fig. 23 give the first useful quantitative corrections to the probe theory in the ion collection regime.

C. SUMMARY OF ONE-DIMENSIONAL EQUATIONS AND SOLUTIONS

Tabulated below in a form useful for computer solution using the Runge-Kutta technique are the equations describing the one-dimensional low and medium pressure discharges. Also included are the first terms in the Taylor series expansion of each of the parameters. This is necessary in order to start out the Runge-Kutta method of solution. In using these formulae it is well to keep in mind the following principal

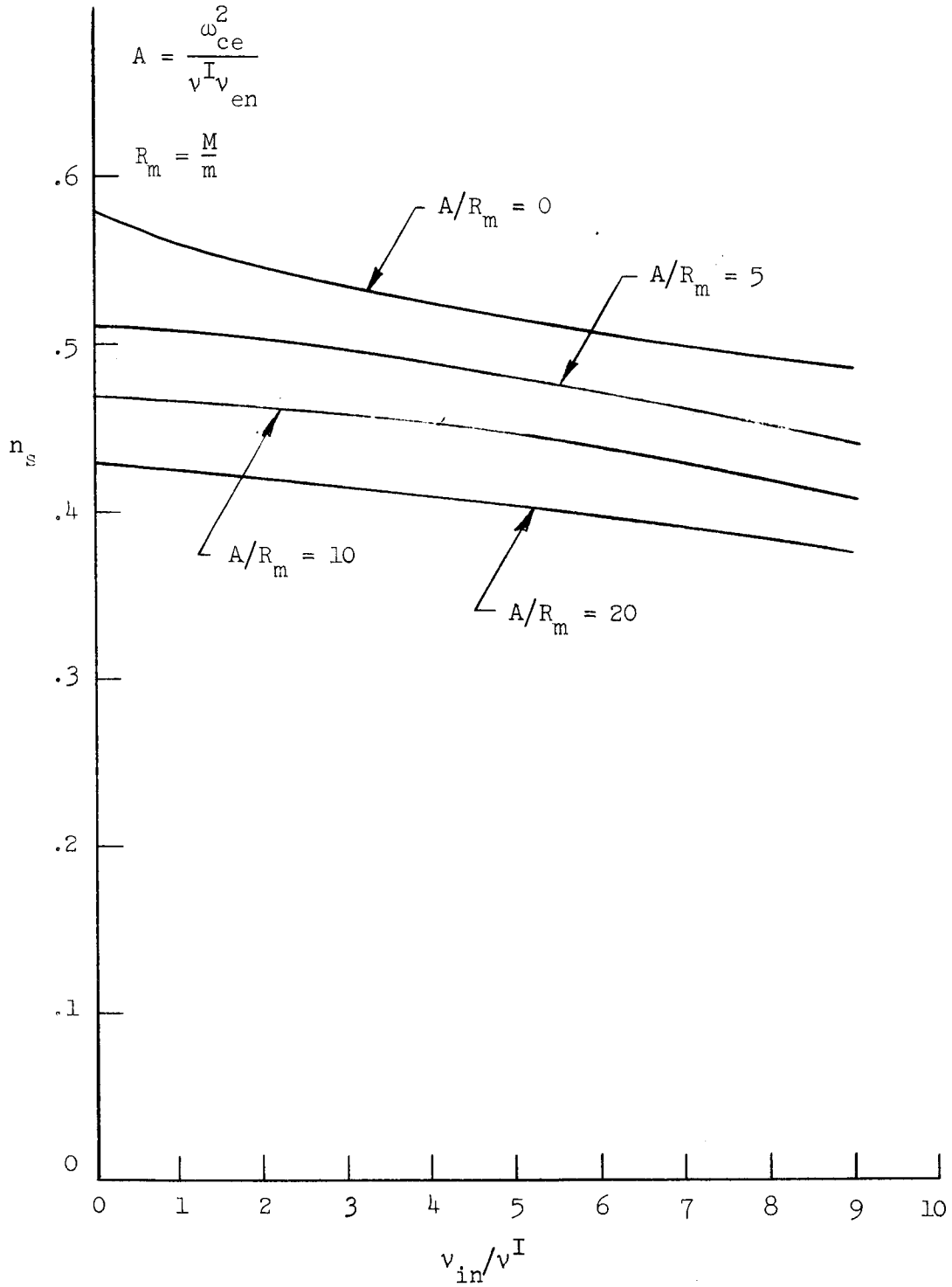

FIG. 23--Normalized ion density at the sheath of a small cylindrical probe for various combinations of magnetic field and ion-neutral collisions.

assumptions which have been used in the derivations:

(1) Charge neutrality is assumed throughout, that is,

$$\frac{n_i - n_e}{n_i + n_e} \ll 1 \quad .$$

(2) In the cases without magnetic field, the electrons are assumed to have a M-B distribution such that

$$n_e = n_{e0} e^{\frac{e\phi}{kT}} \quad .$$

(3) In the cases with a magnetic field, the magnetic field is assumed to be so small as to have a negligible effect on the ions.

(4) The electron temperature is assumed to be uniform throughout the discharge.

Using the formulae of Tables III and IV, any case which is not calculated in the body of Chapter III can be easily solved.

The normalizations used are summarized below:

(1) Planar cases

$$v_1 = \left(\frac{M}{2kT}\right)^{1/2} v_x$$

$$\eta = -\frac{e\phi}{kT}$$

$$U_1 = \ln(n/n_{e0})$$

TABLE III

NORMALIZED EQUATIONS OF THE ONE-DIMENSIONAL PLANAR DISCHARGE

Neglecting kinetic pressure		Including kinetic pressure
Collisionless ("freefall" case)	With collisions	Collisionless ("freefall" case)
$\gamma = 0$	$\gamma = 0$	$\gamma = 0$
$s = \frac{1}{e^{\eta}}\left(\frac{e^{\eta}-1}{2}\right)^{1/2}$	$\frac{dv_1}{ds} = -\frac{[e^{\eta}(1+2v_1^2)+2Cv_1^2]}{2(v_1^2-\frac{1}{2})}$	$s^3 = \frac{3}{4}e^{-2\eta}[se^{\eta} - \frac{1}{2}\tan^{-1}(2se^{\eta})]$
$s = \frac{v_1}{1+2v_1^2}$	$\frac{d\eta}{ds} = -\frac{(2v_1e^{\eta}+Cv_1)}{(v_1^2-\frac{1}{2})}$	$\eta = \ln\left[\frac{v_1^3}{\frac{3}{4}(v_1 - \frac{1}{2}\tan^{-1}(2v_1)}\right]$
	$v_1 = s + \ldots$	
	$\eta = (2+C)s^2 + \ldots$	
	$C = \nu_{in}/\nu^I$	
$\gamma = 1$	$\gamma = 1$	$\gamma = 1$ and 2
$s = -\left(\frac{e^{\eta}-1}{2}\right)^{1/2} + \sqrt{2}\tan^{-1}\left[\left(e^{\eta}-1\right)\right]^{1/2}$	$s = -\frac{v_1}{B} + \frac{1}{\sqrt{2B}}(1+\frac{1}{B})\tan^{-1}(\sqrt{2B}v_1)$	$\frac{dv_1}{ds} = -\frac{(2v_1^2+\frac{1}{2})e^{(1-\gamma)\eta}}{(v_1^2-\frac{1}{2}-3\overline{u_1^2})}$
$s = -v_1 + \sqrt{2}\tan^{-1}(\sqrt{2}v_1)$	$v_1 = \left[\frac{e^{\left(\frac{2B}{1+B}\right)\eta}-1}{2B}\right]^{1/2}$	$\frac{d\eta}{ds} = \frac{3(\overline{u_1^2}/v_1 - v_1)e^{(1-\gamma)\eta}}{(v_1^2-\frac{1}{2}-3\overline{u_1^2})}$
	$B = 1 + \frac{\nu_{in}}{\nu^I}$	$\frac{d\overline{u^2}}{ds} = e^{(1-\gamma)\eta}\frac{\left[\overline{3u_1^2}/2v_1 + 3(\overline{u_1^2})^2/v_1 + v_1^3 - v_1/2\right]}{(v_1^2-\frac{1}{2}-3\overline{u_1^2})}$
$\gamma = 2$	$\gamma = 2$	$\gamma = 1$ and 2
$s = \left(\frac{e^{\eta}-1}{2}\right)^{1/2}[1 - \frac{1}{3}(e^{\eta}-1)]$	$\frac{dv_1}{ds} = -\frac{[e^{-\eta}(1+2v_1^2)+2Cv_1^2]}{2(v_1^2-\frac{1}{2})}$	$v_1 = s + \ldots$
$s = v_1(1 - \frac{2}{3}v_1^2)$	$\frac{d\eta}{ds} = \frac{(2v_1e^{-\eta}+Cv_1)}{2(v_1^2-\frac{1}{2})}$	$\eta = \frac{12}{5}s^2 + \ldots$
	$v_1 = s + \ldots$	$\overline{u_1^2} = \frac{1}{5}s^2 + \ldots$
	$\eta = (1+B)s^2$	
	$B = 1 + \frac{\nu_{in}}{\nu^I}$	

TABLE IV

NORMALIZED EQUATIONS OF THE ONE-DIMENSIONAL CYLINDRICAL AND COAXIAL DISCHARGES

Neglecting Kinetic Pressure ($\overline{u^2} = 0$)			Including Kinetic Pressure
Collisionless, without magnetic field	With collisions	With collisions and a magnetic field	Collisionless, without magnetic field
$\gamma = 0$	$\gamma = 0$, 1, and 2	$\gamma = 1$ only	$\gamma = 0$, 1, and 2
$s = \dfrac{2v_1}{(4v_1^2 + 1)^{3/4}}$	$\dfrac{dv_1}{ds_r} = \dfrac{[(1 + 2v_1^2)e^{(1-\gamma)\eta} - v_1/s_r + 2Cv_1^2]}{(1 - 2v_1^2)}$	$\dfrac{dv_1}{ds_r} = \dfrac{\left[-v_1^2(D + B) + \dfrac{v_1}{2s_r} - \dfrac{1}{2}\right]}{(v_1^2 - \frac{1}{2})}$	$\dfrac{dv_1}{ds_r} = \dfrac{\left[\dfrac{v_1}{2s_r} - (\frac{1}{2} + 2v_1^2)e^{(1-\gamma)\eta}\right]}{(v_1^2 - \frac{1}{2} - 3\overline{u_1^2})}$
$s = \dfrac{(e^{2\eta} - 1)^{1/2}}{e^{2\eta/3}}$			
$\gamma = 1$, and 2			
$\dfrac{dv_1}{ds_r} = \dfrac{\left[\dfrac{v_1}{2s_r} - (v_1^2 + \frac{1}{2})e^{(1-\gamma)\eta}\right]}{(v_1^2 - \frac{1}{2})}$	$\dfrac{d\eta}{ds_r} = \dfrac{2[2v_1 e^{(1-\gamma)\eta} + Cv_1 - v_1^2/s_r]}{(1 - 2v_1^2)}$	$\dfrac{d\eta}{ds_r} = \dfrac{\left[-(1 + B)v_1 + \dfrac{v_1^2}{s_r} - 2v_1^2 D\right]}{(v_1^2 - \frac{1}{2})}$	$\dfrac{d\eta}{ds_r} = \dfrac{\left[\dfrac{v_1^2}{s_r} - \dfrac{3\overline{u_1^2}}{s_r} + \left(3\dfrac{\overline{u_1^2}}{v_1} + v_1\right)e^{(1-\gamma)\eta}\right]}{(v_1^2 - \frac{1}{2} - 3\overline{u_1^2})}$
$\dfrac{d\eta}{ds_r} = \dfrac{\left[\dfrac{v_1^2}{s_r} - 2v_1 e^{(1-\gamma)\eta}\right]}{(v_1^2 - \frac{1}{2})}$		$\dfrac{dU_1}{ds_r} = \dfrac{\left[-(1 + B + D)v_1 - \dfrac{v_1^2}{s_r}\right]}{(v_1^2 - \frac{1}{2})}$	$\dfrac{d\overline{u_1^2}}{ds_r} = \left[\dfrac{\overline{u_1^2}}{s_r} + \left(\dfrac{3(\overline{u_1^2})}{2v_1} + \dfrac{3(\overline{u^2})^2}{v_1} + v_1^3 - \dfrac{v_1}{2}\right) \times e^{(1-\gamma)\eta}\right] \Big/ (v_1^2 - \frac{1}{2} - 3\overline{u_1^2})$
Coaxial	Coaxial	Coaxial	Coaxial
$v_1 = s_r - s_m + \ldots$	$v_1 = s_r - s_m + \ldots$	$v_1 = s_r - s_m + \ldots$	$v_1 = s_r - s_m + \ldots$
$\eta = 2(s_r - s_m)^2 + \ldots$	$\eta = (2 + C)(s - s_m)^2 + \ldots$	$\eta = (1 + B)(s_r - s_m)^2 + \ldots$	$\eta = \frac{12}{5}(s_r - s_m)^2 + \ldots$
		$U_1 = (1+D+B)(s_r - s_m)^2$	$\overline{u_1^2} = \frac{1}{5}(s_r - s_m)^2 + \ldots$
Cylindrical	Cylindrical	Cylindrical	Cylindrical
$v_1 = \dfrac{s_r}{2} + \ldots$	$v_1 = s_r + \ldots$	$v_1 = s_r/2$	$v_1 = \dfrac{s_r}{2}$
$\eta = \frac{3}{4}s_r^2 + \ldots$	$\eta = (\frac{3}{2} + \frac{C}{2})s_r^2 + \ldots$	$\eta = \frac{1}{2}(1 + B)s_r^2$	$\eta = \frac{3}{4}s_r^2 + \ldots$
	$C = \dfrac{v_{in}}{v^I}$	$U_1 = (\frac{3}{4} + D + B)s_r^2$	$\overline{u_1^2} = \frac{1}{4}s_r^2 + \ldots$
		$U_1 = \ln(n/n_{e0})$	
		$D = \dfrac{\omega_{ce}^2}{v^I \nu_{en}} \dfrac{m}{M}$	
		$B = 1 + \nu_{in}/v^I$	

and

$$\overline{u_1^2} = \frac{M}{2kT} \langle \overline{u^2} \rangle$$

$$s = \left(\frac{M}{2kT}\right)^{1/2} \nu I_x \quad .$$

(2) Cylindrical and coaxial cases

$$v_1 = \left(\frac{M}{2kT}\right)^{1/2} v_r$$

$$\eta = -\frac{e\phi}{kT}$$

$$U_1 = -\ln(n/n_{e0})$$

$$\overline{u_1^2} = \frac{M}{2kT} \overline{u^2}$$

$$s_r = \left(\frac{M}{2kT}\right)^{1/2} \nu I_r \quad .$$

One final practical note of interest in the actual solving of the equations. It is more accurate to make a change of independent variable from the normalized distance parameter, s, to the velocity v_1. This is because the derivatives are much better behaved at the Tonks-Langmuir boundary with v_1 as the independent variable and thus the computer solution is more accurate. Fortunately, with the equations in the form given in Tables III and IV this change of variables is easily accomplished.

CHAPTER IV

TWO-DIMENSIONAL CASES – EXACT SOLUTIONS

Solutions for the discharges in a finite length cylinder, between finite length coaxial cylinders and in a rectangular box, have been obtained for the most important case of ion generation proportional to electron density with the pressure term neglected. The particular geometries studied are shown in Fig. 24. The effect of ion-neutral collisions is included so that the results apply in both the low and medium pressure regimes. It can reasonably be expected that these solutions will have the same order of accuracy as the corresponding one-dimensional cases discussed in Chapter III. As far as is known, these results represent the first solutions of this type of problem in more than one dimension. Two-dimensional solutions for the cylindrical geometry case of Fig. 24 have also been obtained for the more restricted case of equal radial and longitudinal electron and ion currents throughout the discharge (ambipolar diffusion). A tabulation of solutions and equations is given at the end of the chapter in a form useful for further computation if desired.

The more general cases without a magnetic field are considered first.

A. WITHOUT A MAGNETIC FIELD

Neglecting the term $\nabla \cdot \overleftrightarrow{\Psi}$ in Eq. (27) and using the condition of a Maxwellian distribution of electrons with equal electron and ion number densities we obtain for the equation of continuity (with $\gamma = 1$)

$$\nabla \cdot \vec{v} + \frac{e}{kT_e} \vec{v} \cdot \nabla\phi = \nu^I \quad , \tag{92}$$

where we have used the Boltzmann distribution of density [Eq. (12)] to eliminate the ion density and for the momentum transfer equation

$$\vec{v} \cdot \nabla \vec{v} + (\nu^I + \nu_{in}) \vec{v} = - \frac{e}{M} \nabla\phi \tag{93}$$

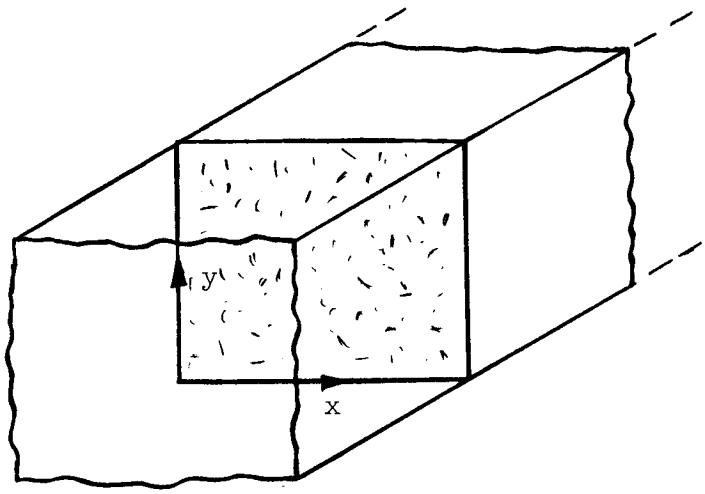

a. Finite-length rectangular box.

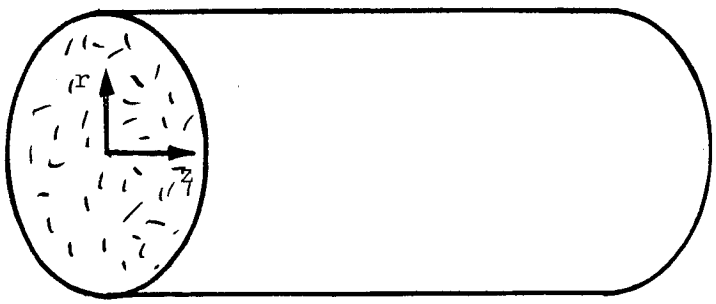

b. Finite-length cylinder.

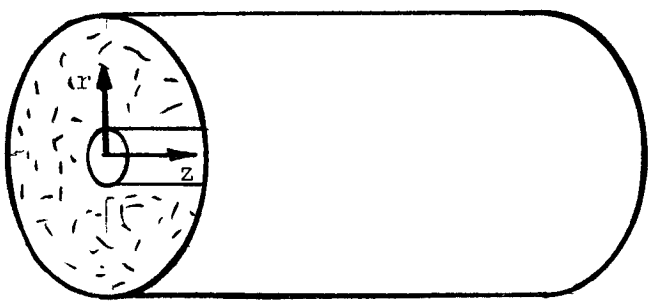

c. Finite-length concentric coaxial cylinders

FIG. 24--Two-dimensional discharge geometries.

where we have brought the collision term $n\nu_{in}\vec{v}$ over to the left-hand side of the equation and divided through by the number density, n. Expanding the $\vec{v} \cdot \nabla \vec{v}$ term in Eq. (93) we obtain the result

$$\nabla\left(\frac{v^2}{2} + \frac{e}{M}\phi\right) - \vec{v} \times \nabla \times \vec{v}$$

$$+ (\nu^I + \nu_{in})\,\vec{v} = 0 \quad . \qquad (94)$$

Now we assume the condition that the curl of velocity or the vorticity is zero throughout the discharge so that the velocity can be expressed in the form

$$\vec{v} = \nabla W \quad ,$$

where W is a scalar function related to the action function in electrodynamics. Using this assumption we can write Eq. (94) as

$$\nabla\left[\frac{v^2}{2} + \frac{e}{M}\phi + (\nu^I + \nu_{in})\,W\right] = 0 \quad , \qquad (95)$$

which is certainly consistent with the assumption of zero vorticity. As the development proceeds in the following paragraphs, we will also see that the assumption of zero vorticity leads to consistent values of the parameters within and on the boundaries of the plasma for this special case of ion generation proportional to electron density $(\gamma = 1)$.

1. Rectangular Box

(a) Derivation of Equations

In the rectangular box geometry of Fig. 24, Eqs. (92) and (94) become, after expanding Eq. (94) into component form and using the

normalizations,

$$s_1 = \nu^I \left(\frac{M}{2kT}\right)^{1/2} x \qquad (96)$$

$$s_2 = \nu^I \left(\frac{M}{2kT}\right)^{1/2} y \qquad (97)$$

$$v_1 = \left(\frac{M}{2kT}\right)^{1/2} v_x \qquad (98)$$

$$v_2 = \left(\frac{M}{2kT}\right)^{1/2} v_y \qquad (99)$$

and

$$\eta = -\frac{e\phi}{kT} \quad ; \qquad (100)$$

$$\frac{\partial v_1}{\partial s_1} + \frac{\partial v_2}{\partial s_2} - v_1 \frac{\partial \eta}{\partial s_1} - v_2 \frac{\partial \eta}{\partial s_2} = 1 \quad , \qquad (101)$$

$$v_1 \frac{\partial v_1}{\partial s_1} + \left(\frac{\nu^I + \nu_{in}}{\nu^I}\right) v_1 = \frac{1}{2} \frac{\partial \eta}{\partial s_1} \quad , \qquad (102)$$

$$v_2 \frac{\partial v_2}{\partial s_2} + \left(\frac{\nu^I + \nu_{in}}{\nu^I}\right) v_2 = \frac{1}{2} \frac{\partial \eta}{\partial s_2} \quad . \qquad (103)$$

We now look for a solution for W of Eq. (95) by assuming that it is separable in the additive form

$$W = W_1(s_1) + W_2(s_2) \quad , \qquad (104)$$

so that v_1 is only a function of s_1 and v_2 is only a function of s_2 . Now, using Eqs. (102) and (103) in Eq. (101) to eliminate $\partial\eta/\partial s_1$ and $\partial\eta/\partial s_2$ we obtain the result

$$(1 - 2v_1^2)\frac{\partial v_1}{\partial s_1} - 2v_1^2\left(1 + \frac{\nu_{in}}{\nu^I}\right) + (1 - 2v_2^2)\frac{\partial v_2}{\partial s_2} - 2v_2^2\left(1 + \frac{\nu_{in}}{\nu^I}\right) = 1 \quad . \tag{105}$$

The first two terms on the left-hand side are only a function of s_1 while the last two terms are only a function of s_2 . That is, we have

$$F_1(s_1) + F_2(s_2) = 1 \quad \text{(a constant)} \quad . \tag{106}$$

For this to be true for all values of s_1 and s_2 , it follows that Eq. (105) must be separable in the form

$$(v_1^2 - \tfrac{1}{2})\frac{\partial v_1}{\partial s_1} + v_1^2\left(1 + \frac{\nu_{in}}{\nu^I}\right) = -\frac{\alpha_1}{2} \tag{107}$$

and

$$(v_2^2 - \tfrac{1}{2})\frac{\partial v_2}{\partial s_2} + v_2^2\left(1 + \frac{\nu_{in}}{\nu^I}\right) = -\frac{\alpha_2}{2} \tag{108}$$

where $\alpha_1 + \alpha_2 = 1$.

Equations (107) and (108) can be integrated to obtain $v_1(v_2)$ as a function of $s_1(s_2)$. The results are

$$Bs_1 = -v_1 + \left(\frac{B}{2\alpha_1}\right)^{1/2}\left(1 + \frac{\alpha_1}{B}\right)\tan^{-1}\left[\left(\frac{2B}{\alpha_1}\right)^{1/2} v_1\right] \tag{109}$$

and

$$Bs_2 = -v_2 + \left(\frac{B}{2\alpha_2}\right)^{1/2} \left(1 + \frac{\alpha_2}{B}\right) \tan^{-1} \left[\left(\frac{2B}{\alpha_2}\right)^{1/2} v_2\right] \qquad (110)$$

where we have defined the parameter, B , as

$$B = 1 + \frac{\nu_{in}}{\nu^I} \quad . \qquad (111)$$

From Eqs. (107) and (108) we again see that the Bohm Criteria at the "wall" comes out as a natural result of the equations, that is, $\partial v_1/\partial s_1 \rightarrow \infty$ when $v_1 = 1/\sqrt{2}$. This is a further indication of the consistency of the formulation.

Using Eqs. (102) and (103) in Eq. (101) the potential can be found as a function of velocity. The results are

$$\eta_1 = \frac{1}{2} \left(1 + \frac{\alpha_1}{B}\right) \ell n \left(\frac{2B}{\alpha_1} v_1^2 + 1\right) \qquad (112)$$

and

$$\eta_2 = \frac{1}{2} \left(1 + \frac{\alpha_2}{B}\right) \ell n \left(\frac{2B}{\alpha_2} v_2^2 + 1\right) \quad . \qquad (113)$$

This in turn can be substituted in Eqs. (109) and (110) to find the potential as a function of distance. The results are

$$Bs_1 = -\left(\frac{\alpha_1}{2B}\right)^{1/2} \left(e^{\left(\frac{2}{1+\alpha_1/B}\right)\eta_1} - 1\right)^{1/2} + \left(\frac{B}{2\alpha_1}\right)^{1/2} \left(1 + \frac{\alpha_1}{B}\right) \tan^{-1} \left[\left(e^{\left(\frac{2}{1+\alpha_1/B}\right)\eta_1} - 1\right)^{1/2}\right] \qquad (114)$$

and

$$Bs_2 = -\left(\frac{\alpha_2}{2B}\right)^{1/2}\left(e^{\left(\frac{2}{1+\alpha_2/B}\right)\eta_2} - 1\right)^{1/2} + \left(\frac{B}{2\alpha_2}\right)^{1/2}\left(1+\frac{\alpha_2}{B}\right)\tan^{-1}\left[\left(e^{\left(\frac{2}{1+\alpha_2/B}\right)\eta_2} - 1\right)^{1/2}\right] \qquad (115)$$

where potential at any point (s_1, s_2) is given by

$$\eta(s_1,s_2) = \eta_1(s_1) + \eta_2(s_2) \quad .$$

For the two-dimensional cases, the ion current at the boundary is still given by Eqs. (46) and (47), but now the current J_i and velocity v are vectors. For the rectangular geometry cases the velocity at any point is given by

$$\vec{v} = \hat{i}v_1 + \hat{j}v_2$$

and the density by

$$n = n_{e0}\, e^{-(\eta_1 + \eta_2)} \quad .$$

(b) Discussion of Calculated Results (Finite Length Rectangular Box)

Using the above formulae all of the parameters of the discharge in a finite length rectangular box can be calculated. As far as is known the results presented below are the first two-dimensional solutions ever obtained for discharges in the low and medium pressure regimes. The usefulness of this modified pressure theory approach is immediately apparent when contrasted with the usual integral equations obtained by Langmuir and which, for two-dimensional cases, appear to be extremely difficult even to formulate.

Several interesting and useful calculated results are as follows. In Figs. 25 and 26 equipotentials for rectangular boxes with two different geometries are plotted as a function of the normalized distance parameter, s . The Tonk's Langmuir (hereafter T-L) boundaries are the outermost straight lines and define the edges of the discharge. It should be noted that only the upper right-hand portion of the box need be presented since the rest of the solution can be obtained by a reflection in the s_1 and s_2 axes. The results appear to be reasonable in that the equipotentials cross the axes at an angle of 90° and near the boundaries the equipotentials begin to approximate the shape of the boundary.

Normalized ion current density to the "wall" of the square box is plotted in Fig. 27 as a function of distance from the axis. Even though the solution does not apply in the sheath region, we have seen that the current calculated at the T-L boundary in the one-dimensional cases is a good approximation to the actual ion current. We would expect the same degree of approximation to hold in the two-dimensional cases.

It is reasonable to expect the ion current density at the T-L boundary to be a good approximation to the actual ion current at the wall since the generation in the sheath region is usually negligibly small. Also shown in Fig. 27 is the angle of the current with respect to the s_1 axis. The case plotted is for no collisions, and we see that the current falls off by about 30% from the center to the edge of the discharge. Again this is a reasonable result since the ion density decreases more rapidly than the total vector velocity increases.

Of more interest than the total vector current is the current normal to the surface at the T-L boundary. Shown in Figs. 28 and 29 is this normalized ion current to the "wall" as a function of distance from the axis of a square box for three different values of ion neutral collision frequency. Figure 28 shows the normalized current

$$j_2 = \frac{n_i}{n_{e0}} v_2 \quad .$$

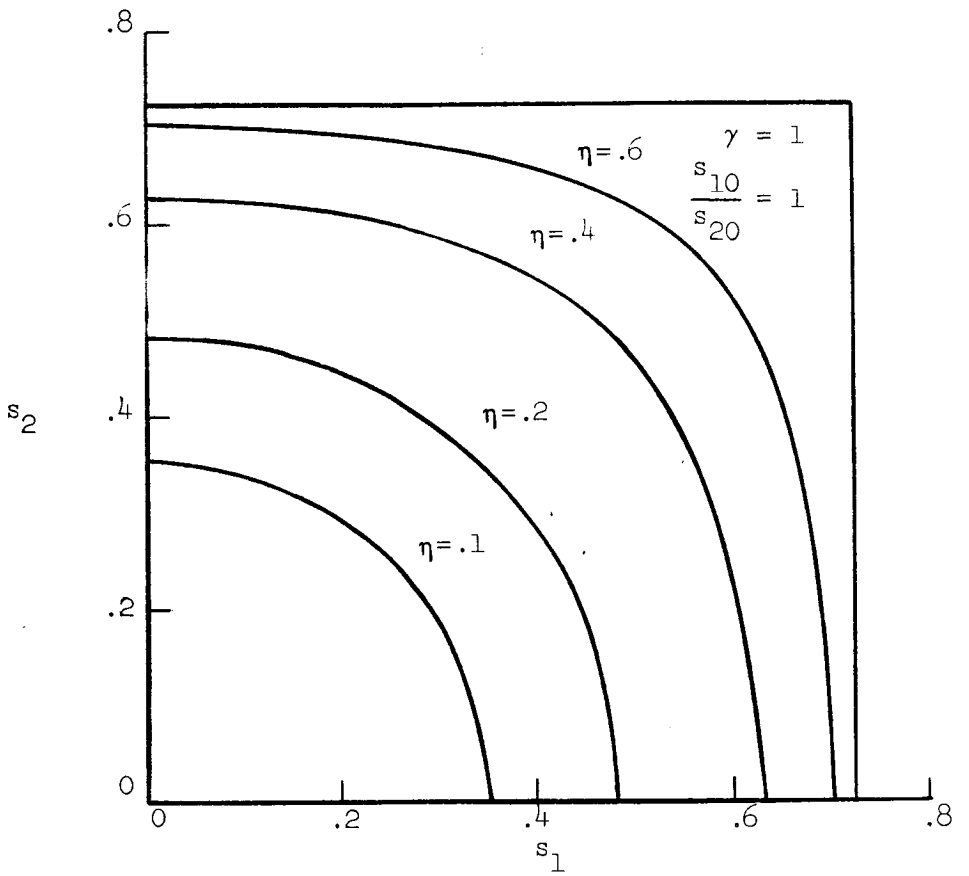

FIG. 25--Equipotentials in a square box.

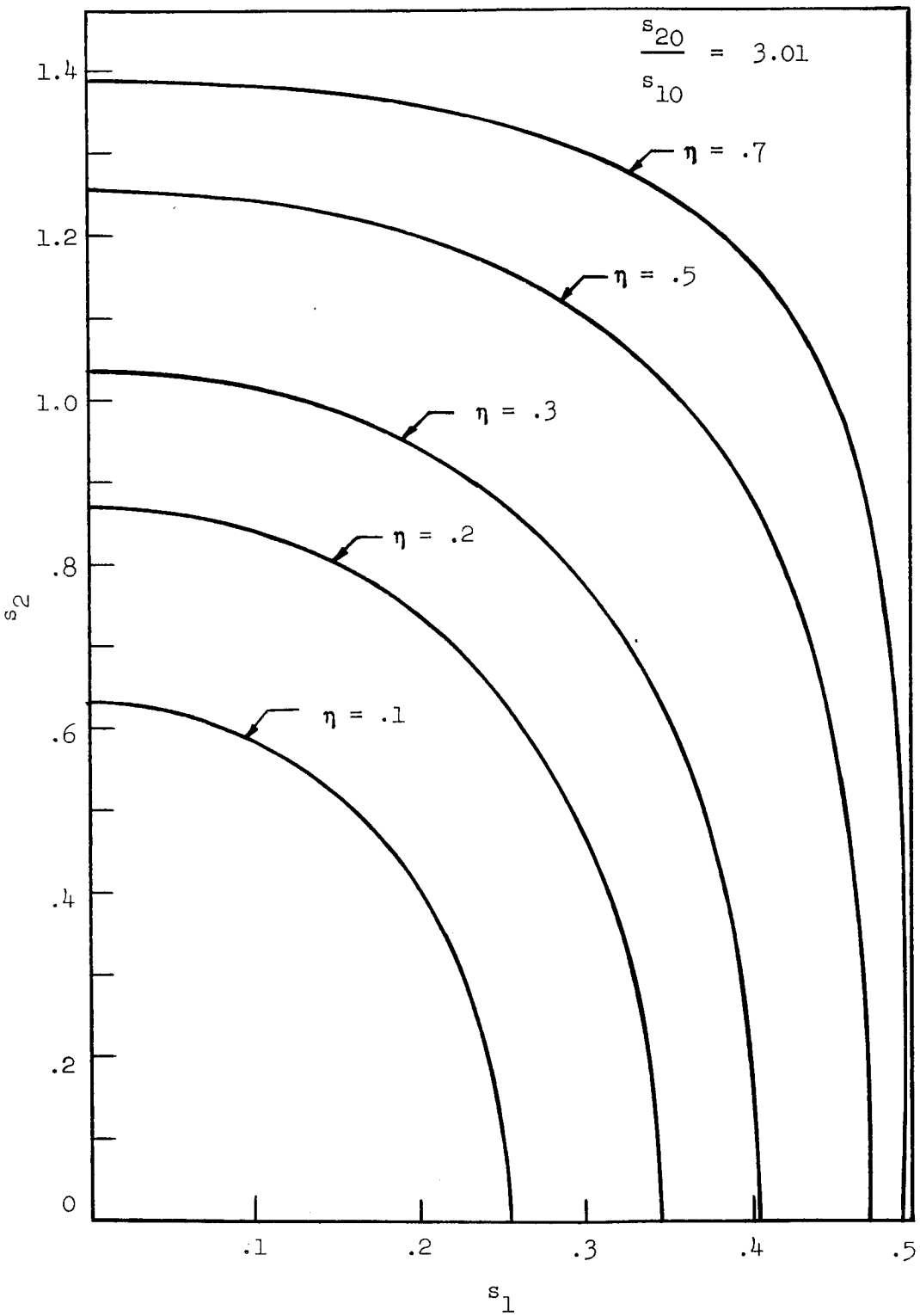

FIG. 26--Equipotentials in a two-dimensional rectangular discharge.

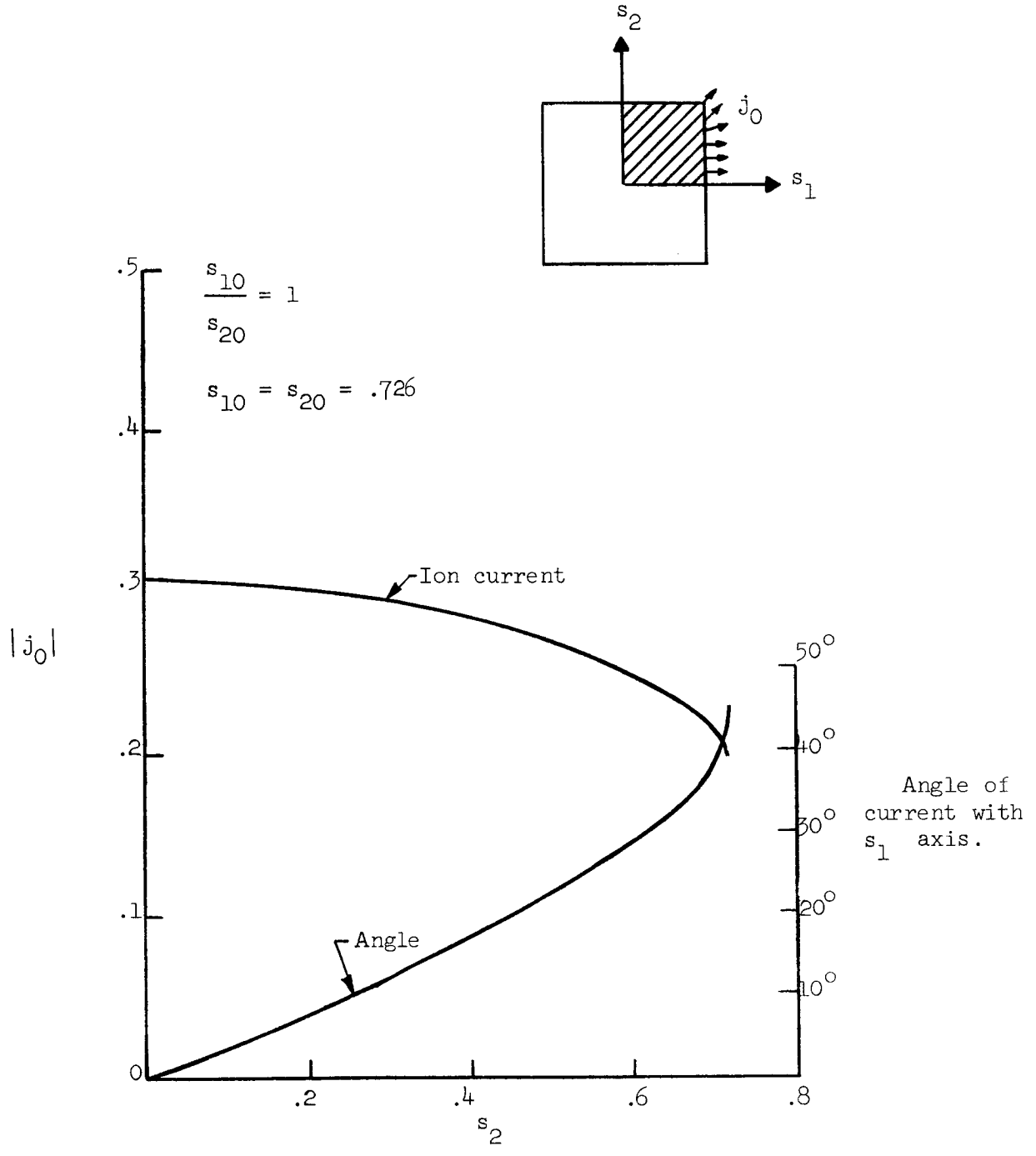

FIG. 27--Magnitude and direction of the ion current at the "wall" of the square box discharge.

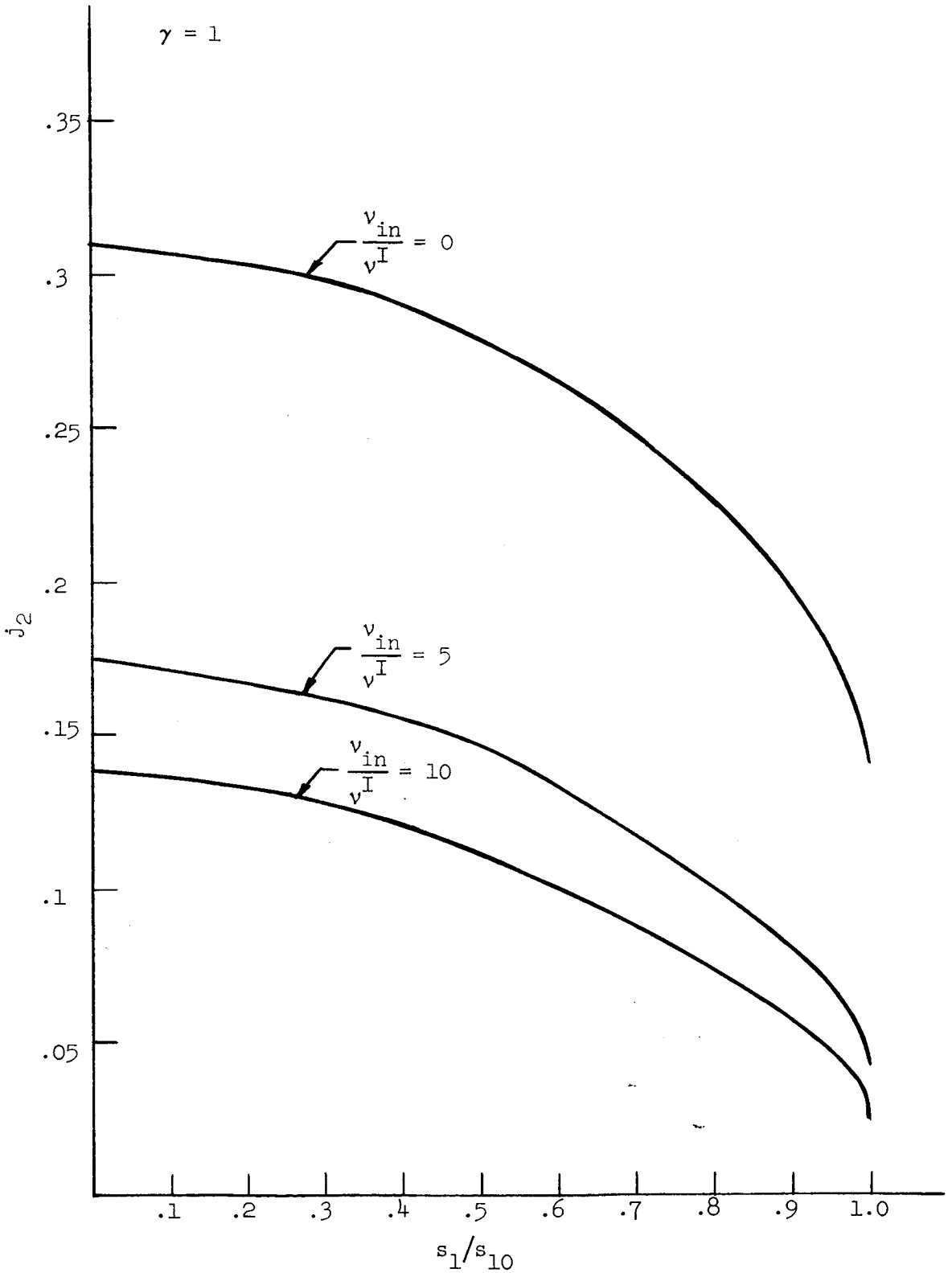

FIG. 28--The effect of collisions on the ion current at the "end" of the discharge in a square box.

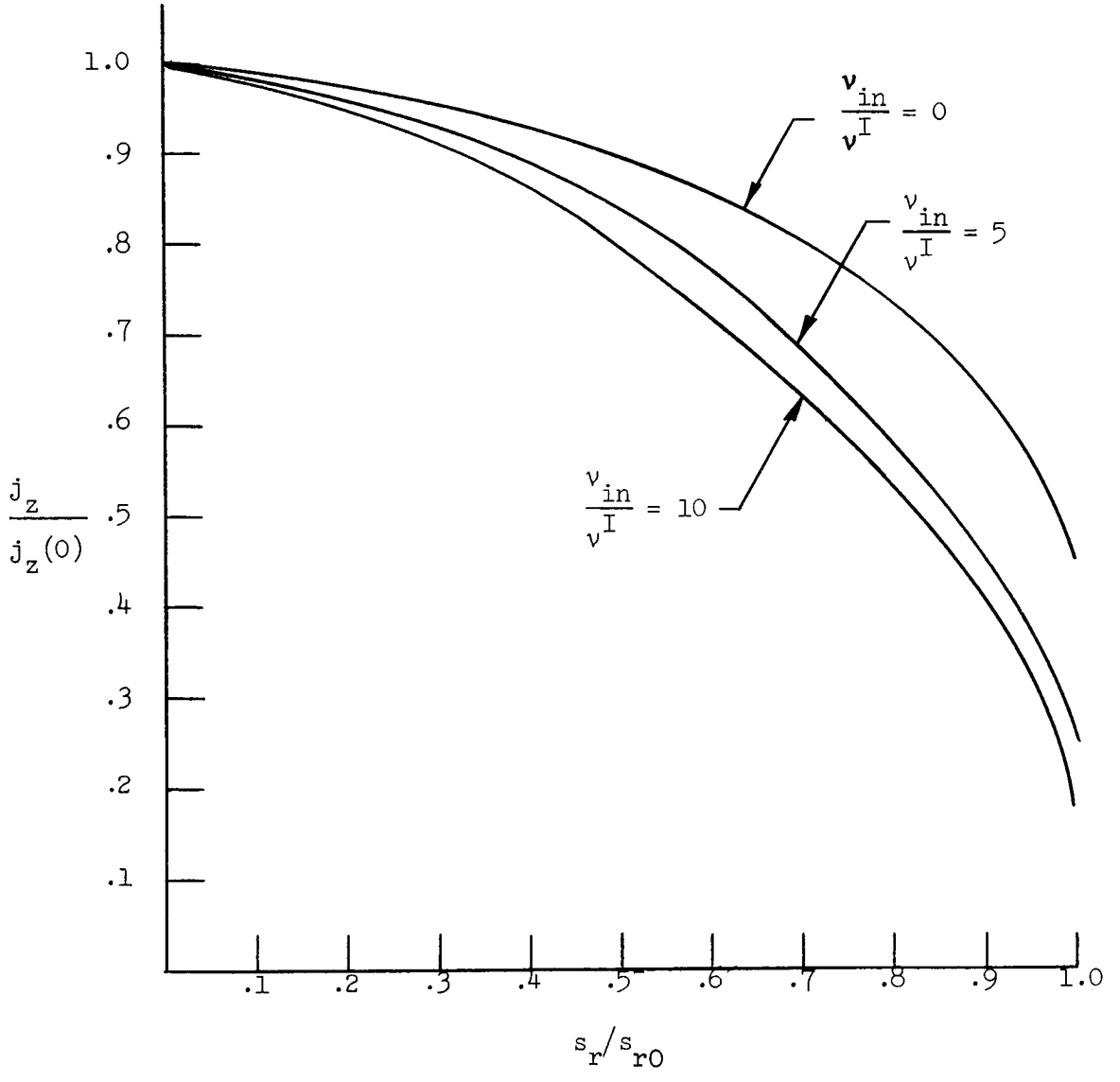

FIG. 29--Axial ion current as a function of radial position at the "end" of the discharge in a square box.

Notice that as the collision frequency is increased from the no collision case to $\nu_{in}/\nu^I = 5$ the current density decreases almost by a factor of two. This is because the ion density necessary to maintain the discharge is less, and this in turn is due to the fact that the ions and ionizing electrons remain in the discharge longer. The effect of collisions on the current density is shown in a different way in Fig. 29. In this figure, the current density is normalized to have the value unity on the s_1 axis. From this figure we see that the ion current density with collisions falls off more rapidly as the collisions frequency increases. The result goes over to the collision dominated or diffusion case as the collision frequency term

$$\nu_{in} \vec{v}$$

begins to dominate the equation of motion and the inertial term

$$\vec{v} \cdot \nabla \vec{v}$$

becomes less and less important. However, it is important to note that the nonlinear inertial term is essential even when there are many collisions present for it cannot be neglected in the determination of the boundary conditions at the walls.

Shown in Fig. 30 is the effect of collisions on the "wall" parameters of the discharge in a rectangular box. Normalized potential and wall distance are plotted as a function of increasing ion-neutral collision frequency. Notice that as the relative collision frequency increases the normalized wall distance decreases. For a square box of a given size this means that the ionizing frequency, necessary to maintain the discharge, decreases as the relative collision frequency increases since from Eq. (96)

$$\nu^I = \sqrt{\frac{2kT}{M}} \frac{s_{10}}{x_0} \quad .$$

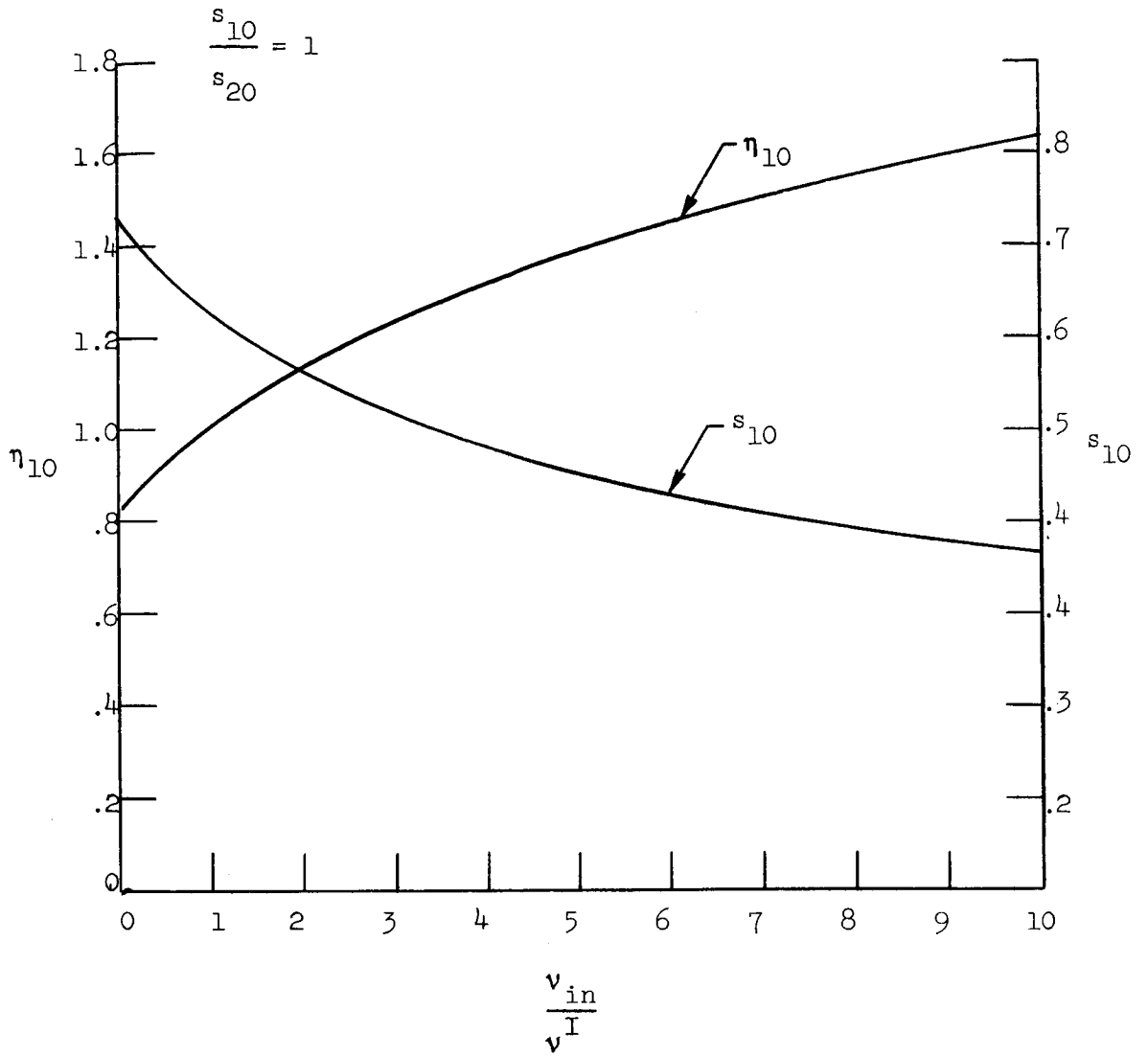

FIG. 30--Wall parameters of the two-dimensional discharge in a square box as a function of the relative ion-neutral collision frequency.

The normalized potential at the "wall" increases with relative ion-neutral collision frequency, thus resulting in a lower density since

$$\frac{n}{n_{e0}} = e^{-\eta} \quad .$$

Using the results of Figs. 31 and 32 we are able to determine two more interesting results. First, we are able, with the aid of Fig. 31, to answer the question of how long a rectangular discharge must be in order to appear "infinite", or in other words, in order that the parameters at the center of the discharge are the same as for an infinitely long $(s_{20}/s_{10} \to \infty)$ box. We see from Fig. 31 that less than 10% error in either normalized wall distance or normalized potential is encountered if the length of the discharge is greater than approximately 5.6 times the height. We will see later that even a shorter (length to radius) cylinder appears essentially infinite. Using Fig. 32 we can obtain some idea of the current to be expected at the end of a long rectangular discharge. From Fig. 32 we see that the normalized potential, η_2 , at the end of a long discharge does not appear to be reaching an asymptotic value. This result is further confirmed if we let α_2 approach infinity in Eq. (113). For v_2 finite we obtain from Eq. (113)

$$\eta_{20} = \lim_{\alpha_2 \to 0} \frac{1}{2} \ln\left(\frac{2Bv_{20}^2}{\alpha_2}\right)$$

or

$$\eta_{20} \to \infty \quad .$$

This means that for a "long" discharge, the density approaches zero and the current out of the end of the discharge must also approach zero. However, we note from Fig. 31 that the ratio of s_{20}/s_{10} must be very large indeed (greater than 16:1) in order for the density to be less than approximately 1/10 of its value at the discharge center.

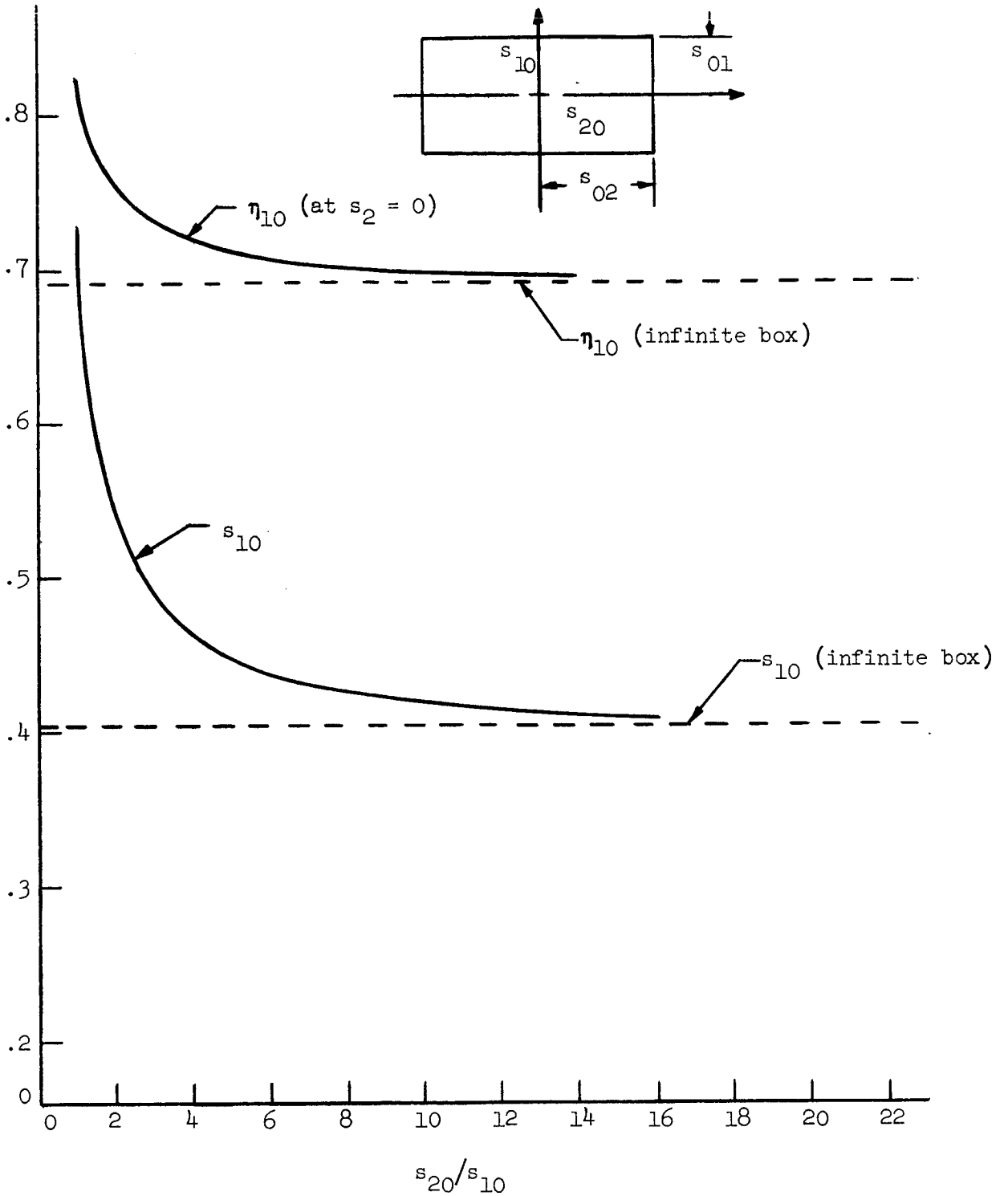

FIG. 31--Normalized wall distance and potential as a function of the length to width ratio in the two-dimensional rectangular discharge.

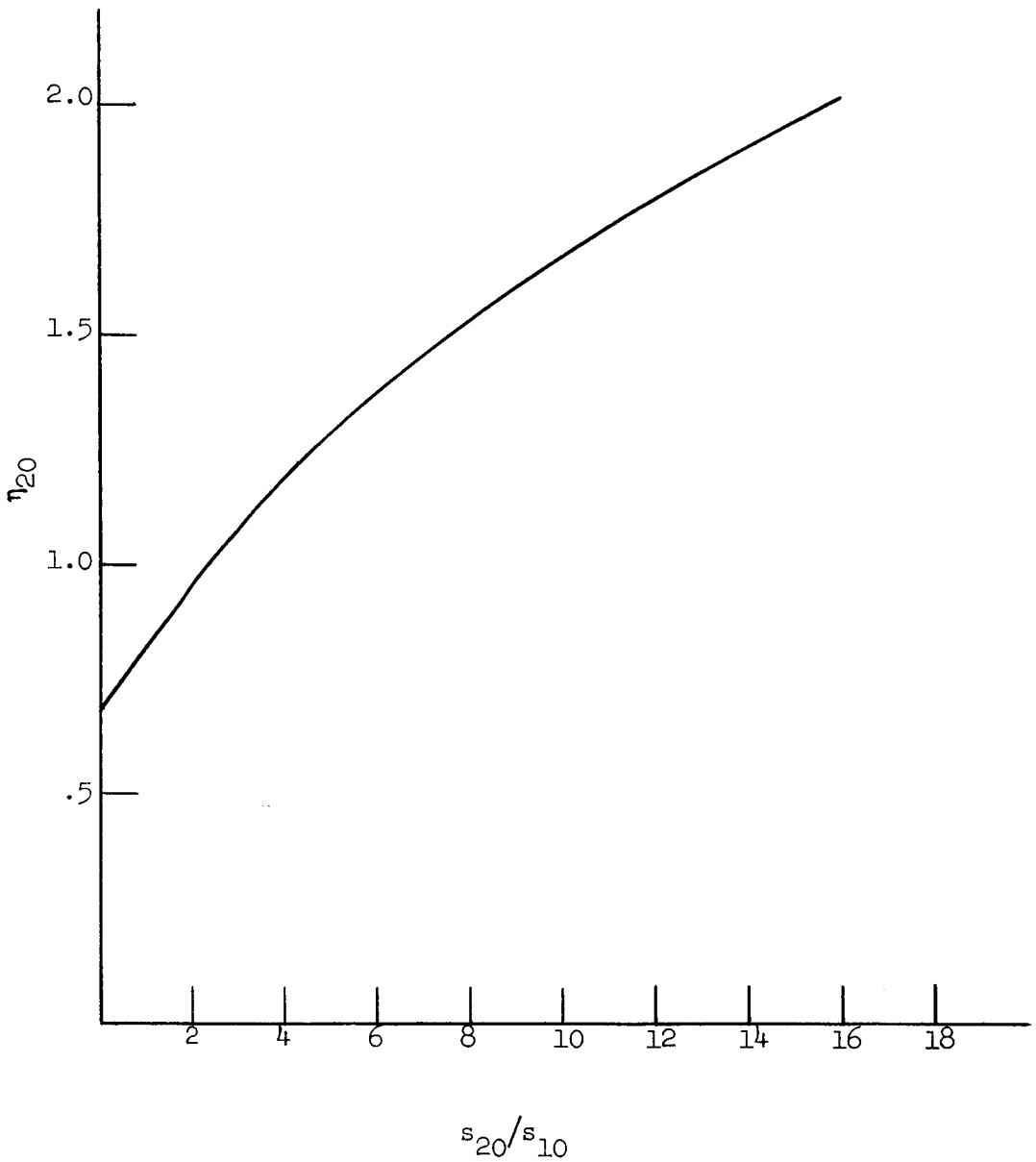

FIG. 32--Wall potential for the two-dimensional rectangular discharge as a function of the ratio of the length to the width of the discharge.

2. Finite Length Cylinder

(a) Derivation of equations

In cylindrical coordinates, neglecting the variation of any parameters in the theta or azimithal direction we obtain for Eqs. (92) and (95) in component form

$$\frac{\partial v_1}{\partial s_r} + \frac{v_1}{s_r} - v_1 \frac{\partial \eta}{\partial s_r} - v_2 \frac{\partial \eta}{\partial s_z} = 1 \quad , \tag{116}$$

$$v_1 \frac{\partial v_1}{\partial s_r} + B v_1 = \frac{1}{2} \frac{\partial \eta}{\partial s_r} \quad , \tag{117}$$

and

$$v_2 \frac{\partial v_2}{\partial s_z} + B v_2 = \frac{1}{2} \frac{\partial \eta}{\partial s_z} \quad , \tag{118}$$

where we have used the normalizations

$$s_r = \nu^I \left(\frac{M}{2kT}\right)^{1/2} r$$

$$s_z = \nu^I \left(\frac{M}{2kT}\right)^{1/2} z$$

$$v_1 = \left(\frac{M}{2kT}\right)^{1/2} v_r$$

$$v_2 = \left(\frac{M}{2kT}\right)^{1/2} v_z \quad .$$

Using the same method of separation of variables as for the rectangular case we obtain for the two-dimensional finite length cylinder, the separated equations:

$$(v_1^2 - \tfrac{1}{2}) \frac{\partial v_1}{\partial s_r} - \frac{v_1}{2s_r} + Bv_1^2 = -\frac{\alpha_r}{2} \tag{119}$$

and

$$(v_2^2 - \tfrac{1}{2}) \frac{\partial v_2}{\partial s_z} + Bv_2^2 = -\frac{\alpha_z}{2} \tag{120}$$

where

$$\alpha_z + \alpha_r = 1 \quad . \tag{121}$$

For this cylindrical case the Bohm Criteria is again satisfied at the boundary since

$$\frac{\partial v_1}{\partial z} \to \infty \tag{122}$$

when

$$v_1 = \frac{1}{\sqrt{2}} \quad . \tag{123}$$

Equation (120) has the same form of solution as the rectangular case, namely

$$Bs_z = -v_2 + \left(\frac{B}{2\alpha_z}\right)^{1/2} \left(1 + \frac{\alpha_z}{B}\right) \tan^{-1} \left[\left(\frac{2B}{\alpha_z}\right)^{1/2} v_2\right] \tag{124}$$

and

$$Bs_z = -\left(\frac{\alpha_z}{2B}\right)^{1/2}\left(e^{\left(\frac{2}{1+\alpha_z/B}\right)\eta_2} - 1\right)^{1/2} + \left(\frac{B}{2\alpha_z}\right)^{1/2}\left(1 + \frac{\alpha_z}{B}\right)\tan^{-1}\left[\left(e^{\left(\frac{2}{1+\alpha_z/B}\right)\eta_2} - 1\right)^{1/2}\right] \quad (125)$$

For the separated solution in the r direction it is again necessary to use the Runge-Kutta procedure and a computer.

In a form useful for computation purposes the separated equations in the r-direction are

$$\frac{\partial v_1}{\partial s_r} = \frac{\frac{v_1}{2s} - \frac{\alpha_r}{2} - v_1^2 B}{\left(v_1^2 - \frac{1}{2}\right)} \quad (126)$$

$$\frac{\partial \eta}{\partial s_r} = \frac{\frac{v_1^2}{s_r} - (\alpha_r + B)\, v_1}{\left(v_1^2 - \frac{1}{2}\right)} \quad . \quad (127)$$

We again note that at the T-L boundary the normalized velocity goes to the value given by the Bohm Criteria independent of the collision frequency or the size or shape of cylindrical discharge. The expansions near the origin necessary to "start" the solution by the Runge-Kutta method together with the normalized equations are summarized at the end of this chapter.

(b) Discussion of calculated results

Shown in Fig. 33 are the calculated equipotentials in a finite length cylinder with a length to radius ratio of 1.57. The general shape of these equipotentials is much like those of the rectangular box, and all of the general comments made in connection with the rectangular discharge apply to the discharge in a finite length cylinder.

One specific difference between the two discharges can be noted when we compare Figs. 34 and 31 which show the parameters of the discharges as the length becomes large. It was noted for the rectangular discharge that as long as the length to height ratio was greater than 5.6:1 the error in assuming an infinite discharge was less than 10%. From Fig. 34 we see that for the cylindrical discharge the length to radius ratio need only be 2.3:1 in order that the "wall" parameters at the center of the discharge differ by less than 10% from the values obtained for an infinitely long discharge.

3. Finite Length, Concentric Coaxial Cylinders

(a) Derivation of equations

The solutions for the discharge parameters between two concentric coaxial cylinders are generated from the same equations as for the cylindrical cases with only a change in the point of zero potential gradient. That is, we choose some value of normalized distance $s = s_m$ as the initial value point where we put

$$\frac{\partial \eta_1}{\partial s_r}(s_m) = 0$$

$$v_1(s_m) = 0$$

$$\eta_1(s_m) = 0$$

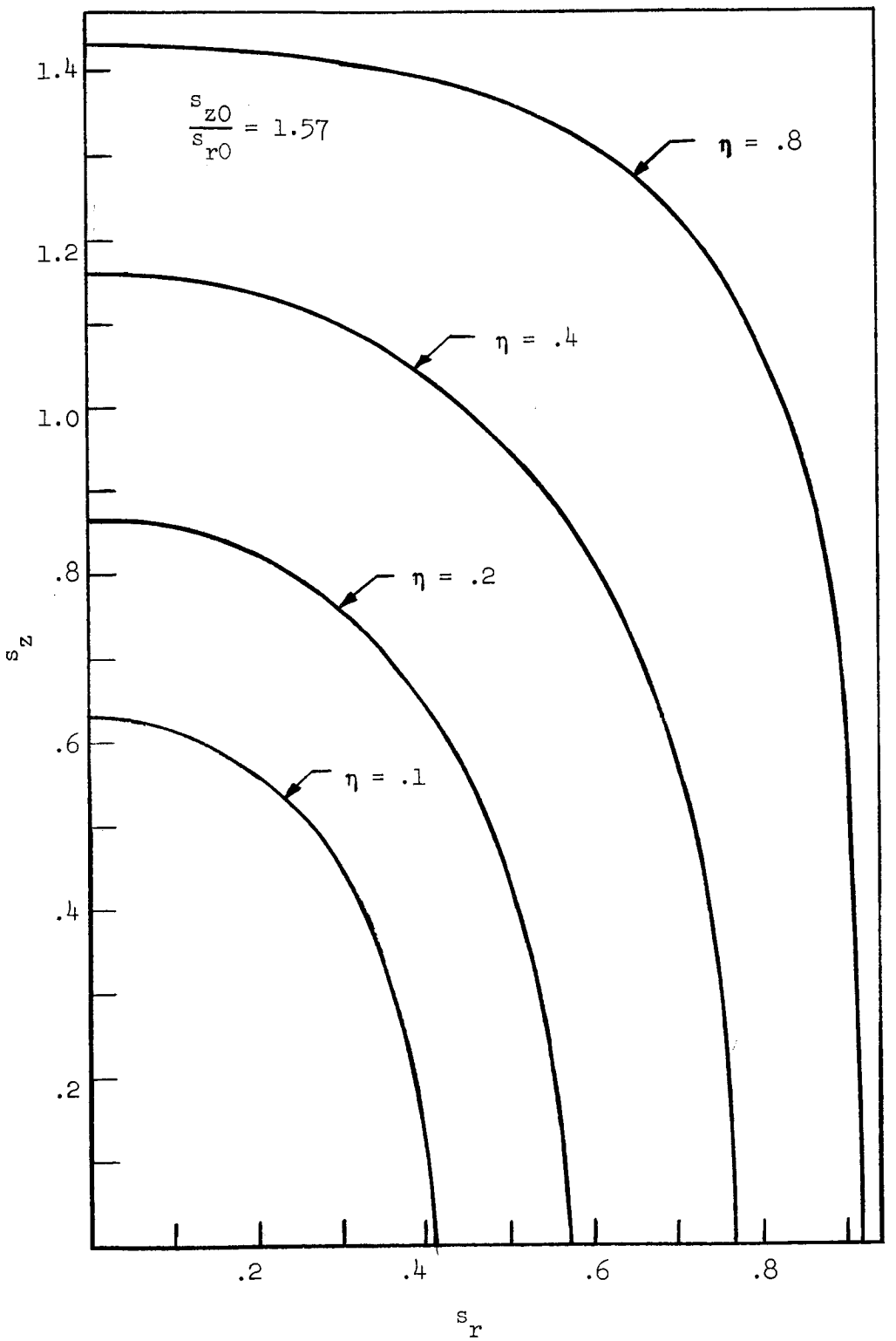

FIG. 33--Equipotentials in a two-dimensional cylindrical discharge.

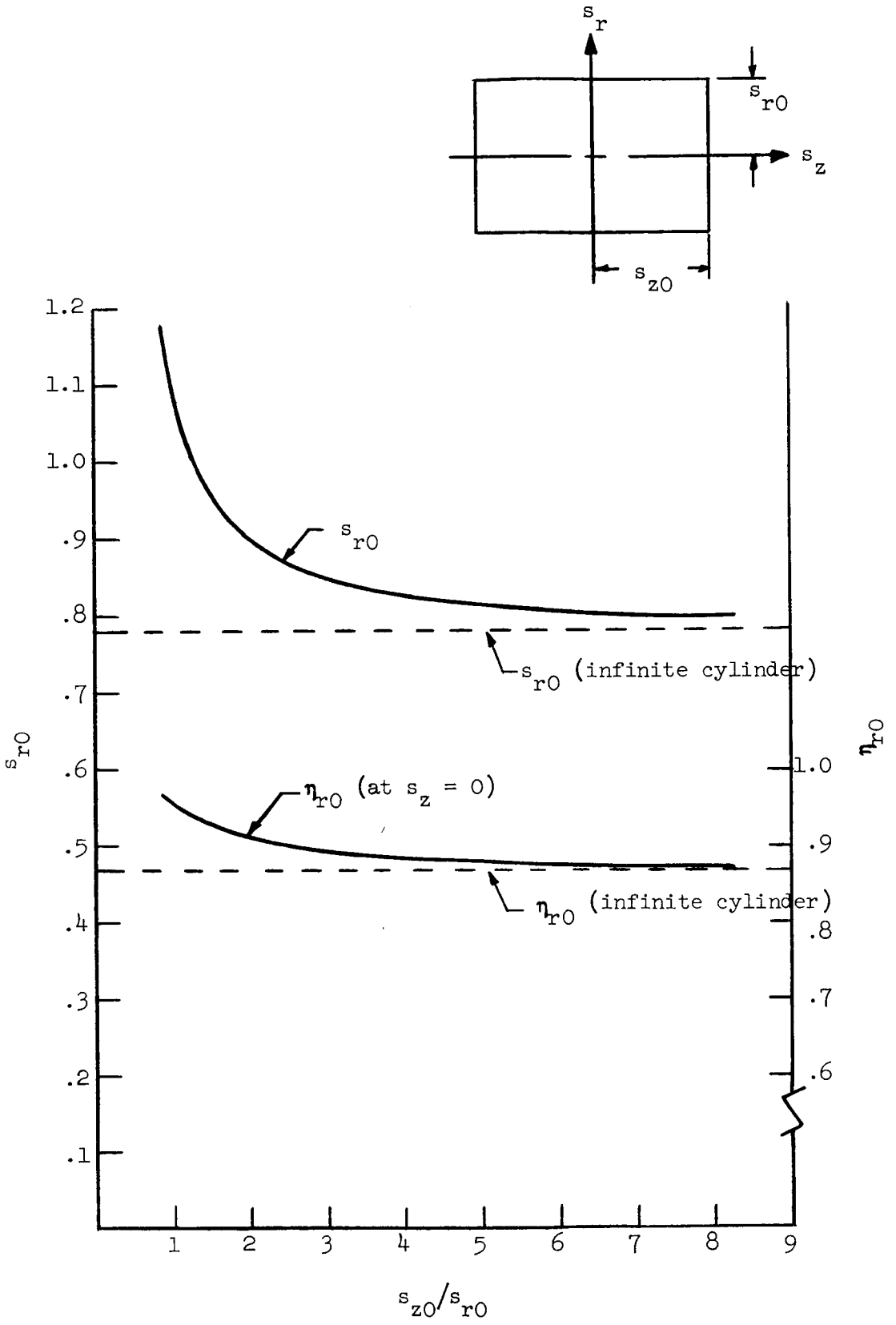

FIG. 34--Normalized wall distance and potential as a function of the length to radius ratio in the two-dimensional cylindrical discharge.

and solve for values of normalized potential and velocity for s greater than s_m and s less than s_m. We again find the velocities at both the inner and outer "walls" are given by the Bohm Criteria.

(b) Discussion of calculated results

The equipotentials for a very small inner conductor are shown in Fig. 35. In this figure the ratio of outer to inner radii is 30:1. In comparing this discharge with nearly the same shape cylindrical discharge of Fig. 33 we see that even a very small center conductor has considerable effect on the shape of the equipotentials at a radial distance of 10% of the outer radius even though the center conductor is only approximately 3.3% of the outer radius.

From the shape of the equipotentials of Fig. 35 one would expect the axial current density to reach a maximum value at approximately 20% of the outer radius of the discharge (at the point of minimum potential since $n/n_{e0} = e^{-\eta}$ and the axial velocity is constant at the wall). That this is true is shown in Fig. 36 where the normalized axial current at the end of the discharge is plotted as a function of radial distance from the center of the discharge. The case considered is for no collisions and with a value of $s_m = 0.2$.

The equipotentials in a discharge with a relatively much larger center conductor are shown in Fig. 37. In this discharge, the ratio of outer to inner conductors (b/a) is equal to 4.48. As b/a goes to unity we would expect this type of discharge to approach the discharge in a rectangular box. Even for the b/a value of Fig. 37 we already see that the equipotentials are becoming somewhat symmetrical.

Normalized axial current density as a function radial distance from the center of the two different discharges of Figs. 35 and 37 is compared in Fig. 38. It is interesting to note that a greater variation in current density is obtained for the discharge with the smallest center conductor.

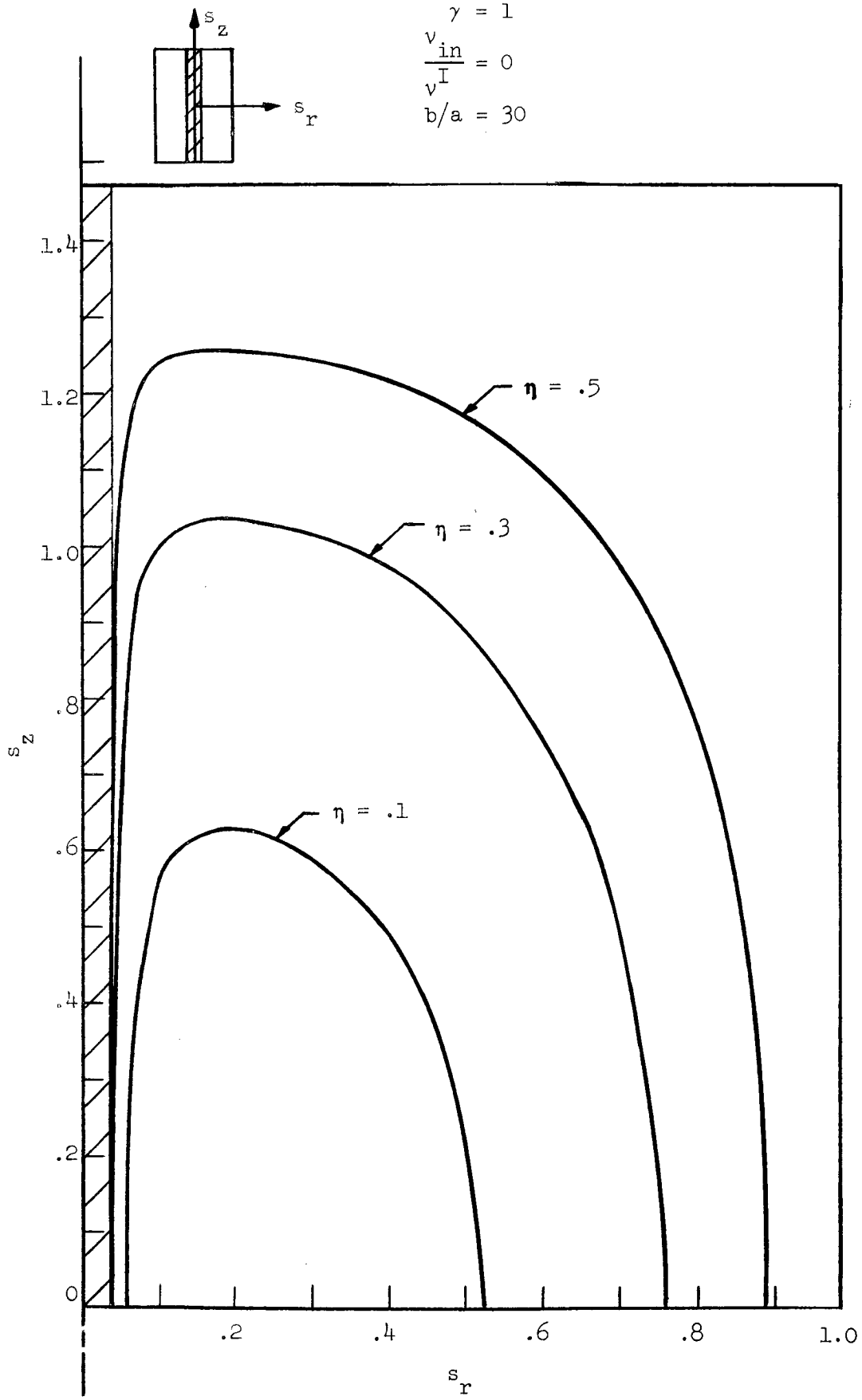

FIG. 35--Equipotentials in a "long" two-dimensional coaxial discharge.

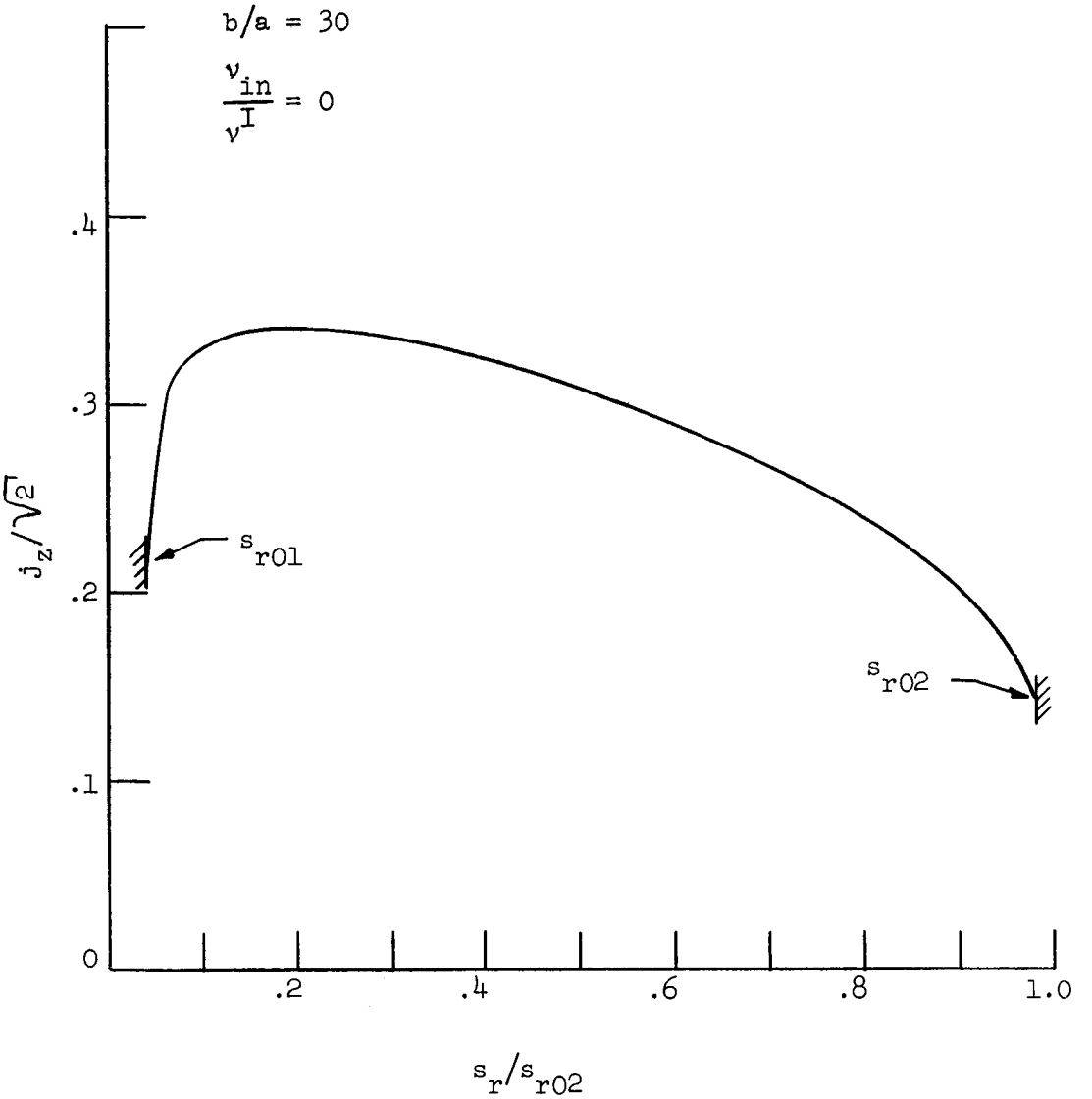

FIG. 36--Axial current as a function of radial distance for a "long" two-dimensional coaxial discharge.

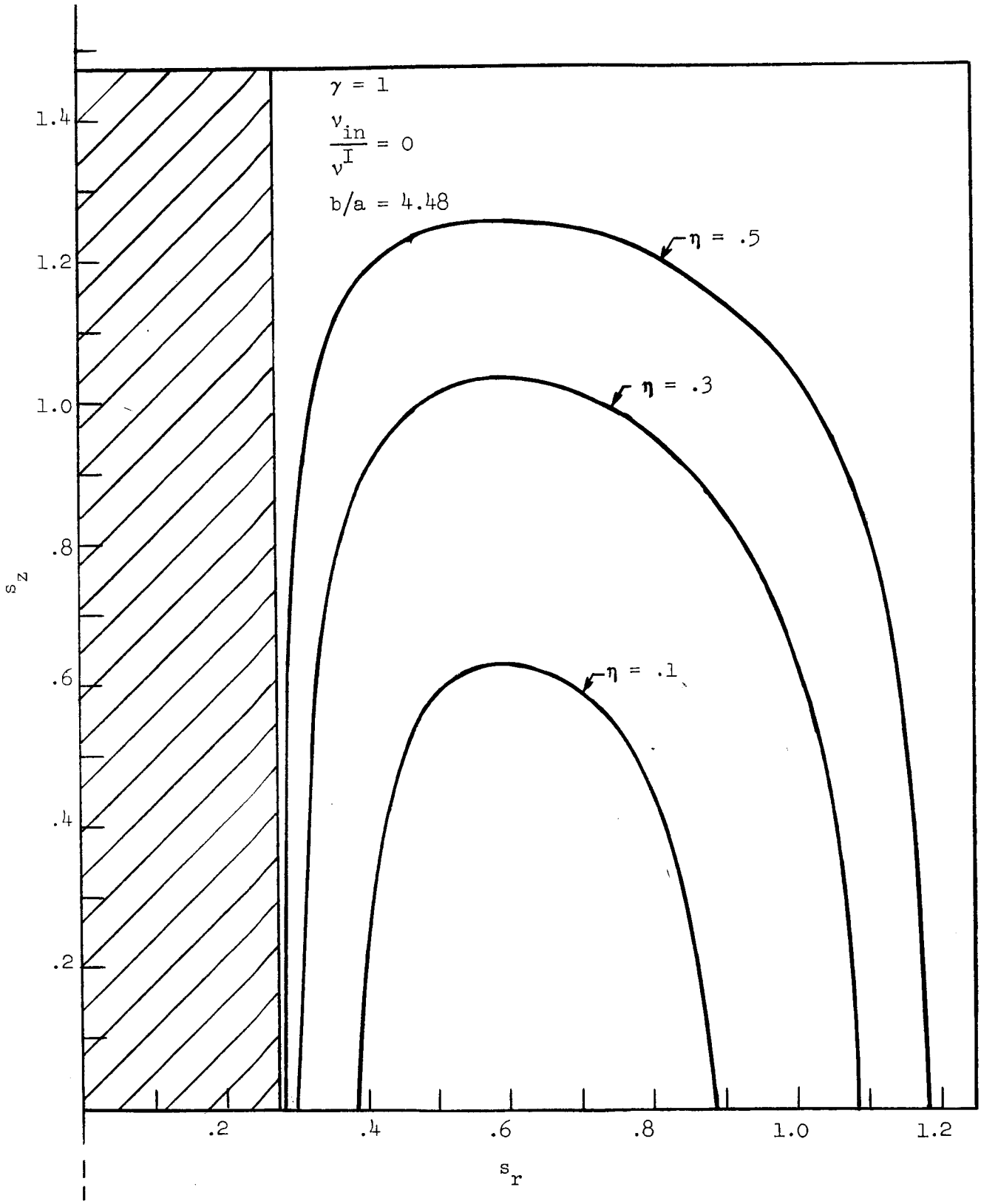

FIG. 37--Equipotentials in a "short" two-dimensional coaxial discharge.

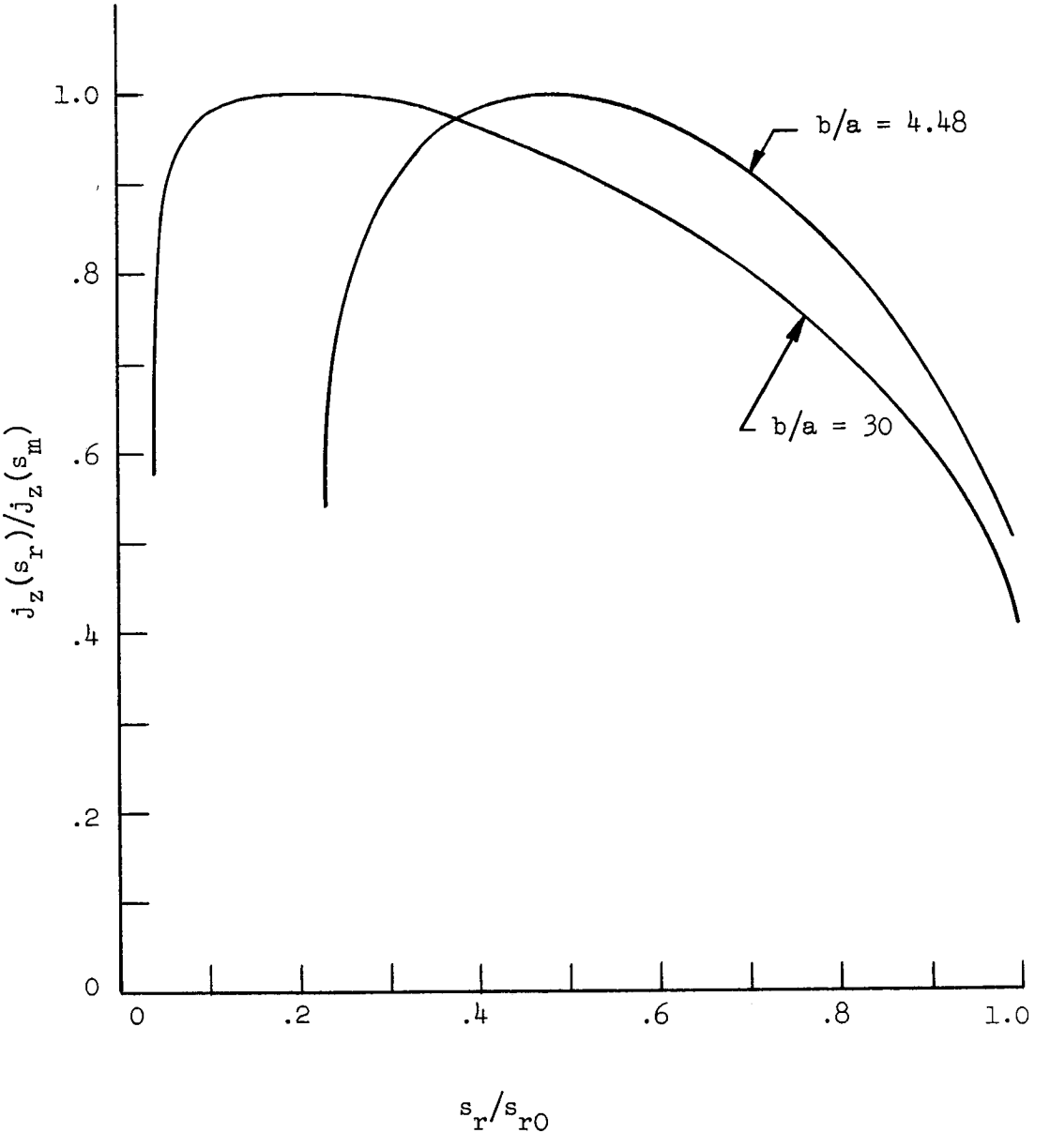

FIG. 38--Comparison of the axial ion current at the end of two finite-length coaxial discharges.

B. THE EFFECT OF A MAGNETIC FIELD IN THE PRESENCE OF COLLISIONS

1. Derivation of Equations

The effect of a longitudinal magnetic field can also be included in the two-dimensional cases provided we make the same assumptions as in the one-dimensional magnetic field cases. It is also necessary to make one further assumption in the two-dimensional cases discussed below. We assume an insulated-wall container so we know that the conditions

$$n_e v_{ez} = n_i v_{iz} \tag{128}$$

and

$$n_e v_{er} = n_i v_{ir} \tag{129}$$

are satisfied at the wall. It is also assumed that Eq. (128) and (129) are satisfied throughout the discharge. This is the common ambipolar diffusion assumption.

Only the case of a finite length cylinder will be carried out in detail since it is the most important case and since the other cases of a rectangular box and finite length coaxial cylinder follow immediately from the cylindrical case.

It is again necessary to solve for the motion of the electrons as well as the ions since the assumption of a M-B electron distribution is no longer valid. For the electrons the equations are

$$\nabla \cdot \vec{v}_e + \vec{v}_e \cdot \frac{\nabla n_e}{n_e} = \nu^I \tag{130}$$

and

$$\frac{kT_e}{m} \frac{\nabla n_e}{n_e} + (\nu^I + \nu_{en}) \vec{v}_e = \frac{e}{m} (\nabla\phi - \vec{v} \times \vec{B}) \quad . \tag{131}$$

Using the fact that $\nu_{en} \gg \nu^I$, normalizing, and expanding the above equations in component form we obtain for Eq. (130)

$$\frac{\partial v_1}{\partial s_r} + \frac{v_1}{s_r} + \frac{\partial v_2}{\partial s_z} + \frac{v_1 \partial U}{\partial s_r} + \frac{v_2 \partial U}{\partial s_r} = 1 \qquad (132)$$

and for Eq. (131), the equations

$$\frac{1}{2}\frac{M}{m}\frac{\partial U}{\partial s_r} + \frac{\nu_{en} v_1}{\nu^I} = -\frac{1}{2}\frac{M}{m}\frac{\partial \eta}{\partial s_r} + \frac{\omega_{ce} v_2}{\nu^I} \qquad (133)$$

and

$$\nu_{en} v_2 = -\omega_{ce} B_z v_1 \qquad (134)$$

$$\frac{1}{2}\frac{M}{m}\frac{\partial U}{\partial s_z} + \nu_{en}/\nu^I \, v_2 = -\frac{1}{2}\frac{M}{m}\frac{\partial \eta}{\partial s_z} \quad , \qquad (135)$$

where we have taken the magnetic field, B_z , to be in the z-direction with

$$\omega_{ce} = \frac{e}{m} B_z$$

$$U = \ell n \, (n/n_{e0})$$

and

$$n_e = n_i = n \quad .$$

Using Eq. (134) in Eq. (133) to eliminate v_2 , we obtain

$$\frac{\partial U_1}{\partial s_r} + \frac{2m}{M}\left(\frac{\nu_{en}^2 + \omega_{ce}^2}{\nu_{en}\nu^I}\right) v_1 = -\frac{\partial \eta}{\partial s_r} \quad . \qquad (136)$$

Equations (132), (135) and (136) constitute the equations for the electrons.

For the ions, again assuming the magnetic field effect to be negligible, the normalized equations are

$$\frac{v_1 \partial v_1}{\partial s_r} + \left(\frac{\nu^I + \nu_{in}}{\nu^I}\right) v_1 = \frac{1}{2}\frac{\partial \eta}{\partial s_r} \quad . \qquad (137)$$

Thus, we have four equations (132), (135), (136), (137) in the four unknowns U_1 , v_1 , v_2 , and η . The procedure of separation of variables is again used with

$$U = U_1(s_r) + U_2(s_z) \qquad (138)$$

$$v_1 = f(s_r) \text{ only} \qquad (139)$$

$$v_2 = f(s_z) \text{ only} \qquad (140)$$

$$\eta = \eta_1(s_r) + \eta_2(s_z) \quad . \qquad (141)$$

Using Eq. (138) through (139) and rearranging the Eqs. (132), (135), (136) and (137) into the form necessary for a computer solution we obtain the separated equations

$$\frac{\partial v_1}{\partial s_r} = \frac{v_1}{2s_r}\Big/\left(v_1^2 - \frac{1}{2}\right) - \left[v_1^2\left(1 + \frac{\nu_{in}}{\nu^I} + \frac{\omega_{ce}^2}{\nu^I \nu_{en} R_m}\right) + \frac{\alpha_1}{2}\right]\Big/\left(v_1^2 - \frac{1}{2}\right)$$

and

$$\frac{\partial \eta_1}{\partial s_r} = \left[- \alpha_1 v_1 - \frac{2}{R_m} \left(\frac{\nu_{en}^2 + \omega_{ce}^2}{\nu_{en} \nu^I} \right) v_1^3 + \frac{v_1^2}{s_r} - \left(1 + \frac{\nu_{in}}{\nu^I} \right) v_1 \right] \Bigg/ \left(v_1^2 - \tfrac{1}{2} \right) \tag{142}$$

$$\frac{\partial U_1}{\partial s_r} = \left\{ \left[\alpha_1 + 1 + \frac{\nu_{in}}{\nu^I} + \frac{m}{M} \left(\frac{\nu_{en}^2 + \omega_{ce}^2}{\nu_{en} \nu^I} \right) \right] v_1 - \frac{v_1^2}{s_r} \right\} \Bigg/ \left(v_1^2 - \tfrac{1}{2} \right) \tag{143}$$

$$\frac{\partial v_2}{\partial s_z} = \left[- \left(1 + \frac{\nu_{in}}{\nu^I} \right) v_2^2 - \frac{\alpha_2}{2} \right] \Bigg/ \left(v_2^2 - \tfrac{1}{2} \right) \tag{144}$$

$$\frac{\partial \eta_2}{\partial s_z} = \left[- \alpha_2 v_2 - v_2 \left(1 + \frac{\nu_{in}}{\nu^I} \right) \right] \Bigg/ \left(v_2^2 - \tfrac{1}{2} \right) \tag{145}$$

and finally

$$\frac{\partial U_2}{\partial s_z} = \left[\alpha_2 v_2 + v_2 \left(1 + \frac{\nu_{in}}{\nu^I} \right) \right] \Bigg/ \left(v_2^2 - \tfrac{1}{2} \right) \quad . \tag{146}$$

These equations, because of their more limited and specific nature, are not included in the summary at the end of this chapter. The Taylor series expansions near the origin are given below for the cylindrical case:

$$v_1 = \frac{\alpha_1}{2} s_r + \ldots$$

and

$$\eta_1 = \frac{\alpha_1}{2}\left[\frac{\alpha_1}{2} + B\right] s_r^2 + \ldots$$

$$U_1 = -\frac{\alpha_1}{2}\left[\frac{\alpha_1}{2} + A + B\right] s_r^2 + \ldots$$

$$v_2 = \alpha_2 s_z + \ldots$$

$$\eta_2 = \alpha_2 B s_z^2 + \ldots$$

$$U_2 = -\alpha_2 B s_z^2 + \ldots$$

where

$$B = 1 + \frac{\nu_{in}}{\nu^I}$$

$$A = \frac{\nu_{in}}{\nu^I} + \frac{\omega_{ce}^2}{\nu^I \nu_{en} R_m}$$

and

$$R_m = \frac{M}{m}$$

2. Discussion of Calculated Results

Of most interest because of the possible application to the study of ion thrustors is the axial current at the end of the coaxial discharge and the effect of magnetic field on this current. Shown in Fig. 39, for the collisionless case of a cylinder with a length to radius ratio of 2:1, is the normalized axial ion current as a function of distance from the z-axis for increasing values of magnetic field.

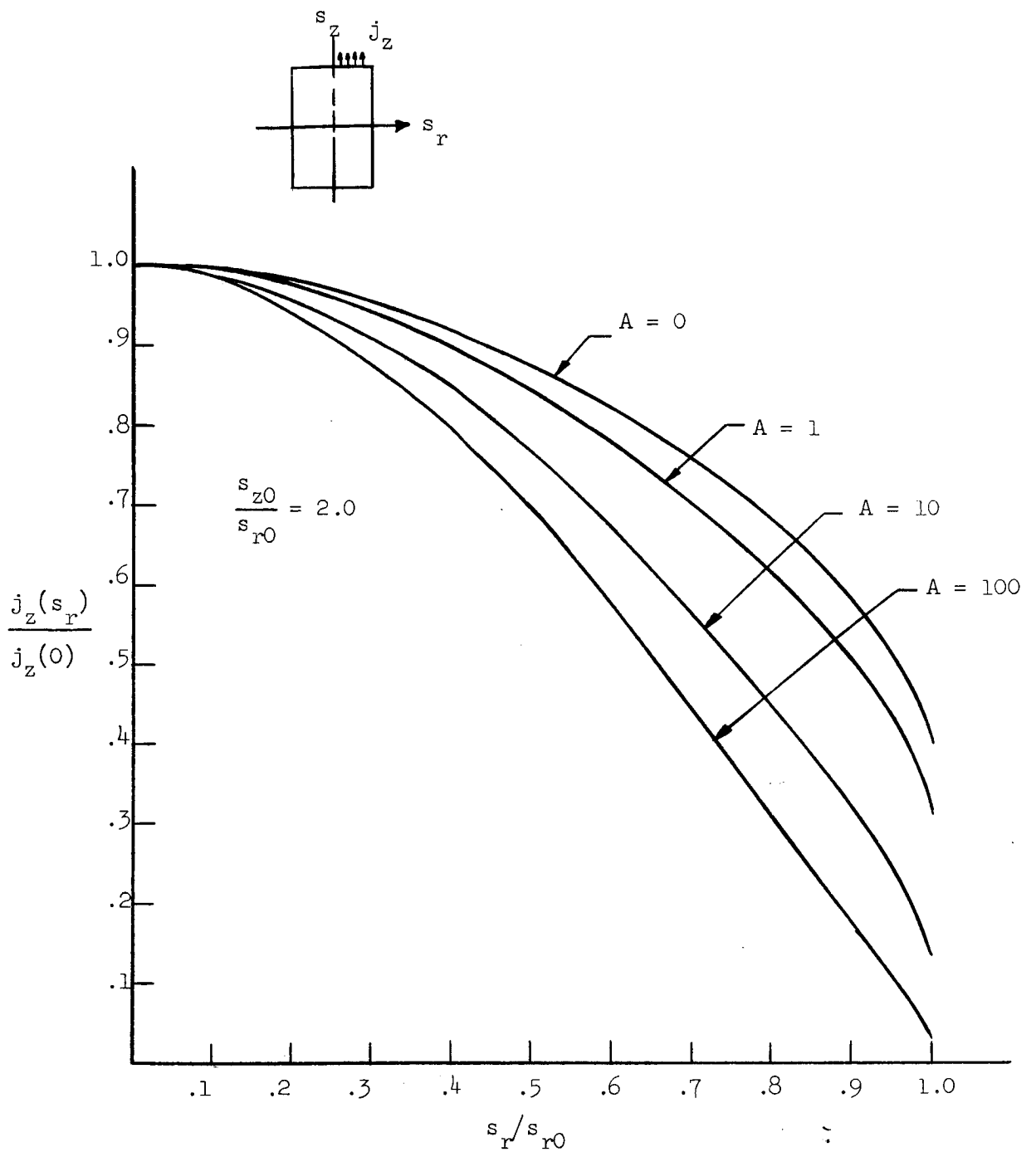

FIG. 39--Axial ion current as a function of radial position for a two-dimensional discharge with an applied axial magnetic field.

The parameter A is directly proportional to magnetic field for this collisionless case. The curves of Fig. 39 show that as the magnetic field is increased the axial current density becomes more and more non-uniform. One might be led to the conclusion that in order to have more uniform current density the magnetic field should be zero. However, this would be an erroneous conclusion since for a given size of discharge the magnetic field increases the percentage of ionization and thus the overall ion current in the axial direction and the overall efficiency of the device.

The primary effect of the magnetic field is to cause the electrons to cycloid many times as they move from where they are generated to the edge of the discharge. The electrons are thus more likely to have an ionizing collision before they reach the wall. Since the axial magnetic field has no effect on the axial motion of either ions or electrons, for a given choice of geometry parameter, α_z , the separated solution in the z direction is unaffected. However, the magnetic field has a large effect on the parameters of the discharge in the r direction, as shown in Fig. 40. Here the normalized length to radius ratio is plotted as a function of magnetic field. We note that as the magnetic field is increased for a given choice of geometry parameters α_r and α_z , the solution applied to a longer and longer discharge. Physically, what is happening is that the collision frequency in the radial direction necessary to maintain the discharge is decreasing as the magnetic field increases. This is a perfectly reasonable physical result in view of the longer time spent by each electron in moving to the "wall."

We should point out that we do not intend to cover all possible shapes and magnetic field situations. Rather we have shown that by presenting some solutions selected to illustrate specific points the results obtained by this general method are physically reasonable. In order to facilitate the calculation of other cases, the equations are presented in all cases in a form useful for computation purposes. In order to use the equations to calculated various geometries, Fig. 41 has been prepared. This figure gives the value of α_r (and thus α_z) to use for various geometries and magnetic fields.

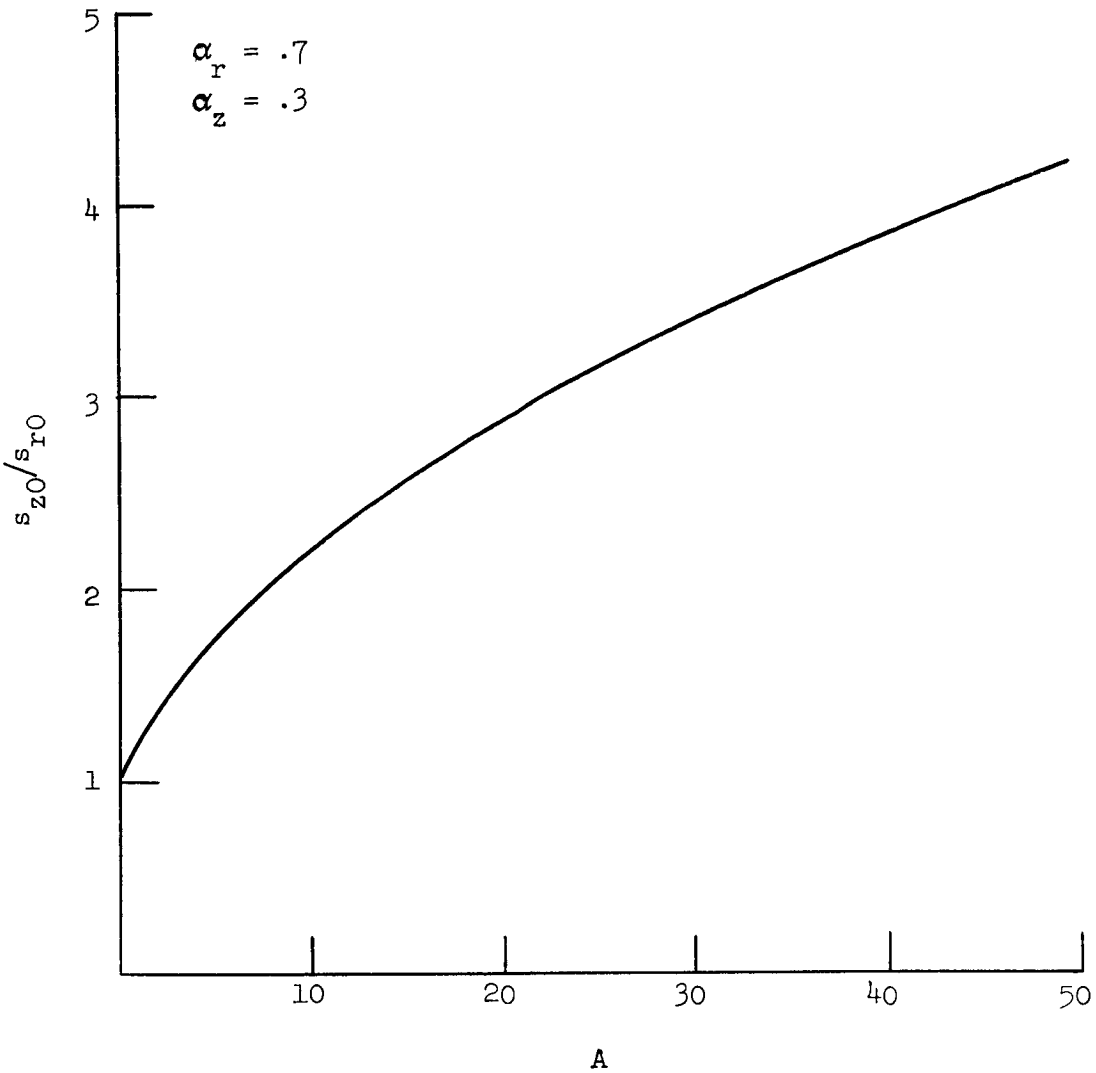

FIG. 40--Effect of magnetic field on the length to radius ratio of the two-dimensional cylindrical discharge.

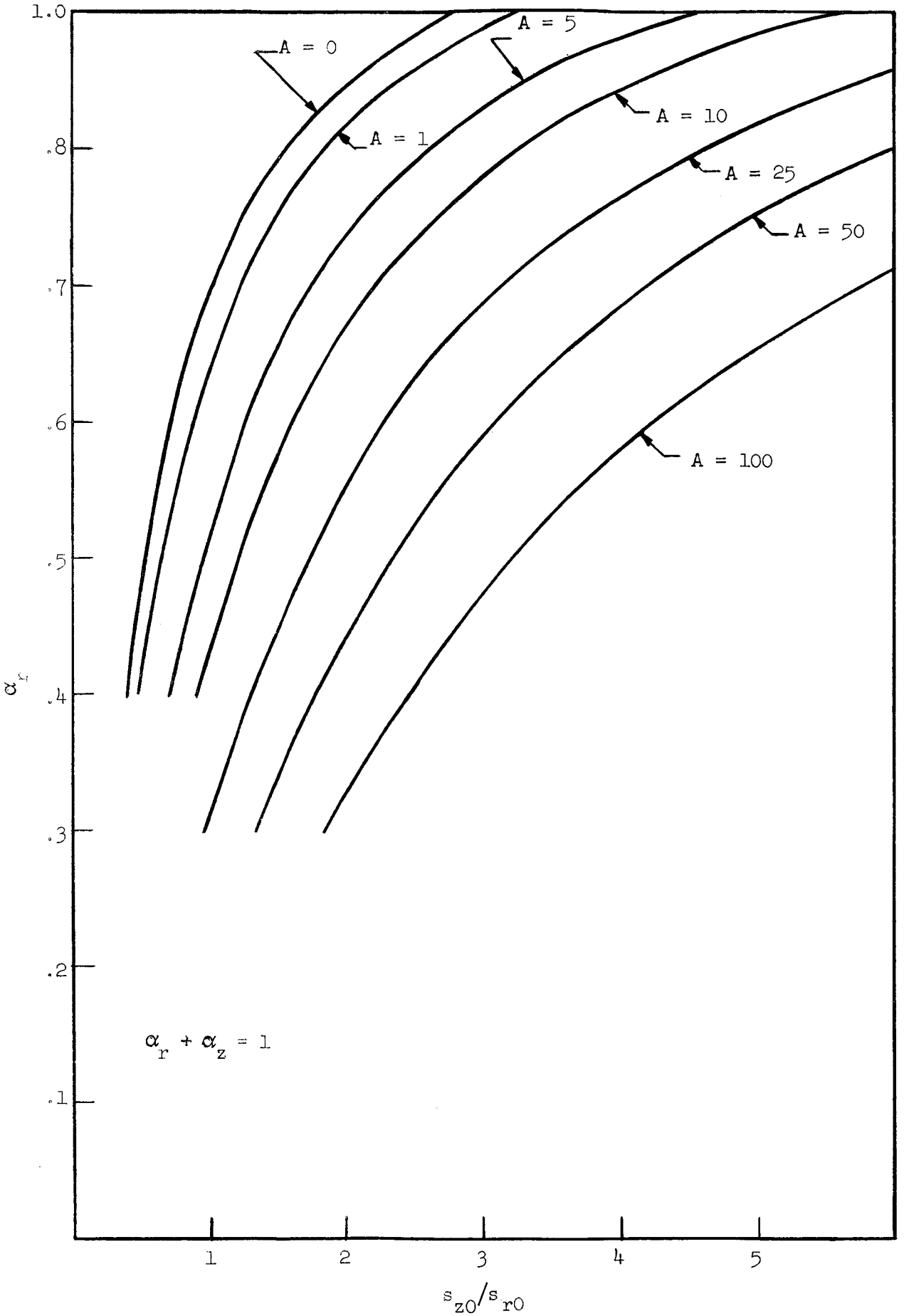

FIG. 41--Shape parameter of the two-dimensional cylindrical discharge as a function of the length to radius ratio for various values of magnetic field.

C. SUMMARY OF TWO-DIMENSIONAL EQUATIONS AND SOLUTIONS

Tabulated below are the equations which describe the discharges in a rectangular box, a finite length cylinder, and a finite length discharge between concentric coaxial cylinders. The same approximations summarized in Part C of Chapter III also apply to the two-dimensional discharges, and these should be kept in mind when applying the equations to a particular discharge. One additional restriction is that the generation rate for all two-dimensional cases is taken as proportional to electron density $(\gamma = 1)$.

The normalizations used are summarized below.

(1) Rectangular geometry:

$$v_1 = \left(\frac{M}{2kT}\right)^{1/2} v_x$$

$$v_2 = \left(\frac{M}{2kT}\right)^{1/2} v_y$$

$$\eta = \eta_1 + \eta_2$$

$$\eta_1 = -\frac{e\phi_1}{kT}$$

$$\eta_2 = -\frac{e\phi_2}{kT}$$

$$n = n_{e0} e^{-\eta} = n_{e0} e^{-(\eta_1+\eta_2)}$$

$$s_1 = \left(\frac{M}{2kT}\right)^{1/2} \nu I_x$$

and

$$s_2 = \left(\frac{M}{2kT}\right)^{1/2} \nu I_y$$

(2) Cylindrical and Coaxial Geometry:

$$v_1 = \left(\frac{M}{2kT}\right)^{1/2} v_r$$

$$v_2 = \left(\frac{M}{2kT}\right)^{1/2} v_z$$

$$\eta = \eta_1 + \eta_2$$

$$\eta_1 = -\frac{e\phi_1}{kT}$$

$$\eta_2 = -\frac{e\phi_2}{kT}$$

$$n = n_{e0} e^{-\eta} = n_{e0} e^{-(\eta_1+\eta_2)}$$

$$s_r = \left(\frac{M}{2kT}\right)^{1/2} \nu I_r$$

$$s_z = \left(\frac{M}{2kT}\right)^{1/2} \nu I_z$$

1. Rectangular Box

The equations of the rectangular box with collisions are:

$$Bs_1 = -v_1 + \left(\frac{B}{2\alpha_1}\right)^{1/2}\left(1 + \frac{\alpha_1}{B}\right)\tan^{-1}\left[\left(\frac{2B}{\alpha_1}\right)^{1/2} v_1\right]$$

$$Bs_2 = -v_2 + \left(\frac{B}{2\alpha_2}\right)^{1/2}\left(1 + \frac{\alpha_2}{B}\right)\tan^{-1}\left[\left(\frac{2B}{\alpha_2}\right)^{1/2} v_2\right]$$

and

$$Bs_1 = -\left(\frac{\alpha_1}{2B}\right)^{1/2}\left(e^{\left(\frac{2}{1+\alpha_1/B}\right)\eta_1} - 1\right) + \left(\frac{B}{2\alpha_1}\right)^{1/2}\left(1 + \frac{\alpha_1}{B}\right)\tan^{-1}\left[\left(e^{\left(\frac{2}{1+\alpha_1/B}\right)\eta_1} - 1\right)^{1/2}\right]$$

$$Bs_2 = -\left(\frac{\alpha_2}{2B}\right)^{1/2}\left(e^{\left(\frac{2}{1+\alpha_2/B}\right)\eta_2} - 1\right) + \left(\frac{B}{2\alpha_2}\right)^{1/2}\left(1 + \frac{\alpha_2}{B}\right)\tan^{-1}\left[\left(e^{\left(\frac{2}{1+\alpha_2/B}\right)\eta_2} - 1\right)^{1/2}\right]$$

where

$$B = 1 + \frac{\nu_{in}}{\nu_I}$$

and

$$\alpha_1 + \alpha_2 = 1 \quad .$$

2. Finite Length Cylinder and Concentric Coaxial Cylinders

a. Axial direction

The equations in the z direction are the same for both the cylindrical and coaxial equations and are given by

$$Bs_z = -v_2 + \left(\frac{B}{2\alpha_z}\right)^{1/2}\left(1 + \frac{\alpha_z}{B}\right)\tan^{-1}\left[\left(\frac{2B}{\alpha_z}\right)^{1/2} v_2\right]$$

and

$$Bs_z = -\left(\frac{\alpha_z}{2B}\right)^{1/2}\left(e^{(\frac{2}{1+\alpha_z/B})\eta_2} - 1\right)^{1/2} + \left(\frac{B}{2\alpha_z}\right)^{1/2}\left(1 + \frac{\alpha_z}{B}\right)\tan^{-1}\left[\left(e^{(\frac{2}{1+\alpha_z/B})\eta_2} - 1\right)^{1/2}\right]$$

b. Radial direction

In the radial direction the equations must again be solved by computer. In a form useful for solution the equations are:

$$\frac{\partial v_1}{\partial s_r} = \frac{\frac{v_1}{2s} - \frac{\alpha_r}{2} - v_1^2 B}{(v_1^2 - \frac{1}{2})}$$

and

$$\frac{\partial \eta_1}{\partial s_r} = \frac{\frac{v_1^2}{s_r} - (\alpha_r + B)\, v_1}{(v_1^2 - \frac{1}{2})} ,$$

where $\alpha_r + \alpha_z = 1$ and depend on the shape of the discharge.

In order to solve the above equations using the Runge-Kutta method it is necessary to expand the solutions in a Taylor series near the initial point. For the finite length cylinder the expansions are

$$v_1 = \frac{\alpha_r}{2} s_r + \ldots$$

and

$$\eta_1 = \frac{\alpha_r}{2}\left(\frac{\alpha_r}{2} + B\right)s_r^2 + \ldots \quad .$$

For convenience of calculation, the value of α_r for various geometries has been plotted in Fig. 42.

Using this figure and given a particular length to radius ratio, α_r can be found and thus α_z from

$$\alpha_z = 1 - \alpha_r \quad .$$

For the coaxial cases, the expansions near the point $s = s_m$ are

$$v_1 = \alpha_r(s_r - s_m) + \ldots$$

and

$$\eta_1 = \alpha_r\,(\alpha_r + B)\,(s_r - s_m)^2 + \ldots \quad ,$$

where the value of s_m determines the ratio of outer to inner radii of the discharge.

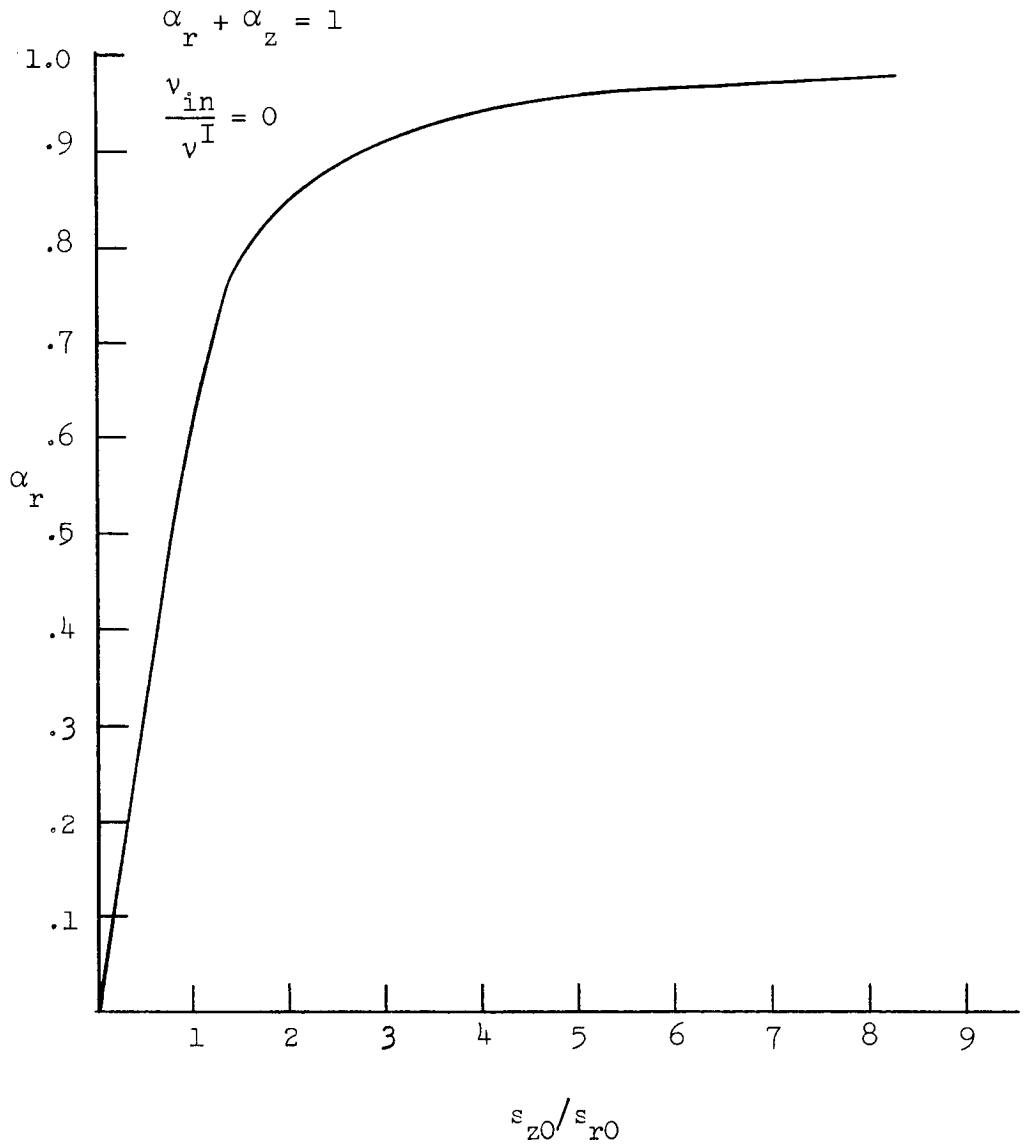

FIG. 42--Shape parameter of the two-dimensional cylindrical discharge as a function of the length to radius ratio of the cylinder

CHAPTER V

NUMERICAL METHODS FOR GENERAL BOUNDARY CONDITIONS AND VARIABLE GENERATION

Although the two-dimensional coaxial and cylindrical cases are certainly the most useful and important because many of the devices of interest tend to conform to these geometries, it would be of considerable interest to be able to solve two-dimensional problems for more general boundary and generation conditions. One application of these more general results would be in a study of discharge shapes for optimizing longitudinal ion current. Another use for a more general analysis would be in studying the effect of a varying generation rate throughout a particular discharge. Thus, in recognition of the value of such a generalization of the problem considerable work was done on trying to formulate finite-difference numerical methods of solving the equations of one- and two-dimensional discharges.

A great deal of difficulty was encountered in trying to solve the general two-dimensional discharge as a boundary value problem. Although some reasonable results were obtained for the one-dimensional cases, only very limited success in solving the general two-dimensional problem was achieved.

It is shown in Appendix C that the separation of variables which allows an exact solution for the case of generation proportional to electron density with zero vorticity cannot be extended to include any other generation condition. Because of the generation term and the curl of the velocity not being zero, the more standard and straightforward fluid type approaches such as a transformation to the hodographic plane cannot be used.[43] It therefore appears that a numerical procedure must be used to obtain more general results.

In this chapter the difficulties associated with a general numerical procedure of solution are first outlined, followed by a discussion of two procedures which were successfully used to solve the one-dimensional

problem as a general boundary value problem. Finally, one of the numerical methods which was successful in one dimension is applied to the two-dimensional problem where it is possible to use this technique to solve only a limited two-dimensional problem because of difficulties with the convergence of the solution.

A. DIFFICULTIES OF THE PROBLEM

All of the cases which have been previously studied in Chapters III and IV have been solved as initial value problems. In order to solve for the discharge configurations with more general boundaries, the equations of the discharge must be solved as boundary value problems. This immediately creates a difficult problem at the outer plasma boundary in that both the derivatives of potential and velocity with respect to distance go to infinity. This means that when numerical procedures are used a computer solution can never give the correct answer at the plasma boundary as long as the distance variable is taken as the independent variable. It also means that obtaining convergence to any solution near the boundary or "wall" of the plasma can be expected to be difficult.

Another difficulty which manifests itself when the plasma problem is set up as a boundary value problem is the appearance in the equations of an unknown distance parameter. In the initial value problem this distance parameter is easily normalized out without restricting the solution. As we will see in the next section, in order to eliminate this distance parameter in the boundary value problem we must restrict the solution to cases for which the generation is not proportional to electron density $(\gamma \neq 1)$. This is a rather severe restriction.

As in many two dimensional problems which one wishes to solve by finite difference procedures there is a problem with obtaining enough computer storage. In the IBM 7090 computer the fast access core contains somewhat less than 32 thousand words of storage. As we will see below, the most straightforward procedure for solving two-dimensional problems cannot be used because of limitations in computer storage.

One final general problem associated with nonlinear partial differential equations of this type is the difficulty, and in most cases the impossibility, of finding the region of convergence for any particular finite difference scheme.

B. ONE-DIMENSIONAL NUMERICAL APPROACHES

All of the numerical methods were initially developed and checked in one dimension since solutions were available for one-dimensional cases by which convergence to the correct solution could be verified.

Two different numerical approaches were used to solve the one-dimensional problem.

1. Newton-Raphson Method

The first method used was a reasonably straightforward application of the Newton-Raphson method.[44] This method of solving simultaneous nonlinear equations is applied as follows: If we call the N equations in the N unknowns which we wish to solve the F_j equations we then have a set of equations of the form

$$\begin{aligned} F_1(\phi_1, \phi_2, \phi_3, \cdots, \phi_N) &= 0 \\ F_2(\phi_1, \phi_2, \phi_3, \cdots, \phi_N) &= 0 \\ &\vdots \\ F_N(\phi_1, \phi_2, \phi_3, \cdots, \phi_N) &= 0 \quad , \end{aligned}$$

where the unknowns are the ϕ_j's . Each of the above equations is expanded in a Taylor series about some initial guessed value of the ϕ_j's , keeping only the lowest order terms in the expansion. The above equations

thus become

$$\sum_{i=1}^{N}\left(\frac{\partial F_1}{\partial \phi_i}\right)_0 \Delta\phi_1 = -F_{10}$$

$$\sum_{i=1}^{N}\left(\frac{\partial F_2}{\partial \phi_i}\right)_0 \Delta\phi_2 = -F_{20}$$

$$\vdots$$

$$\sum_{i=1}^{N}\left(\frac{\partial F_N}{\partial \phi_i}\right)_0 \Delta\phi_N = -F_{N0} \quad ,$$

where the subscript "0" denotes an initial "guessed" value. These simultaneous (now linear) equations are then solved for the $\Delta\phi_j$'s which are in turn used to improve the initially guessed ϕ_{j0}'s which are used to find new $\Delta\phi_j$'s , etc., until a final convergent solution is obtained. First, in order to set up the one-dimensional problem for solution by the N-R method, a new normalization was introduced defining a new distance variable z such that

$$z = s/s_w \quad , \tag{147}$$

where s_w is the normalized distance to the wall. In this new normalization, the one-dimensional equations are (in rectangular coordinates)

$$\frac{dv}{dz} - v\frac{d\eta}{dz} - e^{(1-\gamma)\eta} = 0 \tag{148}$$

and

$$\left[-12v^2 s_w^2 - 3\left(1 - e^{(1-\gamma)\eta}\right)\right]\frac{dv}{dz} + (4v^3 s_w^2 + v)\frac{d\eta}{dz} = 0 \quad , \tag{149}$$

where s_w is treated as another unknown. Next, the region of solution between $z = 0$ and $z = 1$ is divided into a finite number of intervals or mesh points. Equations (148) and (149) are then written in finite difference form at each node of the mesh, being careful to use central differences for the first-derivative terms. These finite difference equations plus the boundary conditions

$$\frac{\partial \eta}{\partial z}(0) = 0$$

$$v(0) = 0$$

and

$$\frac{\partial \eta}{\partial z}(1) = DZ_{max}$$

written also in finite difference from constitute the closed set of equations which were solved by the N-R method, DZ_{max} being the value of the derivative of potential at the outer boundary. Strictly speaking, DZ_{max} should be taken to be infinity at the boundary. However, for computation purposes it was found that a value of DZ_{max} of four would give reasonably good answers for the potential and that higher values did not improve the accuracy at the "wall."

Convergent solutions and reasonably good accuracy were obtained for most of the parameters of the one-dimensional discharge for all three generation rates corresponding to $\gamma = 0$, 1, and 2. The results are shown in Fig. 43. The values of potential plotted in Fig. 43 agree fairly closely with the exact solutions of the same equations from Chapter III which are also plotted on the figure. The computer calculated values of the normalized distance to the wall, s_w, are not in good agreement with the exact solutions due to the problem of accuracy of solution near the plasma boundary where the computer cannot simulate the rapid change of the variables η and v.

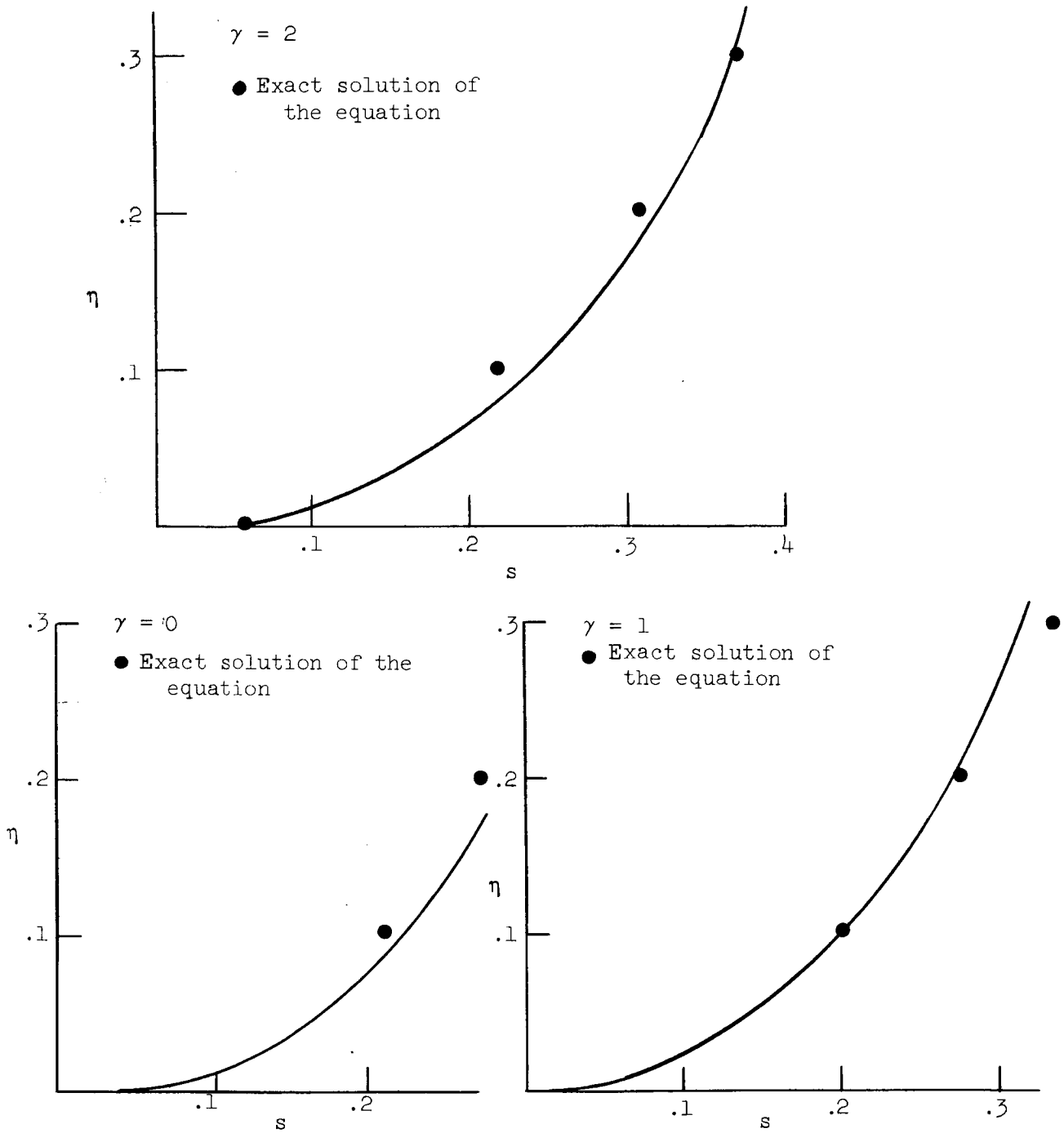

FIG. 43--Normalized potential as a function of position calculated by the numerical Newton-Raphson method compared to the exact solutions of the equations.

Although the N-R method works quite well on the one-dimensional problem it is not easy to apply to the two-dimensional cases due to the limited amount of computer storage available. For a two-dimensional problem divided into only a 10 by 10 grid or 100 mesh points the storage needed would exceed the IBM 7090 core by a factor of three. At each mesh point there would be three unknowns or for a 10×10 mesh a total of 300 unknowns. This would mean that storage would have to be provided for a 300 by 300 coefficient matrix of the 300 linearized finite difference equations. However, within a few years such a problem will not be out of the capability of new computer systems such as the IBM System 360 which will have "unlimited" fast access storage.

Thus, the straightforward N-R method should be kept in mind as a suitable technique for solving these problems in the near future.

2. Time Relaxation Method

The other one-dimensional approach which leads to a convergent solution is the time relaxation method proposed by Lax.[45] In this approach the derivatives with respect to time are kept in the equations and the equations are iterated in time until a steady state is reached. The derivatives with respect to time are written in the following way (in one dimension)

$$\left(\frac{\partial f}{\partial t}\right)_n = \frac{f_n^{t+\Delta t} - \left(\frac{f_{n-1} + f_{n+2}}{2}\right)^t}{\Delta t} , \qquad (150)$$

where n is the mesh point index and $f_n^{t+\Delta t}$ is the value of the dependent variable of interest at time $t + \Delta t$. It is very important that the value of f_n be written as the average of its two nearest neighbors, otherwise this approach does not converge. In general the method proceeds in time in the following manner: an initial value of f^t is guessed, $f^{t+\Delta t}$ is then solved for in terms of f^t, then the new value of $f^{t+\Delta t}$ is used to find $f^{t+2\Delta t}$ and so on until convergence to a steady-state solution is obtained.

In order to program the one-dimensional plasma equations for this method of solution, they are put in the normalized form

$$\frac{\partial \eta}{\partial t} = \nu^I e^{(1-\gamma)\eta} - v \frac{\partial \eta}{\partial z} + \frac{\partial v}{\partial z} \tag{151}$$

and

$$\frac{\partial v}{\partial t} = - v \frac{\partial v}{\partial z} - \nu^I v e^{(1-\gamma)\eta} + \frac{1}{2} \frac{\partial \eta}{\partial z} \tag{152}$$

where ν^I is now an unknown parameter which must be eliminated since no consistent way of finding $\nu^I(t+\Delta t)$ is available. In order to normalize out the parameter ν^I we define a new potential such that

$$\nu^I = e^{(1-\gamma)\eta_0}$$

and

$$u = \eta_0 + \eta \quad .$$

Equations (151) and (152) can then be written as

$$\frac{\partial u}{\partial t} = e^{(1-\gamma)u} - v \frac{\partial u}{\partial z} + \frac{\partial v}{\partial z} \tag{153}$$

and

$$\frac{\partial v}{\partial t} = - v \frac{\partial v}{\partial z} - v e^{(1-\gamma)u} + \frac{1}{2} \frac{\partial u}{\partial z} \quad . \tag{154}$$

These equations are written in finite difference form, ready for programming on the computer, as

$$u_n^{t+\Delta t} = \bar{u}_n^t + \Delta t \left[e^{(1-\gamma)\bar{u}_n^t} - \bar{v}_n^t \left(\frac{u_{n+1}^t - u_{n-1}^t}{2\Delta z} \right) + \frac{v_{n+1}^t - v_{n-1}^t}{2\Delta z} \right] \tag{155}$$

and

$$v_n^{t+\Delta t} = \bar{v}_n^t - \Delta t \left[\bar{v}_n^t \left(\frac{v_{n+1}^t - v_{n-1}^t}{2\Delta z} \right) - \bar{v}_n^t \, e^{(1-\gamma)\bar{u}_n^t} + \frac{1}{2} \frac{u_{n+1}^t - u_{n-1}^t}{2\Delta z} \right] , \tag{156}$$

where

$$\bar{u}_n^t = \frac{u_{n+1}^t + u_{n-1}^t}{2} \tag{157}$$

and

$$\bar{v}_n^t = \frac{v_{n+1}^t + v_{n-1}^t}{2} . \tag{158}$$

The boundary conditions used to obtain a convergent solution are

$$\frac{\partial u}{\partial z}(0) = 0$$

$$v(0) = 0$$

and

$$v(1) = v_{max} ,$$

where v_{max} is chosen to be slightly less than the known value of $1/\sqrt{2}$.

Although the convergence rate is slower than the N-R method, excellent agreement between the exact calculations and the computer calculations are obtained. The results for the case $\gamma = 0$ are shown in Fig. 44. For the one-dimensional problem, the maximum value of $\Delta t/\Delta x$ for convergence can be found explicitly by the method of characteristics.[46] This analysis which is carried out in Appendix D allows us to approach the solution as fast as possible.

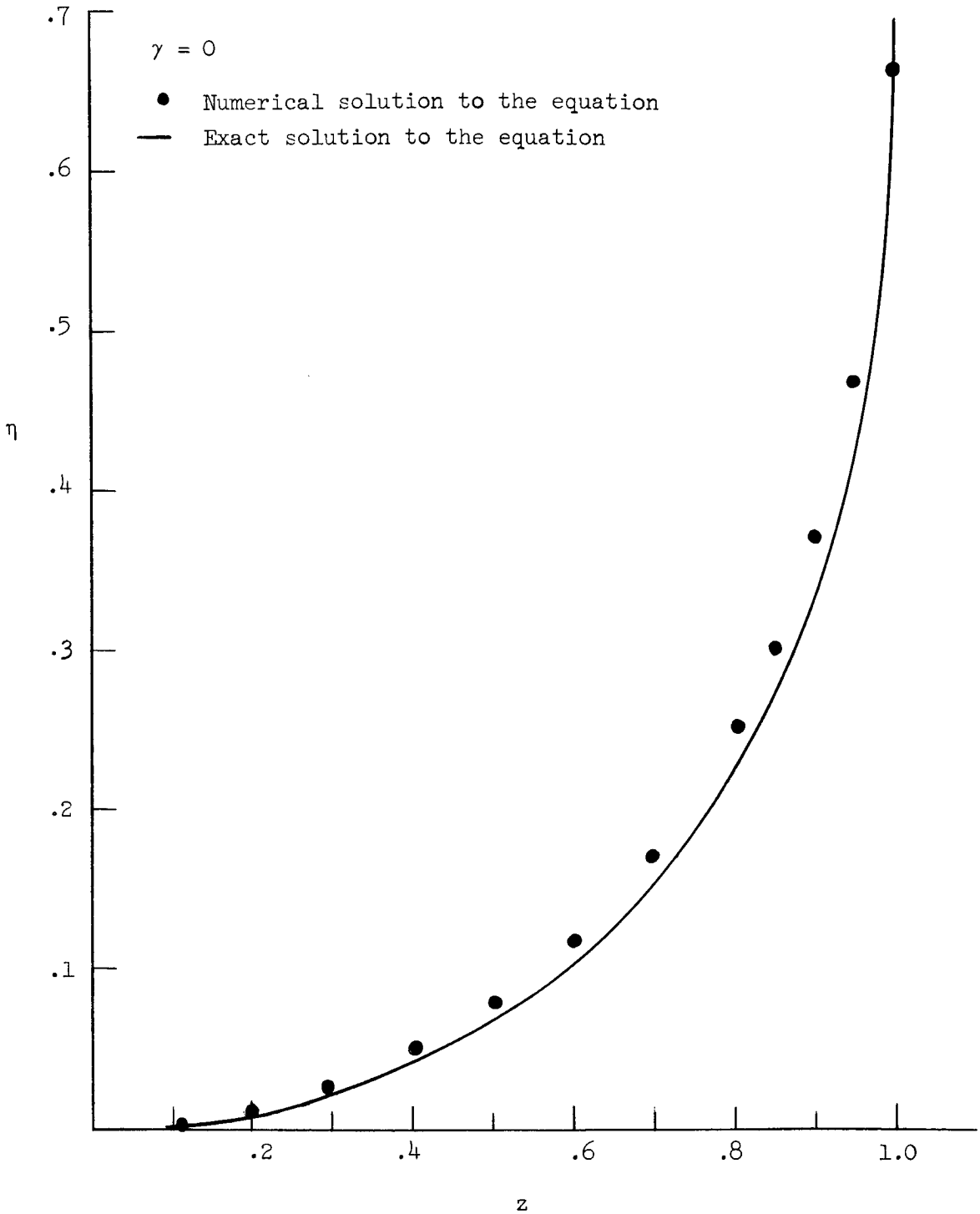

FIG. 44--Normalized potential as a function of position in the one-dimensional planar discharge calculated numerically using the time relaxation method.

Unfortunately, in normalizing out the parameter ν^I, we have automatically excluded the important case of generation proportional to electron density ($\gamma = 1$). In order that ν^I be finite in Eq. (153) we see that η_0 would have to approach infinity for the case $\gamma = 1$ and of course this is not compatible with a computer solution.

Even though the method is somewhat restricted, it was decided that a preliminary investigation of the use of this procedure to solve two-dimensional problems would be undertaken.

C. TWO-DIMENSIONAL TIME RELAXATION APPROACH

For the two-dimensional problems we begin with the equations for the ions

$$\frac{\partial \vec{v}}{\partial \tau} = \frac{1}{2} \nabla \eta - \vec{v} \cdot \nabla \vec{v} - \vec{v} e^{(1-\gamma)u} \tag{159}$$

and

$$\frac{\partial \eta}{\partial \tau} = - e^{(1-\gamma)u} + \nabla \cdot \vec{v} - \vec{v} \cdot \nabla \eta \tag{160}$$

where these equations have been derived by the "moment method" of Chapter II keeping in all variations with respect to time in a consistent manner. In the above equations τ is a normalized time parameter; we have normalized the equations and eliminated the parameter ν^I by the same technique as used for the one-dimensional case. In component form the above equations become (in rectangular geometry)

$$\frac{\partial v_1}{\partial \tau} = \frac{1}{2} \frac{\partial u}{\partial s_1} - v_1 \frac{\partial v_1}{\partial d_1} - v_2 \frac{\partial v_1}{\partial s_2} - v_1 e^{(1-\gamma)u} \tag{161}$$

$$\frac{\partial v_2}{\partial \tau} = \frac{1}{2} \frac{\partial u}{\partial s_2} - v_2 \frac{\partial v_2}{\partial s_2} - v_1 \frac{\partial v_2}{\partial s_1} - v_2 e^{(1-\gamma)u} \tag{162}$$

and

$$\frac{\partial u}{\partial \tau} = \frac{\partial v_2}{\partial s_2} + \frac{\partial v_1}{\partial s_1} - v_2 \frac{\partial u}{\partial s_2} - v_1 \frac{\partial u}{\partial s_1} - e^{(1-\gamma)u} \quad , \qquad (163)$$

where v_1 and v_2 are respectively the normalized x and y velocities, s_1 and s_2 are the normalized x and y distances, and u is the normalized potential.

It is easily shown by eliminating $\partial u/\partial s_1$ between Eq. (163) and (161) that at the "wall" (where $\partial v_1/\partial s_1 \to \infty$) the condition $v_1(s_{10}) = 1/\sqrt{2}$ must be satisfied. Similarly the condition

$$v_2(s_{20}) = \frac{1}{\sqrt{2}}$$

must be satisfied at the "wall." Thus, again we see that the Bohm Criteria comes naturally out of the solution of the two-dimensional problem.

Using exactly the same finite difference procedure as discussed for the one-dimensional case, Eqs. (161), (162), and (163) were programmed for solution on an IBM 7090 computer.

Some difficulty was experienced in obtaining the correct boundary conditions for solution of the two-dimensional case at the outer boundaries where $s_1 = s_{10}$ and $s_2 = s_{20}$. The conditions

$$\left(\frac{\partial v_1}{\partial s_2}\right)_{s_{10}} = 0$$

and

$$\left(\frac{\partial v_2}{\partial s_1}\right)_{s_{20}} = 0$$

plus the conditions

$$v_1 (s_{10}) = v_{1\,max}$$

and

$$v_2 (s_{20}) = v_{2\,max}$$

do not completely define the boundary. It was necessary to assume two further conditions which cannot rigorously be proved true for a general boundary. The conditions assumed were

$$\frac{\partial^2 u}{\partial s_1^2} (s_{20}) = 0$$

and

$$\frac{\partial^2 u}{\partial s_2^2} (s_{10}) = 0 \quad .$$

Convergence to a solution was obtained. However, the solution was severely limited in that convergence could only be obtained for values of $v_{1\,max}$ and $v_{2\,max}$ relatively far away from the boundary ($v_{1\,max}$ and $v_{2\,max}$ were limited to values of 0.45 rather than the known "wall" value of 0.707). Because of this limitation and the previously discussed normalization limiting the solutions to cases other than $\gamma = 1$, work on this approach was not continued.

From the considerable amount of time and effort needed to obtain only limited and certainly not satisfactory solutions to the general two-dimensional problem, we conclude that the difficulties of solving the equations as a boundary value problem have not been overcome and that considerably more work would certainly be necessary in order to obtain useful general solutions. Perhaps even a completely different approach would be necessary in order to overcome the problems discussed above.

CHAPTER VI

EXPERIMENTAL CORRELATION WITH THE THEORY

The theoretical development and procedures discussed above have been used to calculate the behavior of two different low pressure discharges: the so-called oscillating-electron plasma source built by Van Hoven[2] at the Electronic Research Laboratory of Stanford University and the Kaufman ion source tested by workers at the California Institute of Technology.[8] An attempt is made to approximate the oscillating-electron plasma source by a two-dimensional cylindrical discharge. However, only gross qualitative agreement is obtained due to the inability of the theoretical model to take into account the beam or primary electrons from the cathode. Much better agreement between theory and experiment is obtained in the Kaufman ion source where the plasma is treated as three components: ions, Maxwellian electrons, and beam electrons.

A. THE OSCILLATING-ELECTRON PLASMA SOURCE

This low-pressure discharge is shown schematically in Fig. 45 and operates in the following way: Electrons from the indirectly heated cathode are drawn towards the anode, striking neutral mercury atoms and ionizing them to initiate the discharge. It is possible to apply a longitudinal magnetic field to the discharge which is shielded from the region, R , to the left where the plasma streams out through small circular holes in the magnetic shield. The whole device is enclosed in a glass container capable of being continuously pumped and the pressure regulated by means of a pressure sensor and servo-mechanism.

The region enclosed by the magnetic shield was analyzed as a two-dimensional cylindrical discharge. Measurements of the current density were made in region R , as near as possible to the "wall" of the interior region, with a planar Langmuir probe which was capable of being moved from the axis on a radius out to the edge of the discharge. Measurements of

currents were made at two different values of magnetic field. Unfortunately, it was only possible to take a rather limited amount of data since the time available for testing was minimal. The measured results are shown in Fig. 46 where the current density normalized to the value at the center of the discharge is shown as a function of distance from the center of the discharge for no magnetic field, for a magnetic field of 20 gauss, and a magnetic field of 32 gauss. Higher values of magnetic field caused the discharge to assume another mode of operation where the current density differed widely from the ones measured in Fig. 46.

In attempting to approximate the behavior of this device, we chose the finite-length cylindrical discharge as being most nearly like the interior region of the experimental model. The results of calculating the ion current density for this particular shape are shown in Fig. 47. The experimental and calculated results do not agree well at all except that the density for both cases seems to fall off to about the right order of magnitude. A very reasonable explanation of the discrepancy in results is that the primary electrons from the cathode (which are not taken into account in the theoretical model) are causing a larger density of ions on and near the z-axis than the theoretical model could possibly predict. These primary electrons from the cathode have much larger energies than the Maxwellian or plasma electrons and thus near the axis dominate the discharge. Thus, the results show that any theoretical model must include the primary electrons for low pressure discharges of this nature. In the next section we take into account the beam electrons for a Kaufman type ion source and obtain much better agreement between theory and experiment.

B. ONE DIMENSIONAL MODEL OF THE KAUFMAN-TYPE ION THRUSTOR

Shown in Fig. 48 is a schematic diagram of the Kaufman engine or ion thrustor. In its simplest terms the operation of this device can be explained as follows: a mercury gas enters from the left as shown by the arrows where it is then ionized principally by a beam of electrons which is drawn off the cathode. The ions are then accelerated through the openings on the right by a negative potential, mixed with electrons to neutralize the beam, thus providing thrust.

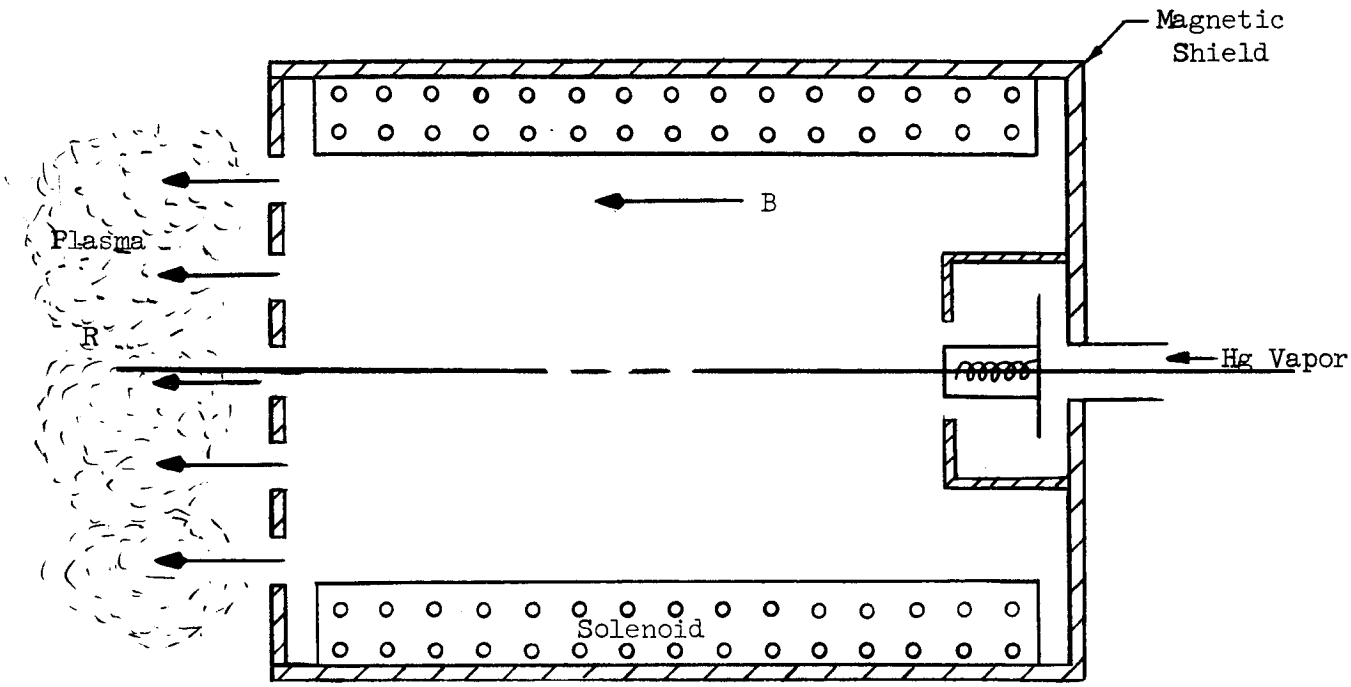

FIG. 45--Oscillating-electron ion source.

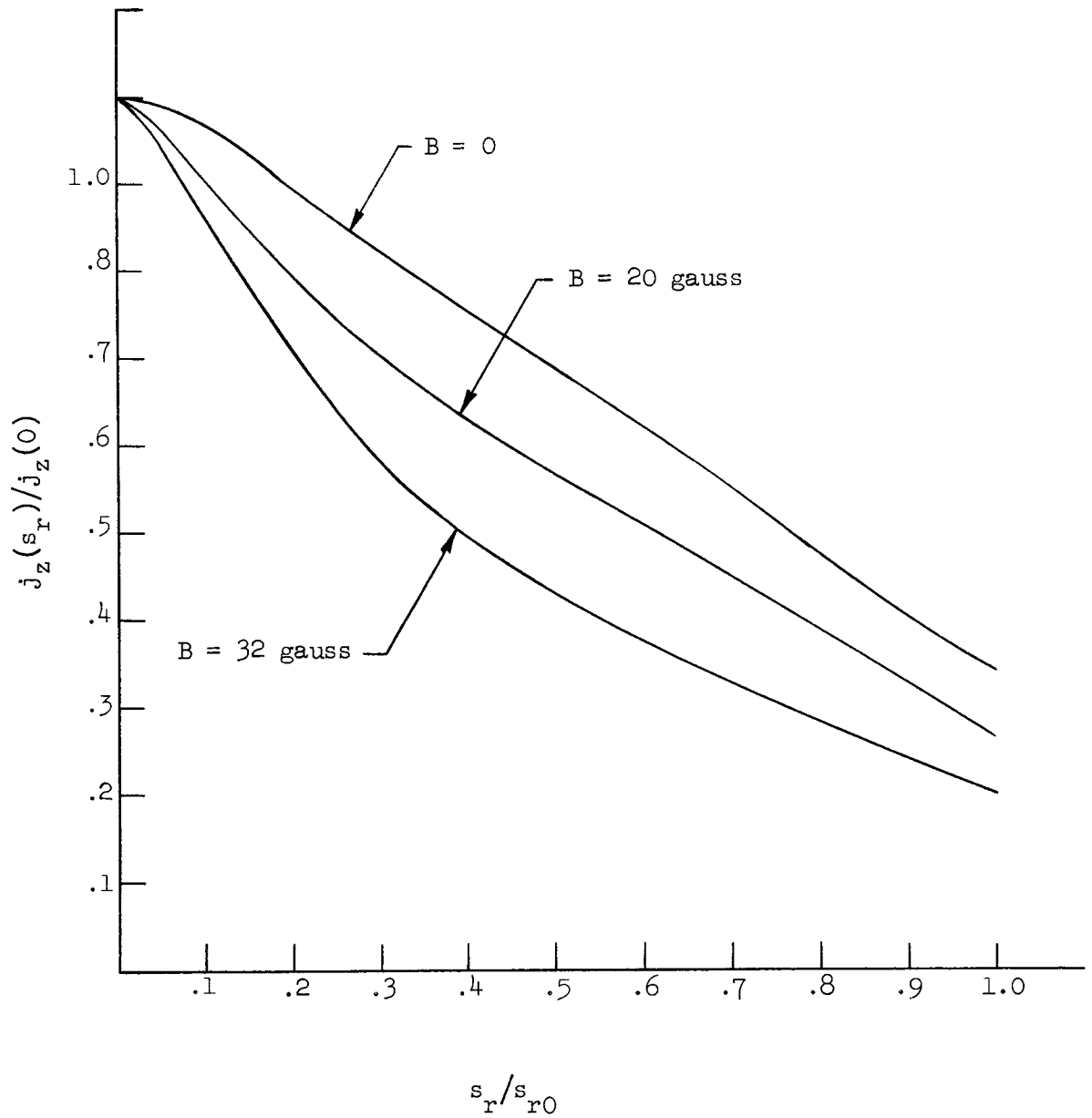

FIG. 46--Measured axial ion current in the oscillating-electron ion-source as a function of radial distance from the axis for three different values of magnetic field.

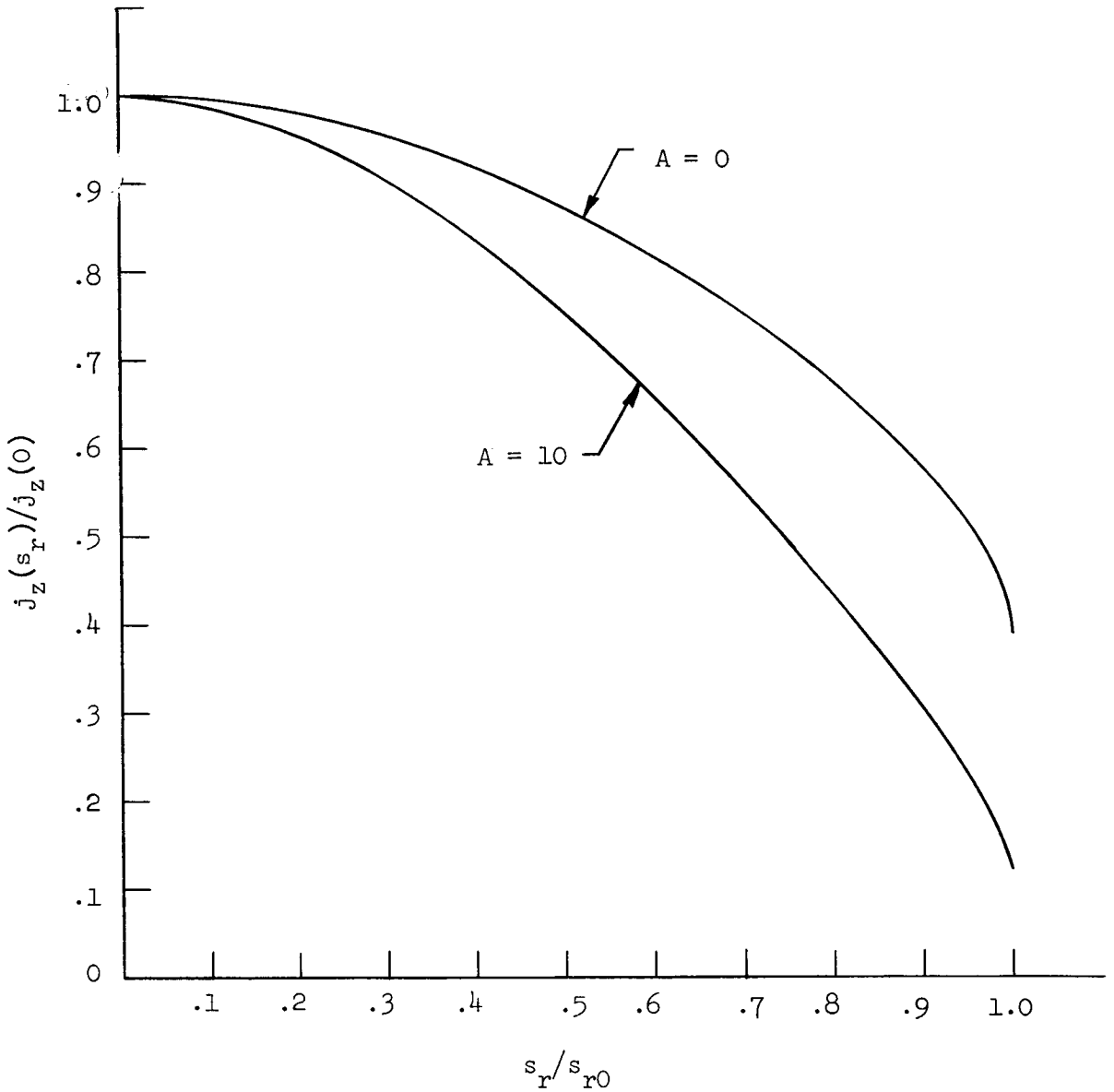

FIG. 47--Calculated axial ion current in the two dimensional coaxial approximation to the oscillating-election ion-source.

Although we will confine our discussion to the Kaufman type ion thrustor the analysis should be applicable to other experimental studies of coaxial type discharges.

1. Mathematical Formulation

In order to be able to analyze this very complicated device, we choose to make the following idealizations:

(1) We assume infinite geometry in the longitudinal or axial direction.

(2) Neutral density variation is neglected.

The usual low pressure operation allows us to make the further approximation that the ion-neutral collisions may be neglected.

Of course, the general formulation is not dependent upon this assumption and the method should be applicable to discharges of higher pressure, as the one discussed by Golant and co-workers[47] where the Maxwellian electrons do most of the ionizing. The geometry is the same as that of the simplified model shown in Fig. 12.

As we have seen, in order to be able to adequately describe a low pressure discharge with primary electrons we must take into account two different species or kinds of electrons: the beam or primary electrons which come from the cathode with a rather high energy, and the thermal or Maxwellian electrons. There is good experimental evidence to support this seemingly arbitrary division of the electrons. Strickfaden and Geiler[8] in their measurements of the Kaufman type ion thrustor found that the Langmuir probe characteristics could be approximately explained by a Maxwellian distribution of electrons with a superimposed, randomly directed but monoenergetic group of electrons at approximately 20-30 eV. Langmuir and Jones[48] in 1928 identified three different main groups of electrons; primary electrons, secondary electrons formed by an ionizing collision of a molecule with a primary electron, and a background of Maxwellian or ultimate electrons. More recent experimental work by Chaghtai[49] and Leckey, Higginson, and Emeleus[50] has confirmed the existence of the two main groups of electrons, an almost monoenergetic group which has fallen through the cathode sheath and acquired random direction with little change in energy and another group of slower near-Maxwellian electrons.

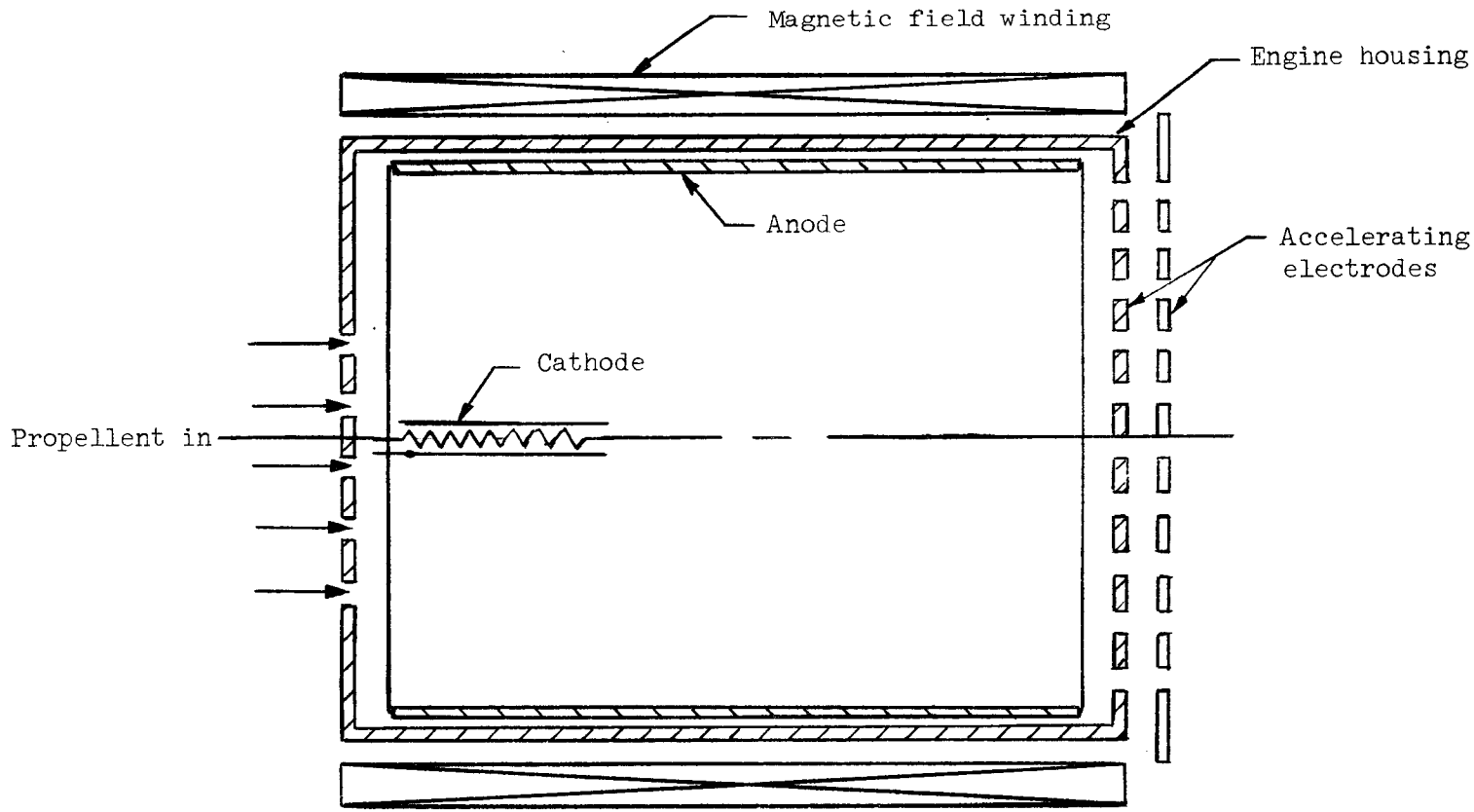

FIG. 48--Schematic diagram of Kaufman engine or ion thrustor.

Using Eq. (167) in Eq. (166) to eliminate $v_{b\theta}$ and normalizing the above equations we obtain for the final one-dimensional beam electron equation

$$\frac{1}{2}\frac{M}{m}\frac{E_b}{E_m}\frac{1}{n_b}\frac{dn_b}{ds_r} + Al\ v_{bl} = -\frac{1}{2}\frac{M}{m}\frac{d\eta}{ds_r} \tag{169}$$

and

$$\frac{dv_{bl}}{ds_r} + \frac{v_{bl}}{s_r} + \frac{v_{bl}}{n_b}\frac{dn_b}{ds_r} = -\frac{1}{p}\ , \tag{170}$$

where

$$E_m = \frac{1}{2}kT_e$$

and

$$Al = \frac{\omega_{ce}^2}{\nu_b^I(\nu_{bn} - \frac{1}{p}\nu_b^I)} - \frac{1}{p} + \frac{\nu_{bn}}{\nu_b^I}$$

and v_{bl} is the normalized radial beam velocity, and we have used the normalization

$$v_{br} = \sqrt{\frac{2kT_e}{M}}\ v_{bl} \tag{171}$$

with

$$r = \sqrt{\frac{2kT_e}{M}}\ \frac{s_r}{\nu_b^I}\ . \tag{172}$$

(a) Beam Electrons

As the beam electrons move to the outer wall and suffer ionizing collisions we would expect them to be Maxwellianized and their density to decrease. We take this into account by assuming that after a given number of ionizing collisions, p, the beam electrons are "instantaneously" Maxwellianized. We thus neglect the secondary or transistional group of electrons.

The first two moment equations for the beam electrons are

$$\nabla \cdot (n_b v_b) = - \frac{1}{p} \nu_b^I n_b \tag{164}$$

where n_b is the primary or beam electron density, ν_b^I is the beam electron ionization frequency, v_b is the average beam velocity, and p is the average number of ionizing collisions necessary to Maxwellianize a beam electron; and

$$\frac{E_b}{m} \frac{\nabla n_b}{n_b} + \vec{v}_b (\nu_{bn} - \frac{1}{p} \nu_b^I) = \frac{e}{m} (\nabla \phi - \vec{v}_b \times \vec{B}_z) \tag{165}$$

where E_b is the equivalent beam energy $(1/2\ m\ \overline{u_b^2})$, ν_{bn} is the beam-neutral collision frequency, and B_z is the magnetic field; uniform and in the z or longitudinal direction.

In component form the above equations may be written as

$$(\nu_{bn} - \frac{1}{p} \nu_b^I)\ v_{br} + \frac{E_b}{m} \frac{1}{n_b} \frac{\partial n_b}{\partial r} = \frac{e}{m} \left(\frac{\partial \phi}{\partial r} + v_{b\theta} B_z \right) \tag{166}$$

$$(\nu_{bn} - \frac{1}{p} \nu_b^I)\ v_{b\theta} = - \frac{e}{m} v_{br} B_z \tag{167}$$

and

$$\frac{\partial v_{br}}{\partial r} + \frac{v_{br}}{r} + \frac{v_{br}}{n_b} \frac{\partial n_b}{\partial r} = - \frac{1}{p} \nu_b^I \quad . \tag{168}$$

We write Eq. (169) as

$$\frac{1}{2} R_E R_m \frac{du_{bl}}{ds_r} + Al\ v_{bl} = - \frac{R_m}{2} \frac{\partial \eta}{\partial s_r} \quad , \tag{173}$$

where

$$R_E = \frac{E_b}{E_m}$$

$$R_m = \frac{M}{m}$$

and

$$u_{bl} = \ell n\ n_b / n_{bO} \quad .$$

(b) Maxwellian Electrons

Again using the condition that the beam ionizing frequency is much greater than the ionizing frequency due to Maxwellian electrons we obtain for the Maxwellian electrons the two normalized equations

$$\frac{dv_{ml}}{ds_r} + \frac{v_{ml}}{s_r} + v_{ml} \frac{\partial u_{ml}}{\partial s_r} = \left(\frac{1 + p}{p} \right) \frac{n_b}{n_m} \tag{174}$$

and

$$\frac{1}{2} R_m \frac{du_{ml}}{ds_r} + v_m\ Bl = - \frac{1}{2} R_m \frac{d\eta}{ds_r} \quad , \tag{175}$$

where

$$Bl = \frac{\omega_{ce}^2}{\nu_b^I\left[\nu_{mn} + \left(\frac{1+p}{p}\right)\frac{n_b}{n_m}\nu_b^I\right]} + \frac{\nu_{mn}}{\nu_b^I} + \left(\frac{1+p}{p}\right)\frac{n_b}{n_m} \quad .$$

(c) Ions

Using the fact that the magnetic field has a negligible effect on the ions we obtain for the ions the two normalized equations

$$\frac{v_{il}\,dv_{il}}{ds_r} + v_{il}\left(\frac{n_b}{n_i} + \frac{\nu_{bn}}{\nu_b^I}\right) = \frac{1}{2}\frac{d\eta}{ds_r} \qquad (176)$$

and

$$\frac{dv_{il}}{ds_r} + \frac{v_{il}}{s_r} + v_{il}\frac{du_{il}}{ds_r} = \frac{n_b}{n_i} \quad . \qquad (177)$$

2. Final Equations for Computation

Using Eqs. (169), (170), (174) – (177) above plus the neutrality condition

$$n_i = n_m + n_e$$

and the condition of equal electron and ion currents

$$n_i v_i = n_m v_m + n_b v_b \quad , \qquad (178)$$

we can eliminate the unknowns n_m and v_m and combine the above equations to give the following forms which are useful for computation purposes:

$$\frac{\partial v_i}{\partial s_r} = \left[\frac{1}{2}\frac{v_i}{s_r(1-R_n)} - \frac{1}{2}\frac{R_n}{(1-R_n)} - v_i^2\left[\frac{C(R_n+1)}{R_E(1-R_n)} + \frac{Bl}{R_m(1-R_n)}\right] + \frac{R_n(Bl-Al)/R_E}{R_m(1-R_n)} v_i v_b\right] \Bigg/ \left[Dv_i^2 - \frac{1}{2}\frac{1}{(1-R_n)}\right] \tag{179}$$

$$\frac{\partial \eta}{\partial s_r} = - v_i\left(\frac{R_n}{1-R_n} + \frac{C}{1-R_n}\right)\left[\frac{-2v_i R_n}{1-R_n} + \frac{v_i^2}{s_r(1-R_n)} - \frac{2v_i^3\, Bl}{R_m(1-R_n)} + \frac{2R_n(Bl-Al)/R_E}{R_m(1-R_n)} v_i^2 v_b\right] \Bigg/ \left[Dv_i^2 - \frac{1}{2}\frac{1}{1-R_n}\right] \tag{180}$$

$$\frac{\partial u_i}{\partial s_r} = \left[v_i\left[D(C + R_n) + \frac{Bl}{R_m(1-R_n)}\right] - \frac{Dv_i^2}{s_r} - \frac{R_n(Bl-Al)/R_E}{R_m(1-R_n)} v_b\right] \Bigg/ \left[Dv_i^2 - \frac{1}{2}\frac{1}{(1-R_n)}\right] \tag{181}$$

$$\frac{\partial u_b}{\partial s_r} = \left[\frac{Al\, v_b}{(1-R_n)R_E R_m} + \frac{v_i(R_n+C)}{R_E(1-R_N)} - \frac{v_i^2}{R_E\, s(1-R_n)} + \frac{2v_i^3\, Bl}{R_m R_E(1-R_n)} - \frac{2v_i^2 v_b}{R_m R_E}\frac{(Bl\, R_n+Al)}{1-R_n}\right] \Bigg/ \left[Dv_i^2 - \frac{1}{2}\frac{1}{(1-R_n)}\right] \tag{182}$$

and

$$\frac{\partial v_b}{\partial s_r} = -\frac{v_b v_i^2}{s_r}\left[D - \frac{1}{R_E(1-R_n)}\right] - \frac{Dv_i^2}{p} + \frac{v_b}{2s_r(1-R_n)} + \frac{1}{2p(1-R_n)} - \frac{v_b^2\, Al}{(1-R_n)R_E R_m}$$

$$- \frac{v_b v_i (R_n+C)}{R_E(1-R_n)} - \frac{2v_i^3 v_b\, Bl}{R_m R_E(1-R_n)} + \frac{2v_b^2 v_i^2}{R_E R_m}\left[Al + \frac{Bl R_n}{1-R_n}\right] + Dv_i^2 - \frac{1}{2}\frac{1}{(1-R_n)} \tag{183}$$

where

$$D = 1 + \frac{R_n}{R_E(1-R_n)} \tag{184}$$

$$C = R_n + \frac{v_{bn}}{v_b^I} \quad . \tag{185}$$

In order to solve the above five equations in the five unknowns, v_i , v_b , u_i , u_b , and η , it is necessary to use numerical methods. Again the Runge-Kutta technique was used with the initial values:

$$v_i = R_{nO}(s_r - s_m) + \ldots \tag{186}$$

$$v_b = -\frac{1}{p}(s_r - s_m) + \ldots \tag{187}$$

$$\eta = R_{nO}(R_{nO} + C_O)(s_r - s_m)^2 + \ldots \tag{188}$$

$$u_b = \frac{Al}{pR_E R_m} - \frac{R_{nO}}{R_E}(R_{nO} + C_O)(s_r - s_m)^2 + \ldots \tag{189}$$

and

$$u_i = -(1-R_{n0})\left[R_{n0}\left(2R_{n0} + \frac{Bl_0}{R_m(1-R_{n0})}\right) + \frac{R_{n0}}{R_m(1-R_{n0})}\left(\frac{Bl_0-Al}{R_E}\right)\frac{1}{p}\right](s_r-s_m)^2 + \cdots \quad . \tag{190}$$

3. Correlation with Experiment

The experimental case chosen for comparison with the above developed theory was taken from a report by Strickfaden and Geiler.[51] This particular set of data was chosen since it corresponds most closely with the theoretical model in that the measurements were taken radially at a longitudinal position where the cathode was still present and no longitudinal accelerating potential was applied. From the data given, average values of the following parameters necessary to obtain a theoretical solution were obtained:

$$R_E = \frac{E_b}{E_m} \approx 6 \quad .$$

Since the beam energy over most of the radial distance was between 20 and 25 eV, and the amount of energy lost per ionizing collision is approximately 10 eV, the number of ionizing collisions of the beam before being Maxwellianized was taken to be three or $p \approx 3$.

The magnetic field given is 17 gauss which determines the value of electron cyclotron frequency $\omega_{ce} = 2.99 \times 10^7/\text{sec}$.

Since the pressure of operation is not given by Strickfaden and Geiler, an estimate was made based on the total density of electrons and on the fact that the percent ionization is quite high. The value of pressure was assumed to be approximately one-tenth of a micron. The average beam-neutral collision frequency was then calculated from the

data given by Brown[37] to be

$$\nu_{bn} \approx 2.5 \times 10^6/\text{sec} \quad .$$

Using the experimental data of Nottingham,[52] the ionization frequency for the beam at approximately 0.1μ pressure and 20 eV is found to be

$$\nu_b^I \approx 5 \times 10^5/\text{sec} \quad .$$

The collision frequency for Maxwellian electrons colliding with neutral atoms was taken from Crawford and Self[32] to be

$$\nu_{en} \approx 2.5 \times 10^6/\text{sec} \quad .$$

Finally the ratio of beam electrons to Maxwellian electrons at the radial position of maximum normalized potential ($s = s_m$) was taken from the experimental data as

$$\frac{n_b}{n_m} \approx 0.3$$

which gives a value of

$$R_n = \frac{n_b}{n_i} = 0.23 \quad .$$

From the scaled drawing of the experimental ion source the ratio of outer to inner diameter (in the region of the cylindrical cathode) was found to be approximately 17:1. Using the above values of the parameters in the equations governing this type of discharge the solutions shown in Figs. 49, 50, and 51 were obtained for the number densities of the various components (ions, beam electrons, and Maxwellian electrons) as a function of radial distance from the center of the discharge.

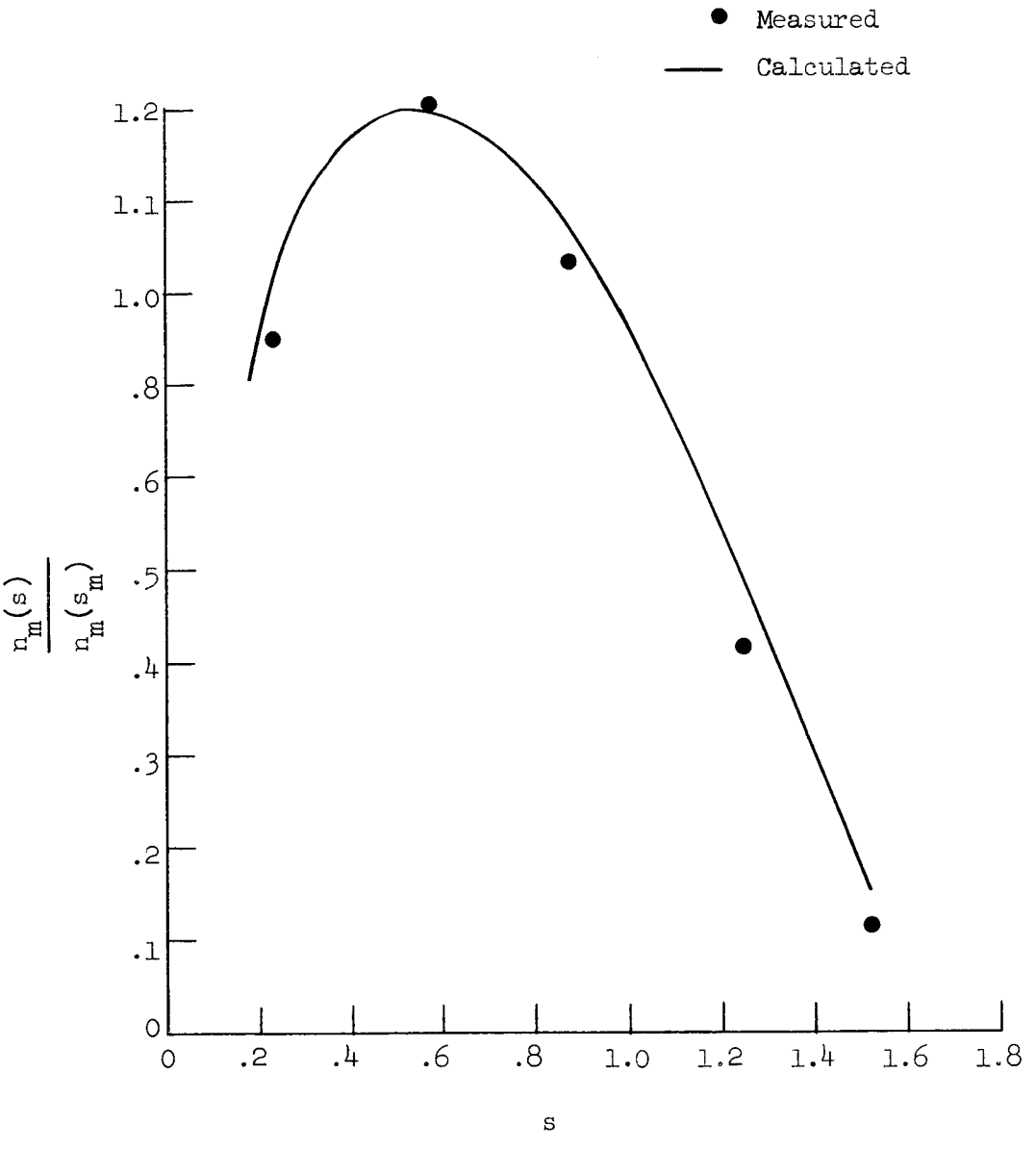

FIG. 49--Calculated and measured Maxwellian electron density as a function of radial position in the Kaufman ion source.

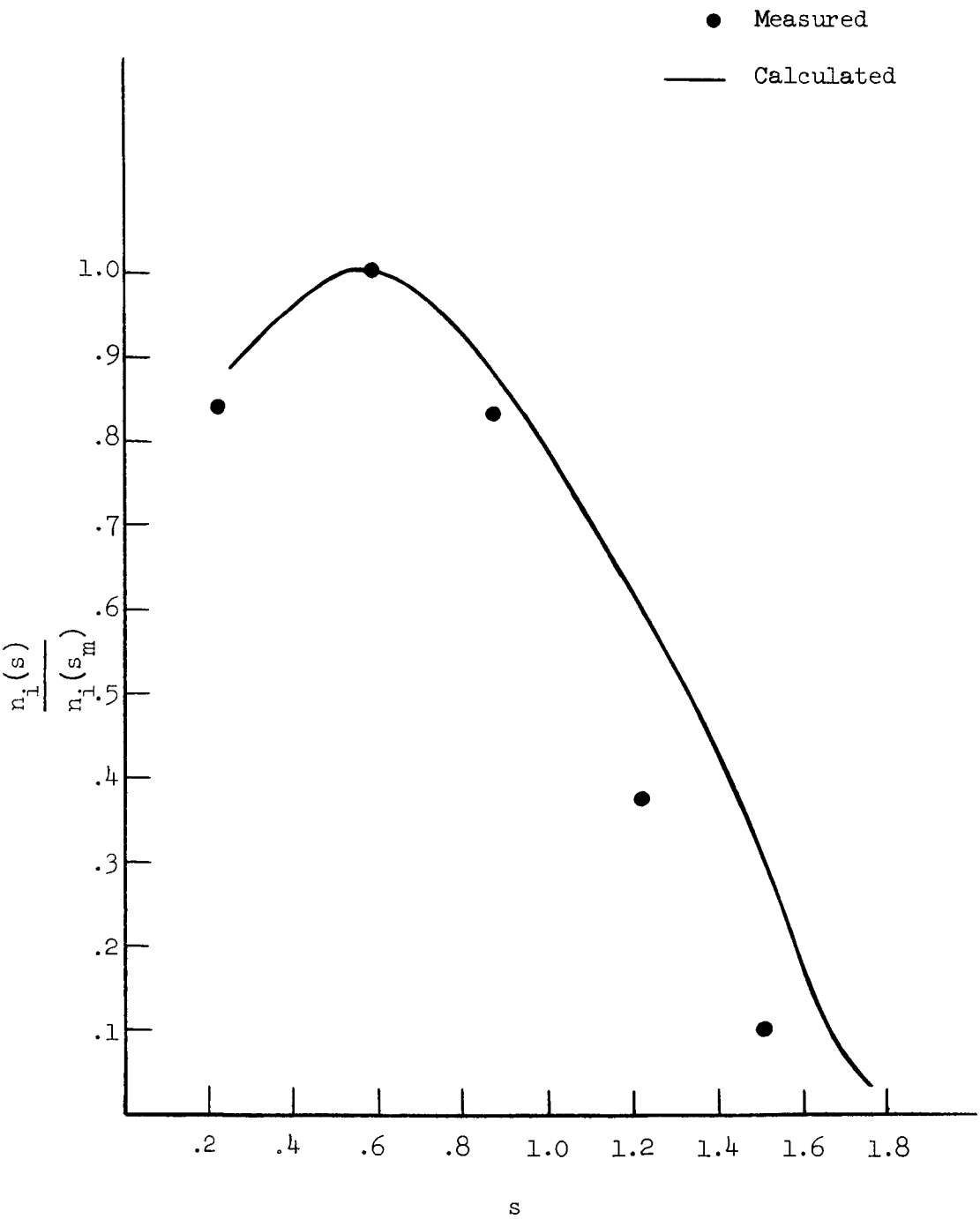

FIG. 50--Ion density as a function of radial position in the Kaufman ion source.

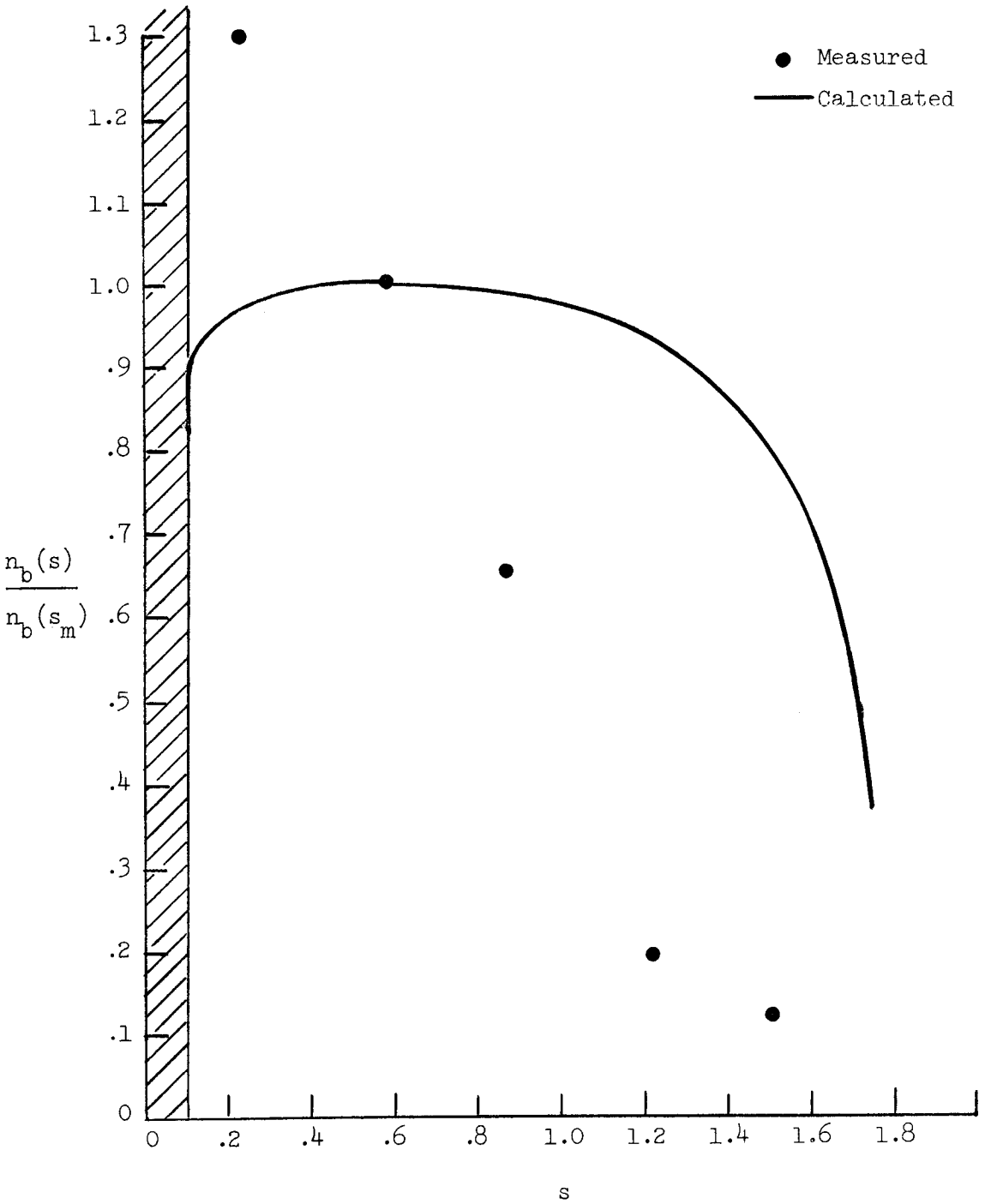

FIG. 51--Calculated and measured beam electron density as a function of radial position in the Kaufman ion source.

Considering the approximations made in the analysis and the uncertainty in the pressure of operation, the results of Fig. 49 for the Maxwellian electron density are amazingly close to the experimental values also plotted in the figure.

The results of Fig. 50 which compares the theoretically calculated and measured values of ion density are also quite good, although it is seen that the measured ion density begins to fall off more rapidly than the calculated values as the edge of the discharge region is approached. This discrepancy is due to the rather large variance in the calculated and measured values of beam electron density shown in Fig. 51. We see that the measured value of beam density falls off much more rapidly than the calculated values. However, we believe that there is a reasonable explanation for this difference in the one dimensional approximation made in the theoretical model. First, we have assumed the cathode extends over the full length of the discharge when in fact it only extends over approximately 40% of the discharge. Thus, the supply of beam electrons is not as large as we have assumed. Second, the discharge is finite in length and the beam electrons, because they are more energetic, can be expected to supply most of the current to the walls and to the ends of the discharge. Making a rough estimate of the loss of beam electrons to the ends of the discharge based on the area we would expect approximately 44% of the beam to be lost to the ends of the discharge. Thus, the total density of beam electrons might reasonably be expected to fall off at a rate much higher than that predicted by the theory. In fact we would expect the density to be down greater than 40% from the calculated value.

We thus conclude from the above comparisons of calculated and measured densities that the theoretical model does in fact approximate the behavior of the Kaufman source reasonably well and should be useful in studying this type of discharge.

CHAPTER VII

CONCLUSIONS AND RECOMMENDATIONS FOR FURTHER STUDY

The general modified pressure theory approach described in this work has been shown to be applicable to a large number of one- and two-dimensional dc discharges in the low and medium pressure regimes. Not only is it possible to describe the parameters of two-component plasmas but three-component (ion, neutral, and Maxwellian electrons; ion, beam electron, and Maxwellian electrons) plasmas can also be described using this same general approach. The effects of ion-neutral collisions and an applied magnetic field can also be included without any major modification of the theory.

Correlation with previous theoretical and experimental work shows that this approach, although approximate, gives reasonably good agreement with both previous theories and experiment for the parameters of most interest in the study of plasmas.

Among the many areas which this work opens up for investigation the following are suggested as being most profitable for further study:

(1) An extension of the theory to include Poisson's equation and thus the sheath region of the discharges.

(2) Further improvement of the one-dimensional model of the Kaufman ion source to include an electron beam velocity at the potential minimum and perhaps three kinds of electrons.

(3) Further development of the one-dimensional theory to include the spherical Langmuir probe as well as the cylindrical probe and a general study of the application of the pressure theory approach to probe theory in the presence of a magnetic field.

(4) A study of the effects of neutral density variations on the parameters of a discharge with the neutral atoms diffusing off the walls would be very interesting and useful in predicting current limiting in low-pressure discharges.

APPENDIX A

THE EFFECT OF NEUTRAL DENSITY VARIATION ON THE PARAMETERS OF THE ONE-DIMENSIONAL DC DISCHARGE

In order to obtain an approximate idea of how the parameters change when the neutral density is not uniform, we make the following assumptions:

(1) The degree of ionization is such that the discharge is not dominated by electron-neutral collisions so that we still have

$$n_e = n_{e0}\, e^{e\phi/kT} \quad .$$

(2) Ion-neutral collisions are assumed to be much less frequent than ionizing collisions.

(3) The neutral density variation is known and this variation is maintained by a flow of neutral gas in a direction perpendicular to the ion flow.

(4) Neutral gas velocity is much less than the ion velocity, i.e.,

$$v_g << v_i$$

where v_g is the average neutral gas velocity.

(5) Kinetic pressure is neglected in the momentum transfer equation for the ions.

The above assumptions would apply reasonably well to a discharge where the ions are continually being drawn out of one end of the discharge and the neutral gas continually supplied at the other end (Kaufman-like ion source). However, the above assumptions would not apply to a "closed" system where the neutral gas is being supplied by a flow from the walls of the discharge.

With the above assumptions the first two moment equations for the ions became for a planar discharge with generation proportional to electron density

$$\frac{d(n_i v_i)}{dx} = n_g n_e \alpha^I \tag{A.1}$$

and

$$\frac{n_i v_i dv_i}{dx} + \alpha^I n_g n_e v_i = -\frac{e}{M} n_i \frac{\partial \phi}{\partial x} \quad . \tag{A.2}$$

Expanding and normalizing Eqs. (A.1) and (A.2) we obtain

$$\frac{dv_1}{ds} - \frac{v_1 d\eta}{ds} = \frac{n_g(s)}{n_{g0}} \tag{A.3}$$

and

$$\frac{v_1 dv_1}{ds} + \frac{n_g(s)}{n_{g0}} v_1 = \frac{1}{2} \frac{d\eta}{ds} \quad , \tag{A.4}$$

where n_{g0} is the neutral gas density at $s = 0$ and $n_g(s)$ is a known function of s. Using Eq. (A.4) in Eq. (A.3) to eliminate $d\eta/ds$ we obtain

$$\left(\frac{1 - 2 v_1^2}{2v_1^2 + 1} \right) \frac{dv_1}{ds} = \frac{n_g(s)}{n_{g0}} \quad . \tag{A.5}$$

Integrating we obtain

$$\sqrt{2} \tan^{-1} v_1 - v_1 = \int_0^s \frac{n_g(s)}{n_{g0}} \, ds \quad . \tag{A.6}$$

Let us suppose that the neutral variation is given by

$$\frac{n_g(s)}{n_{g0}} = 1 - as \quad ,$$

where "a" is an unspecified constant. This would be a reasonable assumption for a Kaufman type ion source being supplied with neutrals from a point in the center of the discharge. Equation (A.6) then becomes

$$\sqrt{2}\,\tan^{-1} v_1 - v_1 = s - \frac{as^2}{2} \qquad (A.7)$$

Notice in Eq. (A.6) that the Bohm Criteria is still satisfied at the "wall" where the velocity is

$$v_{10} = \frac{1}{\sqrt{2}} \quad .$$

We can thus find the distance to the "wall" by using the value of v_{10} given above in Eq. (A.7) and then solving for s_0 . When we do this we obtain the result

$$s_0 = \frac{1}{a} - \frac{1}{a}\sqrt{1 - 0.81a} \quad .$$

The above equation has been solved for several values of the parameter "a" corresponding to various values of the percent change in neutral gas density between the center and edge of the discharge. The results are shown in Table A.1. For this particular case a 12.9% change in the neutral density only results in a 6.71% change in the "wall" distance.

We would also like to know how the "wall" potential η_0 is affected. Using Eq. (A.3) in Eq. (A.5) to eliminate n_g/n_{g0} , we find

$$\frac{4v_1^2}{2v_1^2 + 1}\,\frac{dv_1}{ds} = \frac{d\eta}{ds}$$

TABLE A.I

Effect of Neutral Density Variation On Distance To "Wall"

a	s_0	$\frac{n_{g0} - n_{gw}}{n_{g0}}$
0	0.403	0
0.1	0.42	4.2%
0.2	0.425	8.4%
0.3	0.430	12.9%

or

$$\frac{4v_1^2}{2v_1^2 + 1} dv_1 = d\eta \quad .$$

This is the same result as obtained without neutral density variation and thus the wall potential is not effected by a neutral density variation.

We conclude therefore that the assumption of uniform neutral gas density is reasonably good as long as it is known that the variation is less than approximately 10% in going from the center to the edge of the discharge. For large variations in the neutral gas density, large errors in the discharge parameter will most certainly result.

APPENDIX B

THE EFFECT OF INITIAL ION VELOCITY ON THE PARAMETERS OF THE ONE DIMENSIONAL DC DISCHARGE

In this work we have assumed that the ions are generated with zero velocity. More accurately, we know that they are generated with a Maxwellian distribution (M.D.) of velocity. In one dimension, the ion distribution function at generation should be written as

$$f_{gi}(w_g) = \frac{M}{2kT_g\pi} \cdot e^{-\frac{M}{2kT_g} w_g^2} ,$$

where T_g is the background or neutral gas temperature, and w_g is the gas velocity.

If we again use the "moment method" of solution of the Boltzmann equation we see that the equation of continuity is unchanged when the initial velocity distribution is taken into account, since the generation term will be

$$\int_{-\infty}^{\infty} G \int_{-\infty}^{\infty} \frac{a}{\pi} e^{-aw_g^2} \delta(w-w_g)\, dw_g\, dw = G \int_{-\infty}^{\infty} \frac{a}{\pi} e^{-aw_g^2} dw = G .$$

In fact, as long as the generation function, G, does not depend on the ion velocities, w, the equation of continuity is given by

$$\frac{d}{dx}(nv) = G \qquad (B.1)$$

The momentum transfer equation is also unchanged since the momentum change due to the generation term is given by

$$G \int_{-\infty}^{\infty} w \left[\int_{-\infty}^{\infty} \sqrt{\frac{a}{\pi}}\, e^{-aw_g^2}\, \delta(w-w_g)\, dw_g \right] dw = G \int_{-\infty}^{\infty} \sqrt{\frac{a}{\pi}}\, we^{-aw^2}\, dw = 0 .$$

The momentum transfer equation is thus given by

$$\frac{d}{dx}(nv^2) + \frac{d}{dx}(\overline{nu^2}) = -\frac{e}{m} n \frac{d\phi}{dx} . \qquad (B.2)$$

The equation of heat transfer has an additional term, given by

$$G \int_{-\infty}^{\infty} w^2 \left[\int_{-\infty}^{\infty} \sqrt{\frac{a}{\pi}}\, e^{-aw_g^2}\, \delta(w-w_g)\, dw_g \right] dw = G \int_{-\infty}^{\infty} w^2 \sqrt{\frac{a}{\pi}}\, e^{-aw^2}\, dw = \frac{GkT_g}{M} .$$

Thus we obtain

$$\frac{d}{dx}(nv^3) + 3\frac{d}{dx}(\overline{nvu^2}) + \frac{d}{dx}(\overline{nu^3}) = -\frac{2e}{M} nv \frac{d\phi}{dx} + G\frac{kT_g}{M} \qquad (B.3)$$

for the heat transfer equation. Using the "standard" normalizations, Eqs. (1), (2) and (3) become

$$n\frac{dv}{ds} - nv\frac{d\eta}{ds} = g \qquad (B.4)$$

$$\frac{d}{ds}(nv^2) + \frac{d}{ds}(\overline{nu^2}) = \frac{1}{2} e^{-\eta} \frac{d\eta}{ds} \qquad (B.5)$$

$$\frac{d}{ds}(nv^3) + 3\frac{d}{ds}(\overline{nvu^2}) + \frac{d}{ds}(\overline{nu^3}) = nv\frac{d\eta}{ds} + \frac{1}{2} g \frac{T_g}{T_e} . \qquad (B.6)$$

Integrating (B.5), we obtain

$$nv^2 + \overline{nu^2} = -\frac{e^{-\eta}}{2} + C .$$

Now, when $\eta = 0$, we have $v = 0$ and we take

$$\overline{u^2}|_0 = \frac{kT_g}{M} \quad \text{(un-normalized)}$$

or

$$\overline{u^2}|_0 = \frac{1}{2}\frac{T_g}{T_e} \quad \text{(normalized)}$$

Therefore, we obtain

$$C = \frac{1}{2}\left(1 + \frac{T_g}{T_e}\right)$$

and

$$\overline{nu^2} = \frac{1}{2}\left(1 + \frac{T_g}{T_e}\right) - \frac{1}{2}e^{-\eta} - nv^2 \quad . \qquad \text{(B.7)}$$

Normally we would neglect the heat flux term and solve for the dependent variables v , $\overline{u^2}$, and η . However, for this case we cannot neglect the heat flux term and still obtain consistent results at the origin. We find a consistent value of $d/dx\,(\overline{nu^2})$ in the following manner. We rewrite (B.6) in the form

$$nv\frac{d}{ds}(v^2 + 3\overline{u^2}) + g(v^2 + 3\overline{u^2}) + \frac{d}{ds}(\overline{nu^3}) = nv\frac{d\eta}{ds} + \frac{1}{2}g\frac{T_g}{T_e} \quad .$$

From symmetry, we know that $v = 0$ at the origin, and therefore

$$3\overline{u^2}(0)\, g + \frac{d}{ds}[n(0)\,\overline{u^2}(0)] = \frac{1}{2}g\frac{T_g}{T_e} \quad ,$$

or

$$\frac{d}{ds}(\overline{nu^3})\Big|_0 = \frac{1}{2} g \frac{T_g}{T_e} - \frac{3}{2} g \frac{T_g}{T_e}$$

or

$$\frac{d}{ds}(\overline{nu^3})\Big|_0 = - g \frac{T_g}{T_e} \qquad (B.8)$$

We cannot retain $\overline{u^3}$ as a variable since the equations will not then form a closed set. As a reasonable approximation we take $\overline{u^3}$ a constant and equal to the value determined above to make the equations consistent at the origin. When we do this (B.6) becomes [after substituting for g from (B.4) and for $\overline{u^2}$ from (7)]

$$v \frac{d\eta}{ds}(4v^2 + 1 + 3\tau) + \frac{dv}{ds}[-12v^2 + 3(e^{\eta} - 1) + 3v(e^{\eta} - 1)] = 0 \quad , \qquad (B.9)$$

where

$$\frac{T_g}{T_e} = \tau$$

We now solve for v and η near the origin. From the equation of continuity we can solve for $d\eta/ds$ to get

$$\frac{d\eta}{ds} = \frac{dv}{ds} - e^{(1-\gamma)\eta} \quad .$$

Using this in (B.9), we find that (after collecting terms)

$$\frac{dv}{ds} = \frac{e^{(1-\gamma)\eta}(4v^2 + 1 + 3\tau)}{[-8v^2 + 1 + 3\tau + 3(e^{\eta} - 1) + 3\tau(e^{\eta} - 1)]} \quad .$$

From this equation we obtain

$$\frac{dv}{ds}(0) \approx \frac{(1 + 3\tau)}{(1 + 3\tau)} = 1 \quad . \tag{B.10}$$

Similarly, we can obtain the first term in the expansion of η near the origin. Since $\eta(0) = \partial\eta/\partial s(0) = 0$, we know that

$$\eta = as^2 + \ldots \quad .$$

Keeping terms to second order in (B.9) , we obtain

$$\eta = \frac{12}{5}\left(1 + \frac{9}{5}\tau\right) s^2 + \ldots \quad . \tag{B.11}$$

Langmuir also has considered this problem. However, he only obtained a solution near the origin. For the case $\tau << 1$ he calculated

$$\eta = \frac{\pi^2}{4}(1 - 2\tau)\, s^2 + \ldots$$

or

$$\eta = 2.46\,(1 - 2\tau)\, s^2 \quad ,$$

where our calculation gives

$$\eta = 2.4\,(1 - 1.8\tau)\, s^2 + \ldots \quad .$$

The agreement is reasonably good. We can now solve (B.9) to see what the effect of finite τ will be on the potential, current, etc., at the wall. Since T_e is normally much greater than T_g , we would expect the effect to be small. Solving for the parameters at the wall for various ratios of $T_g/T_e = \tau$, we obtain the values shown in Table B.I (for $\gamma = 0$) . Since $\tau = T_g/T_e$ would normally be expected to be of the order of 0.01 the effect of initial ion temperature can

be neglected as we have done in previous calculations.

TABLE B.1

Values of η_0 and s_0 for Various Ratios of T_g/T_e ($\gamma = 0$)

T_g/T_e	s_0	η_0
0	0.345	~ 0.786
0.025	0.358	~ 0.780
0.05	0.351	~ 0.786

APPENDIX C

LIMITATION OF THE SEPARATION OF VARIABLES TECHNIQUE

Consider the two equations governing the two-dimensional discharge in the case where the kinetic pressure is taken to be equal to zero. These two equations are

$$\nabla \cdot (n\vec{v}) = G \qquad (C.1)$$

and

$$\vec{v} \cdot \nabla\vec{v} + \frac{G}{n}\vec{v} = -\frac{e}{m}\nabla\phi \quad . \qquad (C.2)$$

Using the vector identity

$$\vec{v} \cdot \nabla\vec{v} = \nabla\frac{v^2}{2} - \vec{v} \times \nabla \times \vec{v} \quad ,$$

(C.2) can also be written as

$$\nabla(\frac{v^2}{2} + \frac{e}{m}\phi) - \vec{v} \times \nabla \times \vec{v} + \frac{G}{n}\vec{v} = 0 \quad . \qquad (C.3)$$

Let us now assume that $\nabla \times \vec{v} = 0$ so that (C.3) becomes

$$\nabla(\frac{v^2}{2} + \frac{e}{m}\phi) + G\vec{v} = 0 \quad . \qquad (C.4)$$

In order for (C.4) to be consistent we see by taking the curl it must be true that

$$\nabla \times \frac{(G\vec{v})}{n} = 0 \quad . \qquad (C.5)$$

Now

$$G = n^{\gamma} \quad ,$$

so that Eq. (C.5) may be written as

$$\nabla \times (n^{\gamma-1} \vec{v}) = 0 \quad .$$

Using the vector identify $\nabla \times \psi\vec{A} = \psi\nabla \times \vec{A} + \nabla\psi \times \vec{A}$ on the above equation we obtain

$$n^{\gamma-1} \nabla \times \vec{v} + (\gamma - 1) \nabla n \times \vec{v} = 0 \quad ,$$

which is zero only if

$$(\gamma - 1) \nabla n \times \vec{v} = 0 \quad . \tag{C.6}$$

For the case $\gamma = 1$, Eq. (C.6) is always true but for $\gamma \neq 1$, Eq. (C.6) cannot, in general, be shown to be equal to zero and therefore the assumption that $\nabla \times \vec{v} = 0$ is not consistent in general for any value of γ except $\gamma = 1$, which corresponds to a generation rate of ions proportional to electron density.

APPENDIX D

DETERMINATION OF MAXIMUM TIME INTERVAL FOR CONVERGENCE IN THE ONE-DIMENSIONAL CASE

To apply the method of characteristics, we write the one-dimensional equations in the form

$$\frac{\partial \eta}{\partial t} + e^{(1-\gamma)\eta} - \frac{\partial v}{\partial z} + v\frac{\partial \eta}{\partial z} = 0 \qquad (D.1)$$

and

$$\frac{\partial v}{\partial t} + e^{(1-\gamma)\eta}\, v + v\frac{\partial v}{\partial z} - \frac{1}{2}\frac{\partial \eta}{\partial z} = 0 \qquad (D.2)$$

Equations (D.1) and (D.2) are then written in matrix form as

$$\begin{bmatrix} 1 & 0 \\ 0 & 1 \end{bmatrix} \begin{bmatrix} \frac{\partial \eta}{\partial t} \\ \frac{\partial v}{\partial t} \end{bmatrix} + \begin{bmatrix} v & -1 \\ -1/2 & v \end{bmatrix} \begin{bmatrix} \frac{\partial \eta}{\partial z} \\ \frac{\partial v}{\partial z} \end{bmatrix} = \begin{bmatrix} -e^{(1-\gamma)\eta} \\ -v\, e^{(1-\gamma)\eta} \end{bmatrix} \qquad (D.3)$$

We then multiply the first term in Eq. (D.3) by λ and form a matrix of the coefficients of the various derivatives of η and v to obtain the matrix

$$\begin{bmatrix} \lambda & 0 \\ 0 & \lambda \end{bmatrix} + \begin{bmatrix} v & -1 \\ -1/2 & v \end{bmatrix} = \begin{bmatrix} \lambda + v & -1 \\ -1/2 & \lambda + v \end{bmatrix}$$

We next take the determinant of this matrix and set it equal to zero, to obtain

$$(\lambda + v)^2 - \frac{1}{2} = 0$$

or

$$\lambda = \pm \sqrt{\frac{1}{2}} - v \qquad (D.4)$$

Now λ is equal to $\Delta z/\Delta t$ and we wnat the maximum value of λ such that Eq. (D.4) is satisfied. From Eq. (D.4), using the fact that $v_{(max.)} = 1/\sqrt{2}$ (Bohm Criteria), we obtain

$$|\lambda_{(max.)}| = |(-\frac{1}{v_2} - \frac{1}{v_2})| = \sqrt{2}$$

Since $\lambda = \Delta z/\Delta t$ we obtain a value of Δt given by

$$\Delta t_{(max.)} = \frac{\Delta x}{\sqrt{2}} \qquad (D.5)$$

Thus, for a given value of Δx in order to obtain convergence Δt must be less than .707 times Δx .

REFERENCES

1. G. S. Kino and E. K. Shaw, Phys. Fluids 9, 587 (1966).
2. G. Van Hoven, Phys. Rev. Letters 17, 169 (1966).
3. J. W. Davis, A. W. Angelbeck, and E. A. Pinsley, AIAA J. 1, 2497 (1963).
4. H. R. Kaufman, NASA TN D-585 (1961).
5. D. J. Kerrish, IRE Trans. Space Electron Telemetry 8, 188 (1962).
6. E. A. Pinsley, E. C. Lary, and R. G. Meyerand, Jr., AIAA J. 2, 401 (1964).
7. D. J. Kerrisk and T. D. Masek, AIAA J. 3, 1060 (1965).
8. W. B. Strickfaden and K. L. Geiler, AIAA J. 1, 1815 (1963).
9. H.R. Kaufman and P. D. Reader, Progress in Astronautics and Rocketry, Vol. 5, Electrostatic Propulsion (Academic Press Inc., 1961).
10. L. Tonks and I. Langmuir, Phys. Rev. 24, 876 (1929).
11. I. Langmuir, Collected Works of Irving Langmuir (Pergamon Press, Ltd., New York, 1961), Vols. 4 and 5.
12. S. A. Self, Phys. Fluids 6, 1762 (1963).
13. S. A. Self, Microwave Laboratory Report No. 1185, Stanford University (1964).
14. S. A. Self, J. Appl. Phys. 36, 456 (1965).
15. E. R. Harrison and W. B. Thompson, Proc. Phys. Soc. 72, 2145 (1959).
16. A. Caruso and A. Cavaliere, Nuovo Cimento 26, 1389 (1962).
17. B. Klarfeld, Soviet Phys. JETP 5, 913 (1938).
18. R. J. Bickerton and A. von Engle, Proc. Phys. Soc. 69-B, 468 (1955).
19. K.-B. Persson, Phys. Fluids 5, 1625 (1962).
20. E. R. Mossberg, Jr., and K.-B. Persson, Phys. Fluids 7, 1829 (1964).
21. J. L. Delcroix, Plasma Physics (John Wiley and Sons, London, 1965), p. 166, Ibid., chapter 7, and Appendix 10B.
22. D. L. Rose and M. Clark, Jr., Plasmas and Controlled Fusion (John Wiley and Sons, New York, 1961), chapter 6.

23. J. Jeans, The Dynamical Theory of Gases (Dover, New York, 1954), chapter 9.
24. J. L. Delcroix, Introduction to the Theory of Ionized Gases (Interscience Pub. Inc., 1960), chapter 8, Ibid, 85.
25. L. Spitzer, Jr., Physics of Fully Ionized Gases (Interscience Publishers, New York, 1962), p. 23.
26. I. Langmuir, Phys. Rev. 26, 585 (1925).
27. I. Langmuir, Zeits. Phys. 46, 271 (1927).
28. I. Langmuir. Proc. Nat. Acad. Sci. 14, 627 (1928).
29. D. Gabor, E. A. Ash, and D. Dracott, Nature 176, 916 (1955).
30. N. A. Vorob'eva, Yu. M. Kagan, and V. M. Milenin, Soviet Phys. JETP 8, 423 (1963).
31. N. A. Vorob'eva, Yu. M. Kagan, et al., Soviet Phys. JETP 9, 114 (1964).
32. F. Crawford and S. A. Self, Int. J. Elect. 18, 569 (1965).
33. W. Ott, Institut für Plasmaphysik, Garching b. München, Germany Report 2/19, (1963).
34. R. S. Harp, Microwave Laboratory Report No. 1175, Stanford University, Stanford, California (1964).
35. A. von Engle, Ionized Gases (Oxford, 1965), p. 114.
36. W. P. Allis, Encyclopedia of Physics, Vol. 21 - "Gas Discharges" (Springer-Verlag, Berlin, 1965), p. 383.
37. S. C. Brown, Basic Data of Plasma Physics (M.I.T. Press and J. Wiley, Inc., New York, 1959), p. 3.
38. S. A. Self and H. N. Ewald, "Static Theory of a Discharge Column at Intermediate Pressures," Institute for Plasma Research, Report No. 46, Stanford University (1966).
39. D. Bohm, The Characteristics of Electrical Discharges in a Magnetic Field Eds. Guthrie and Wakerling (New York, 1949), chapter 3.
40. S. A. Self, private communication (1966).
41. D. Bohm, E. Burhop, and H. Massey, The Characteristics of Electrical Discharges in a Magnetic Field Eds. Guthrie and Wakerling (New York, 1949), chapter 2.

42. J. E. Allen, R. Boyd, and P. Reynolds, Proc. Phys. Soc. (London), B70, 297 (1957).
43. S-I Pai, Introduction to the Theory of Compressible Flow (D. Van Nostrand Co. Inc., Princeton, N. J., 1958), chapter 8.
44. J. B. Scarborough, Numerical Mathematical Analysis Fifth Ed. (John Hopkins Press, 1962), p. 199.
45. P. D. Lax, Comm. Pure and Appl. Math. 7, 159 (1954).
46. G. Forsythe and W. Wasow, Finite Difference Methods for Partial Differential Equations (J. Wiley, 1959), p. 38.
47. V. E. Golant et al., Soviet Phys. JETP 9, 737 (1964).
48. I. Langmuir and H. Jones, Phys. Rev. 31, 357 (1928).
49. M. Chaghtai, Proc. Phys. Soc. 63, 768 (1950).
50. G. Leckey et al., Nature 198, 1187 (1963).
51. W. Strickfaden and K. Geiler, TR No. 32-417, Jet Prop. Lab., Cal. Int. Tech., Pasadena, Calif. (1963), p. 12.
52. W. Nottingham, Phys. Rev. 55, 203 (1939).

DISTRIBUTION LIST SUMMARY REPORT II

CONTRACT NAS 3-4100

	Addressee	Number of Copies
1.	National Aeronautics and Space Administration Washington, D. C. 20546 Attn: RNT/James Lazar	1
2.	NASA-Lewis Research Center 21000 Brookpark Road Cleveland, Ohio 44135	
	Attn: Spacecraft Technology Procurement Section (M.S. 54-2)	1
	Attn: Technology Utilization Office (M.S. 3-19)	1
	Attn: Technical Information Division (M.S. 5-5)	1
	Attn: Library (M.S. 60-3)	2
	Attn: Spacecraft Technology Division	
	a. C. C. Conger (M.S. 54-1)	1
	b. R. J. Rulis (M.S. (54-3)	2
	c. S. G. Jones (M.S. 54-3)	5
	Attn: Electric Propulsion Laboratory (M.S. 301-1)	
	a. W. Moeckel	1
	b. H. R. Kaufman	1
	Attn: Report Control Office (M.S. 5-5)	1
3.	NASA Scientific and Technical Information Facility P. O. Box 33 College Park, Maryland 20740 Attn: NASA Representative RQT-2448	6
4.	NASA-Marshall Space Flight Center Huntsville, Alabama 35812 Attn: Ernest Stuhlinger (M-RP-DIR)	1
5.	Research and Technology Division Wright-Patterson AFB, Ohio 45433 Attn: AFAPL (APIE-2)/R. F. Cooper	1
6.	AFWL Kirtland AFB, New Mexico Attn: WLPC/Capt. C. F. Ellis 87417	1
7.	Aerospace Corporation P. O. Box 95085 Los Angeles, California 90045 Attn: Library/Technical Documents Group	1

	Addressee	Number of Copies
28.	Office of Naval Research Power Branch - Room 2509 Washington, D. C. 20025 Attn: J. A. Sotkowski	1
29.	Cornell University Graduate School of Aeronautical Engineering Ithaca, New York 14851 Attn: E. L. Resler, Jr.	1
30.	Rensselaer Polytechnic Institute Troy, New York Attn: E. H. Holt	1
31.	Astrosystems, Inc. 82 Naylon Avenue Livingston, New Jersey 07039 Attn: R. E. Wiech, Jr.	1
32.	Space Sciences, Inc. 301 Bear Hill Road Waltham, Massachusetts 02154 Attn: J. M. Proud	1
33.	Philco Corporation Newport Beach, California 92660 Attn: R. Spongbert/ATC	1
34.	Litton Systems, Inc. Beverly Hills, California 90213 Attn: A. S. Penfold	1
35.	Space Sciences Corporation Natick, Massachusetts Attn: A. Winston	1
36.	Ford Motor Company Astronautics Newport Beach, California 92660 Attn: S. R. Bryon	1
37.	General Electric Company Missile and Space Division Space Sciences Laboratory P. O. Box 8555 Philadelphia, Pennsylvania 19101 Attn: P. Gloevsen	1

	Addressee	Number of Copies
38.	California Institute of Technology 1201 East California Street Pasadena, California 91109 Attn: Professor R. W. Gould	1
39.	University of California Lawrence Radiation Laboratory Livermore, California 94550 Attn: S. A. Colgate	1
40.	University of California Radiation Laboratory Berkeley, California 94720 Attn: R. K. Wakerling	1
41.	University of Illinois Department of Electrical Engineering Urbana, Illinois 61801 Attn: L. Goldstein	1
42.	University of Michigan 3506 East Engineering Building Ann Arbor, Michigan 48106 Attn: Electron Tube Laboratory	1
43.	The Royal Institute of Technology Stockholm 70, Sweden Attn: B. Agduv	1
44.	Stevens Institute of Technology Department of Physics Hoboken, New Jersey 07030 Attn: W. H. Bostick	1
45.	University of Washington Department of Electrical Engineering Seattle, Washington 98105 Attn: H. Golde	1
46.	Bell Telephone Laboratories Murray Hill, New Jersey 07971 Attn: Dr. Buchbaum	1
47.	University of British Columbia Department of Electrical Engineering Microwave Laboratory Vancouver 6, British Columbia, Canada	1

UNCLASSIFIED

Security Classification

DOCUMENT CONTROL DATA - R & D

(Security classification of title, body of abstract and indexing annotation must be entered when the overall report is classified)

1. ORIGINATING ACTIVITY *(Corporate author)*
Stanford University
Stanford, California

2a. REPORT SECURITY CLASSIFICATION
UNCLASSIFIED

2b. GROUP
N/A

3. REPORT TITLE
ONE AND TWO-DIMENSIONAL STEADY STATE LOW PRESSURE DISCHARGE THEORY

4. DESCRIPTIVE NOTES *(Type of report and, inclusive dates)*
Interim Report (Summary Report II)

5. AUTHOR(S) *(First name, middle initial, last name)*
Shaw, E. K.

6. REPORT DATE	7a. TOTAL NO. OF PAGES	7b. NO. OF REFS
November, 1966	170	52

8a. CONTRACT OR GRANT NO.	9a. ORIGINATOR'S REPORT NUMBER(S)
NAS 3-4100	M. L. Report No. 1495
b. PROJECT NO.	
c.	9b. OTHER REPORT NO(S) *(Any other numbers that may be assigned this report)*
d.	NASA CR-54665

10. DISTRIBUTION STATEMENT

11. SUPPLEMENTARY NOTES	12. SPONSORING MILITARY ACTIVITY
N67-28745	National Aeronautics and Space Admin. Office of Scientific & Technical Information Attn: AFSS-A, Washington, D. C. 20546

13. ABSTRACT

It is shown that a pressure theory approach, although approximate, when modified to take into account ion generation can be used to accurately describe a wide variety of dc discharges in the low- and medium-pressure regimes.

Solutions are found for the parameters of the discharges in one-dimensional planar, cylindrical, and coaxial geometries for various generation rates and including both the effects of ion-neutral collisions and an applied magnetic field. The results for the one-dimensional collisionless cases are compared with the more exact formulation of Langmuir and found to be in good agreement.

In the limit of a small inner conductor, the one-dimensional coaxial solutions are shown to be useful in determining the properties of cylindrical Langmuir probes in the ion collection regime. The results are compared to present collisionless probe theories and found to be in good agreement.

For the most important case of ion generation proportional to electron density, two-dimensional solutions for the parameters of the discharges in a rectangular box, a finite length cylinder, and between finite length concentric coaxial cylinders are found for the first time.

Calculated parameters for both the one- and two-dimensional discharges are presented graphically for a number of representative cases and the equations are tabulated and summarized in such a way as to be easily applied to other cases.

The theory is also used to describe the behavior of two experimental devices: the so-called oscillating-electron ion source and the Kaufman ion source.

Author

14. KEY WORDS	LINK A		LINK B		LINK C	
	ROLE	WT	ROLE	WT	ROLE	WT
Low pressure discharge theory						
Ion generation						
Langmuir probes						
Collisionless probe theory						
One and two-dimensional discharge theory						
Oscillating-electron ion source						
Kaufman ion source						